UNIVERSITY OF READING

Department of Meteorology

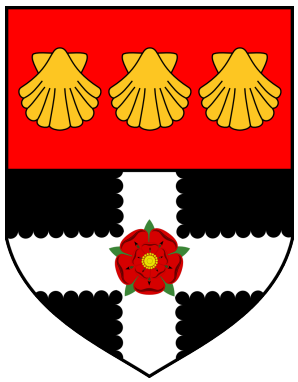

Representing thunderstorm electrification for lightning forecast evaluation

Ben Courtier

A thesis submitted for the degree of Doctor of Philosophy

April, 2020

Declaration

I confirm that this is my own work and the use of all material from other sources has been properly and fully acknowledged.

Ben Courtier

Abstract

Forecasts of lightning in the Met Office's Unified Model (MetUM) are known to over-forecast the total number of lightning flashes in the UK. One of the difficulties in understanding why this happens comes from the dependence of the lightning forecast on the convective forecast. This problem can be mitigated using a more physically representative forecasting method to compare against and by comparing lightning production in modelled thunderstorms to that in observed thunderstorms.

In order to provide a more physically representative forecasting method a new, explicit thunderstorm electrification and lightning scheme is implemented within the MetUM. This scheme uses non-inductive collisional charging to represent the charge generated on hydrometeors and produce a charge density distribution. From this, the magnitude of the electric field is calculated, with appropriate thresholds selected to allow initiation of lightning events. It is shown that this scheme accurately represents observed thunderstorm charge magnitude and structure.

Results from the new electrification scheme are compared with those from the existing lightning parameterisation within the MetUM, and to natural lightning observations in two case studies. The new electrification scheme performs well in both a scattered, fair weather convection case study in the UK and an organised, deep convection case study in the US. It shows realistic lightning coverage and reproduced the daily lightning flash accumulation relatively accurately. The collision-separation efficiency is found to be a key parameter and therefore a potential source of uncertainty in the scheme. Through comparison with the new scheme, the existing MetUM parameterisation is shown to be producing lightning in a manner that is too closely dependent on the rainfall accumulation, which it is suggested is related to its poor performance in the UK case study.

Observations of single cell thunderstorms are used to investigate the production of lightning in thunderstorms in the UK. It is found that prior to the onset of lightning production, single cell thunderstorms show an increase in storm core area. Model simulations of similarly intensifying thunderstorms show that, during these intensifications, the updraft velocity and area both increase, as does the graupel mass in the storm core. It is shown that the new electrification scheme can reproduce the increase in updraft area and graupel mass in intensifying storms, whereas the existing lightning parameterisation does not reproduce any of these parameters. The use of this new electrification scheme, whilst not operationally feasible with existing computer power, provides a research tool with which to further improve lightning forecasting.

Authorship of papers

The following paper has been included in this thesis. The components and estimated percentage of the work carried out by the candidate have been indicated.

Courtier, BM, Stein, THM, Harrison, RG, Hanley, KE, Wilkinson, JM. Intensification of single cell storms prior to lightning onset. *Atmos Sci Lett.* 2019; 20:e873. https://doi.org/10.1002/asl.873

Contribution 80%

B.C. completed the analysis with advice from T.H.M.S., R.G.H. and K.E.H. B.C. wrote the study with input from all authors.

Acknowledgements

First and foremost, I would like to thank my supervisors Thorwald Stein, Giles Harrison, Jonathan Wilkinson and Kirsty Hanley for their insight, guidance and support throughout this project. Without their help this thesis would not exist. I would also like to thank my monitoring committee Chris Westbrook and Matt Owens for their guidance and constructive feedback on my work.

I would like to thank Maff Glover and Tom Allen at the Met Office for their invaluable help with understanding the computational aspects of the UM.

Thank you to all those on Lyle 5 across the years, to those I've lived with, and to the wider PhD community for all the great times spent together throughout this time. Finally, thank you to my family and friends for your support throughout the last few years, particularly my parents for your unwavering love and support.

Contents

Chapter 1

Introduction

1.1 Introduction

Thunderstorms and the lightning produced by them are some of the most complex and powerful elements of the Earth-atmosphere system. Lightning not only presents a danger to life (Elsom and Webb, 2014) but also to infrastructure and transport, such as power lines and aircraft. Lightning is a high speed phenomenon that originates high within thunderstorms, this makes it difficult to study using either in-situ or remote observations. Lightning has not typically been included within operational numerical weather prediction models because of its erratic nature and the small scale of the phenomenon.

More recently, the increase in use of convection permitting models has allowed for parameterisations of lightning to be included in operational models. The Met Office recently included a lightning parameterisation within their high resolution model, the UKV. Wilkinson (2017) evaluated this parameterisation against lightning observations within the UK. It was found that the parameterisation used in the UKV, while relatively accurate in terms of location, over-predicted the intensity and total coverage of the lightning flash rate.

The cause of the over-prediction is difficult to determine. When parameterising lightning flash rate, the typical approach (and the approach used in McCaul *et al.* (2009), whose parameterisation is used within the UM) is to use convective parameters that are related to the production of charge or the intensity of convection. However, given that the convection forecast is often itself inaccurate in terms of both location and intensity, it is difficult to separate the errors of the convective forecast from the errors of the lightning parameterisation.

Previous studies have developed more physically based, explicit electrification and lightning schemes for high resolution models (e.g. Fierro *et al.*, 2013; Barthe *et al.*, 2012; Mansell *et al.*, 2005). These are more physically accurate than the parameterisations based on empirical relationships, as such they can be used a "model truth" to compare parameterisations against. This allows for the diagnosis of whether it is the parameterisation or the underlying model causing the poor representation of lightning flash rate.

Within this thesis, a new explicit thunderstorm electrification and lightning scheme is implemented within the Met Office's Unified Model (MetUM) to allow for a more objective evaluation of the current parameterisation. This scheme is compared to observations of lightning in both the UK and the US. The current McCaul *et al.* (2009) parameterisation is compared against the new scheme. Radar observations of single-cell thunderstorm development are also used to examine the evolution of lightning in thunderstorms and to further test the physical accuracy of both the new scheme and the McCaul *et al.* (2009) parameterisation.

1.2 Thesis contents

The aim of this thesis is to address the deficiencies of the prediction of lightning within the MetUM. This is undertaken through objective and subjective analysis of how well the MetUM captures thunderstorm physics and development and comparing a complex, explicit electrification scheme to a lightning parameterisation.

This thesis is organised as follows: In chapter 2 the data and methodologies consistent to the entire thesis are presented including an overview of the MetUM. In chapter 3 a new physically-based electrification scheme developed for the MetUM is introduced and examples of the charging mechanisms and generated charge structure are examined. In chapter 4 the electrification scheme is tested in two case studies and several aspects of the difference between the new electrification scheme and the existing McCaul *et al.* (2009) based parameterisation are discussed. Chapter 5 examines the evolution of thunderstorm structure related to lightning, in

particular to the onset of lightning. This analysis is replicated using the electrification scheme in chapter 6 and the microphysical accuracy of both lightning forecast methods is investigated. Finally chapter 7 summarises and draws conclusions from the previous chapters and future work is proposed in chapter 8.

1.2.1 A note on terminology

Throughout this thesis the mechanisms of charge generation and charge separation are discussed. "Charge separation" is often used as a term to describe the separation of charge in graupel - ice crystal collisions. However here, to avoid confusion, it will exclusively be used to refer to the process of separating the oppositely (but equally) charged graupel and ice crystals following the collision. The creation of net charge on each particle will be referred to as charge generation.

1.3 Charge generation

How charge is generated within thunderstorms has been a well researched topic with many conflicting theories. Early theories such as ion capture charging and conductive charging are now considered to be ineffective at producing the large amounts of charge observed in thunderstorms; a complete review of these theories is given by Saunders (2008). The main theories that are still currently considered important are the inductive charging mechanism and Non-Inductive Charging (NIC) mechanism.

The first of these, as the name suggests, relies on the induced polarisation of particles in a vertical electric field. As a cloud droplet or smaller ice particle collides and then rebounds off a polarised ice particle, charge is transferred from the polarised particle to the other. These two particles are then separated by their different fall speeds.

Non-inductive charging does not need an electric field to generate charge. Instead, it relies on the charge separated during collisions between graupel and ice crystals. As in the inductive charging mechanism, the particles must collide and then separate for charge to be generated. The charged particles are then separated from one another through gravitational separation. This is currently the primary theory of thunderstorm charging.

1.3.1 Inductive Charging

The inductive charging mechanism involves two colliding hydrometeors in a pre-existing electric field. The hydrometeors involved are usually considered to be an ice particle and a supercooled liquid particle. This is because collisions between two liquid particles almost always result in the particles coalescing (MacGorman and Rust, 1998, p. 63) and therefore not generating any charge. Two ice particles, however, have a much lower combined conductivity and therefore not much charge is generated within the collision (Illingworth and Caranti, 1985).

The ambient electric field causes the particles to become polarised. Then, when

the particles collide through differential fall speeds, the positive region of one particle will collide with the negative region of the other. A small amount of liquid from the drop is left behind, thereby transferring charge from one particle to the other (Aufdermaur and Johnson, 1972) leaving each with a net charge.

The obvious issue with this mechanism as the sole charging mechanism for a thunderstorm is that there needs to be a pre-existing electric field. The fair weather electric field is not strong enough to polarise hydrometeors sufficiently to charge a thunderstorm. Aufdermaur and Johnson (1972) calculated that an electric field on the order of 10 kVm^{-1} is needed to maintain or increase the charge within a thunderstorm. This means that there must be another method of charge generation to, at least initially, create a large electric field within a storm.

1.3.2 Non-Inductive Charging

The NIC mechanism usually relies on the collisions of graupel and ice crystals to produce an equal and opposite charge in the two particles. Many experiments have taken place to investigate the magnitude and sign of the charge generated and the dependencies of the NIC process (e.g. Takahashi, 1978; Jayaratne *et al.*, 1983; Saunders, 1993; Saunders and Peck, 1998). These experiments involved sweeping a rimed probe through an ice cloud within a cloud chamber. The temperature, speed of the probe, cloud water content and properties of the ice crystals were controlled and investigated.

The experiments undertaken by Takahashi (1978) found that the magnitude and sign of charge transferred to a rimed probe depended on both the temperature and cloud water content (CWC) during riming. Jayaratne *et al.* (1983) affirmed these dependencies in a similar experiment. They also included warmed, dry, rimed particles as a target for collisions with ice crystals and found that the warmed graupel did not charge any more than cold, dry graupel. Therefore concluding that the active process of riming (and the presence of liquid water) was more important for charge transfer than the warming effect of riming. In the same set of experiments they examined several other variables including the ice crystal size and the rimer ve-

locity. The charge transferred per event was found to increase with both increasing crystal size and rimer velocity.

The primary theory of how charge is generated within these collisions is the relative diffusional growth rate theory of charge transfer (Baker *et al.*, 1987). This theory states that charging will be positive to the particle that is growing faster from vapour diffusion at the time of the collision. It is worth noting that this theory takes into account the diffusional growth of vapour during the process of droplets freezing onto a particle's surface.

The mechanism behind this theory relies on the fact that the speed with which an ice particle grows affects the local spatial ionisation within the ice. That is, the faster a particle grows, the more rough edges and inhomogeneities there are within the particle, at these locations the OH^- and H^+ ions become dissociated (Dash and Wettlaufer, 2001). The OH^- ions are still held to the overall structure with some remaining hydrogen bonds, the H^+ ions, however, are free to move within the particle. The positive ions tend to move closer towards the centre of the particle, creating a net negative charge on the outside of the particle and a net positive charge in the centre of the particle.

If two particles collide, there will be a small amount of melting that occurs due to the collision. In liquid water the H^+ and OH^- ions become dissociated and therefore free to move. Because it is just the very outer layers of the ice particles that melt, there will be a difference in H^+ concentration between the two particles. If the ice crystals have a higher concentration at the particle surface, the H^+ ions will move down the concentration gradient, therefore giving the graupel particle a net positive charge and the ice crystal a net negative charge. This is represented in Figure 1.1, where the graupel particle is growing faster and therefore charges positively.

Saunders *et al.* (1991) expanded on the work of Jayaratne *et al.* (1983) by using effective liquid water content (EW) rather than cloud water content as the independent variable, where EW is the cloud water content available to be rimed (i.e. the product of the CWC and the collision-collection efficiency). They related the

EW and riming rate to the relative diffusional growth rate theory by speculating that charging is positive (to graupel) in high EW and at high temperatures, where water to provide vapour deposition is plentiful and does not immediately freeze to the surface of the graupel. In the opposite scenario with low temperatures or low EW, the vapour deposition on graupel is low as there is less liquid water available to provide moisture and drops freeze rapidly when making contact with graupel.

Saunders and Peck (1998) further examined the sign and magnitude of the charge transfer with respect to Rime Accretion Rate (RAR) and Effective Water (EW). These two quantities give more information about the active riming rate during the charge transfer than cloud water content or liquid water content. It was found that graupel could charge negatively to relatively high temperatures given a sufficiently low RAR. The dependency on RAR implicitly includes within it sensitivity to liquid water content, graupel/droplet collection efficiency and size/number of droplets.

Because of the large number of varying results from different laboratories, Takahashi *et al.* (2017) used videosondes to measure the charge and shape of particles and other videosondes to measure the CWC, by capturing droplets onto a scrolling film. The results from their study were compared against previous laboratory studies. They found that the average charge reversal temperature (the temperature at which the sign of the charge transferred to graupel changes between positive and negative) was -11 °C when the CWC was low. Compared to Takahashi *et al.* (2017), the positive charging of graupel at warm temperatures and low CWC was not well represented by Saunders and Peck (1998) who suggested that graupel should generally charge negatively at these temperatures.

One question that has not been covered by the literature is the change to charge generation by the combined effect of the inductive and non-inductive charging methods. If (in the case of an electric field pointed toward the surface and graupel charging positively through the NIC method) the electric field causes the base of the particle to become more positively charged through the polarisation of the particle this should reduce the net negative charge within the graupel's surface layer, thereby reducing the charge generated within the NIC process.

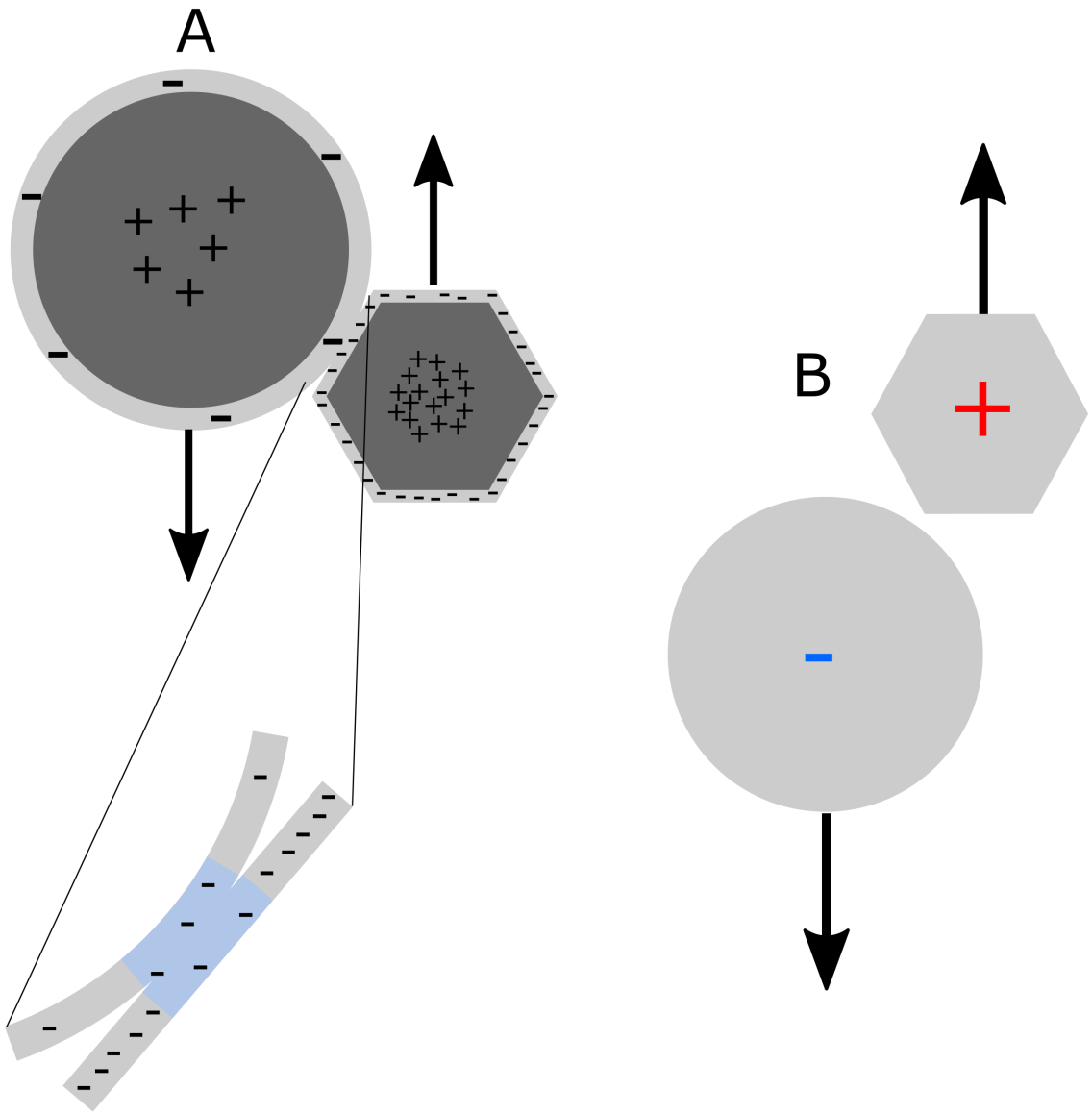

Figure 1.1: A schematic of the relative diffusional growth rate theory for charge separation between an ice crystal and graupel particle, where the ice crystal is growing faster from diffusion. Small black pluses and minuses refer to local ions, the large coloured plus and minus refer to the particle charge. The blue section of ice particle shows the collisional melting. A shows the graupel and ice crystal particles colliding and B shows the result of the collision.

1.4 Thunderstorms

1.4.1 Thunderstorm charge

Lightning and thunderstorm electrification have been of interest to scientists for centuries. For example, Benjamin Franklin famously proposed an experiment using

a kite to conduct electricity from a thunderstorm to the surface and create a spark. Thomas-François Dalibard performed the experiment in 1752 with a metal rod, proving that thunderstorms are electrified and implying lightning is an electrical phenomenon (Franklin may have also performed the experiment later in the same year using his original kite design).

Later, Wilson (1916, 1924) proposed a dipole charge structure within thunderstorms based on measurements of the electric field beneath thunderstorms. A tripole charge structure was theorised by Simpson and Scrase (1937) and Simpson and Robinson (1941) based on balloon-borne measurements of the electric field in thunderstorms. The tripole charge model became the pre-eminent model of thunderstorm charge structure for most of the rest of the 20th century. Eventually, after further measurements with weather balloon borne electric field meters by Marshall and Rust (1991) and reviewing of past data by Rust and Marshall (1996) a number of more complex structures were reported involving between four and ten charge centres. Stolzenburg *et al.* (1998) suggest a composite charge structure (based on 49 soundings through several types of thunderstorm) of four charge centres within the convective region of the storms and six charge centres outside of the updraft, shown in Figure 1.2. These charge regions are not necessarily present in every thunderstorm in the configuration shown in Figure 1.2 particularly outside of the updraft.

Stolzenburg *et al.* (1998) suggest that the three lower charge layers within the updraft are likely a result of the NIC process. In the case of Figure 1.2 the positive charging of graupel at warmer temperatures accounts for the lower positive charge layer, the main negative charge layer is attributed to the negatively charged cloud ice from charging at warmer temperature and the negatively charged graupel from charging at colder temperatures, finally the positively charged cloud ice from charging at colder temperatures produces the upper positive layer. Outside the updraft region the charge layers are created through similar mechanisms, but the weaker updraft (or downdraft) creates more complex charge structure as different particles are not separated as much.

The highest layer in the convective region shown in Figure 1.2 is not necessarily generated by the same processes as the other charge regions. The top layer of charge suggested by Stolzenburg *et al.* (1998) is a screening layer. This forms from the difference in conductivity between the cloud and clear air. The conduction current that forms as part of the global atmospheric circuit causes accumulation of charge on both the upper and lower cloud boundaries. Due to the presence of charged precipitation and inductive charging this charge layer is rarely observed at the bottom of the cloud, but at the top of the cloud the layer can be distinct.

The most common arrangement of the charge layers within the updraft is: a lower positive charge layer, main negative layer, upper positive layer and a negative screening layer at the top cloud boundary, as shown in Figure 1.2. This is not always the case, MacGorman *et al.* (2005) present observations of storms in which each charge layer specified by Stolzenburg *et al.* (1998) is of opposite sign; these storms are referred to as inverted polarity. Often the charge structure is more complex than this idealised case, however the lower and main charge layers in the updraft region are the layers that are usually largest in magnitude.

Bruning *et al.* (2007) suggested that their observations support the conceptual model of Stolzenburg *et al.* (1998). Bruning *et al.* (2007) observed a multicell thunderstorm in Oklahoma using both a Lightning Mapping Array (LMA; see section 1.7.2) and a balloon-borne electric field meter in order to locate the charge centres. Both methods observed the typical polarity tripole structure, the electric field meter also observed a negative screening layer at the top of the cloud, as well as two much smaller charge layers at the bottom of the cloud. The difference in charge structure from each method highlights one of the issues with inferring charge regions from LMA observations. These can only find charge regions which lightning strokes propagate through, meaning that some regions could easily be missed.

In a separate field campaign Wiens *et al.* (2005) observed a supercell thunderstorm in Kansas. This supercell had an inverted polarity. However, the charge structure was not as simple for much of the storm's lifetime as the conceptual model of Stolzenburg *et al.* (1998) or the example of Bruning *et al.* (2007): the storm often

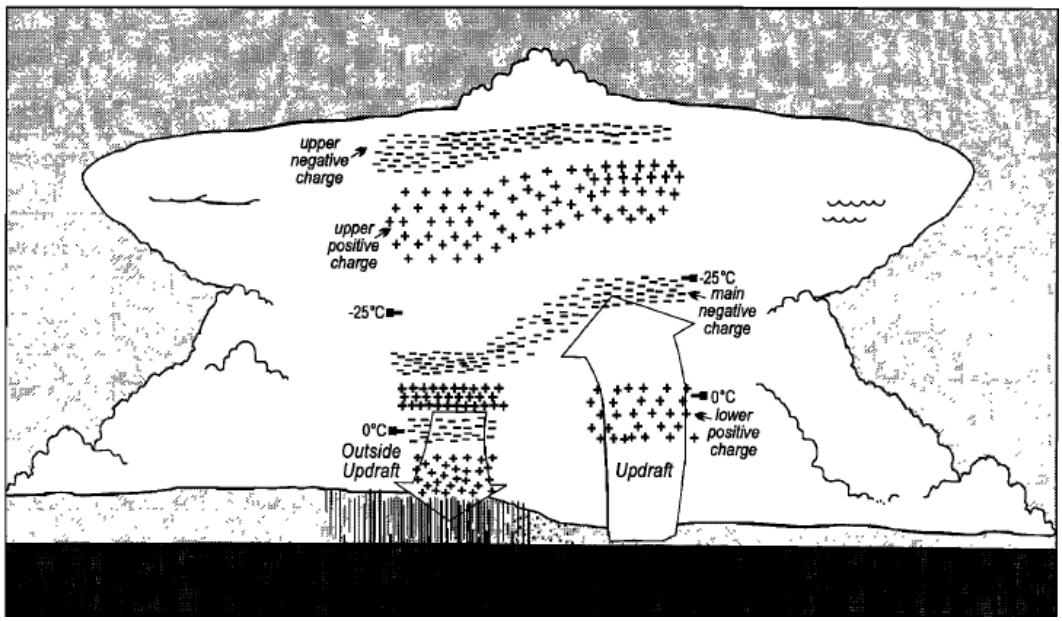

Figure 1.2: A model of the theoretical thunderstorm charge structure within and outside of the updraft from Stolzenburg *et al.* (1998). The specific charge regions are highly variable, particularly outside of the updraft.

showed five charge layers with some of the charge layers being separated horizontally rather than the typical vertical separation. This shows that while the Stolzenburg *et al.* (1998) model is a good base of typical thunderstorm charge structure, there are often variations to that model.

In-situ observations of the charge regions within thunderstorms have been used to study the charge density of both precipitation (Marshall and Marsh, 1993) and cloud particles (Marshall and Stolzenburg, 1998). Using a videosonde with a built in induction ring to observe both the shape and charge of cloud particles, Takahashi *et al.* (1999) report that the maximum particle charges were around 50 pC in Japanese winter thunderstorms. Charge of both signs was carried on graupel and ice (crystals and aggregates) throughout the depth of the cloud in the majority of the cases observed, as shown in Figure 1.3. This contrasts with the findings of Mo *et al.* (2007) where 98% of the charged particles were charged positively. The work of Mo *et al.* (2007) did examine a collapsing, weakly electrified cloud, as opposed to a thunderstorm. The earlier work of Marshall and Marsh (1993); Marshall and Stolzenburg (1998) does agree with the results of Takahashi *et al.* (1999). These

observations help to confirm the theory of charging through graupel-ice collisions and subsequent gravitational separation.

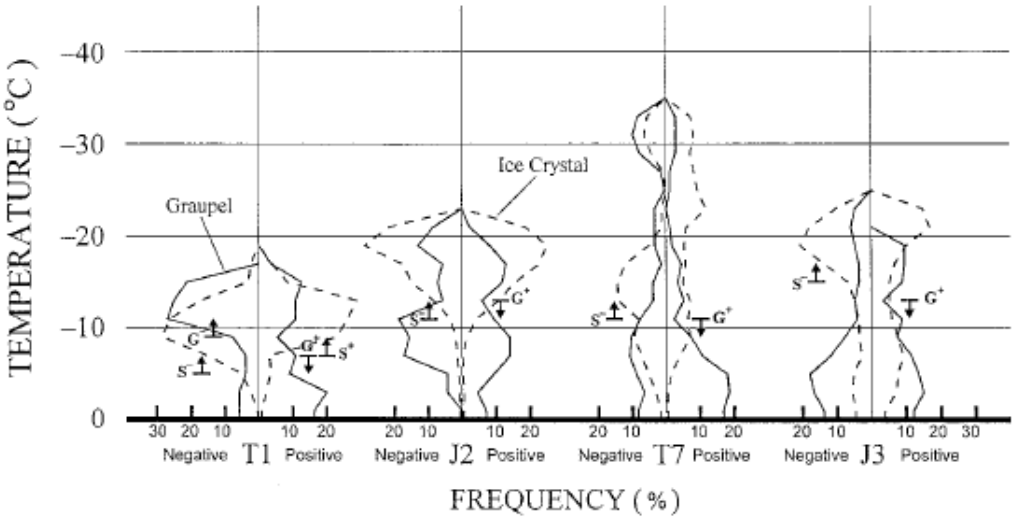

Figure 1.3: Selected cases of Takahashi *et al.* (1999) where reversal temperatures were identified. Smoothed frequency of positive and negative graupel and ice crystals are shown. The reversal temperatures are indicated by small arrows for both graupel and ice crystals. Modified from Takahashi *et al.* (1999, © American Meteorological Society. Used with permission.)

1.4.2 Lightning and thunderstorm microphysics

The microphysics of a thunderstorm play a vital role in the development of the electrical structure and in the accumulation of charged particles to create the charge centres that are needed to generate lightning.

As discussed in detail in section 1.3, charge generation requires graupel, ice crystals or aggregates and supercooled water droplets. In order for all three of these to be present at the same time an updraft is generally required. This allows for liquid droplets to be lofted well above the freezing level, to where ice crystals are growing and also gives plenty of opportunity for riming to occur, thereby creating graupel. This mixed phase region has been shown to be related to lightning flash rates (e.g. Carey and Rutledge, 1996; Liu *et al.*, 2012) and is understood to be where the majority of charge is generated within the storm (Latham *et al.*, 2004).

The total flash rate is related to the velocity of the updraft, but a stronger

relation is generally observed between the total flash rate and the volume of the updraft (Deierling and Petersen, 2008). This suggests that a larger number of particles generating charge outweighs the increased charge that is generated through the fewer, larger particles that are colliding at the greater velocities that are present in a stronger, but narrower, updraft.

Observational studies have related the total lightning flash density to various parameters relating to ice in a thunderstorm, including cloud ice mass (Deierling *et al.*, 2008) and precipitating ice flux (Petersen *et al.*, 2005). Mattos *et al.* (2016) used dual-polarimetric radar parameters to infer statistical relationships between regions of hydrometeors and lightning VHF sources (i.e. lightning channel location). They found that in vertical radar profiles with high VHF source rates (>14 km^{-2}) there were signatures of supercooled raindrops in the lower mixed-phase region. They also observed ice crystals aligned vertically with the electric field in the glaciated region.

Deierling *et al.* (2008) examine in further detail the suggested relationship of Blyth *et al.* (2001), that lightning flash rate is proportional to the product of the downward flux of precipitating ice mass and the upward flux of non-precipitating ice mass. They find that for storms in both Alabama and the High Plains there is a strong correlation between flash rate and the two variables. They suggest that due to the different environments in Alabama and the High Plains the relationship is "robust and relatively invariant". However, given that the majority of storms in both areas had flash rates of 1 min^{-1} or greater, it is questionable whether the relationship could be identified in the UK where flash rates are often lower. Deierling *et al.* (2008) finish by suggesting that ice mass derived from the flash rate (which is observable from satellites as well as global detection networks) could be a useful observational method in areas with poor radar coverage.

However, lightning flash rate doesn't always increase with increasing ice mass. The presence of lightning holes in particularly strong updrafts and hail cores is well documented (e.g. Krehbiel *et al.*, 2000; Emersic *et al.*, 2011; DiGangi *et al.*, 2016). These lightning holes do not occur just in lightning flash origin density observations,

but also in flash extent density observations. It is thought these regions contain less charge due to the growth of hail including a wet growth phase where the collisions between graupel and ice result in the two particles coalescing rather than separating and generating charge (Emersic *et al.*, 2011).

1.4.3 Lightning in thunderstorm development

The initial electrification of a thunderstorm begins as soon as the cloud forms, when screening charge layers can form, and early in the storm development, ice crystal - ice crystal collisions without any supercooled liquid water present can cause electrification (Dye and Bansemer, 2019). However, these changes are difficult to detect without in-situ observations. The size and intensity of the storm does not necessarily translate directly to electric field magnitude. Dye *et al.* (1986) observed a storm with no significant change in electric field even though an "organized updraft and growing precipitation were present".

Once the electrification process begins in earnest, a lightning flash can follow relatively quickly. In their observations Dye *et al.* (1986) reported an intra-cloud flash only eight minutes after the field intensification began.

Three thunderstorms observed by Stolzenburg *et al.* (2015) showed an initial change in electric field between 5 and 10 minutes before the first lightning flash. However, the electric field only began to rapidly increase around 3 minutes before first lightning flash. They note that, prior to the initial electric field change being measured, there was reflectivity of 40 dBZ or greater observed at the $-5\,^{\circ}\mathrm{C}$ level. In each case the first lightning flash was an intracloud flash.

Lightning jumps are sudden increases in the lightning flash rate, they are related to severe weather occurrence, such as strong winds, hail or tornadoes. A statistical examination of observations of the microphysics and timing of lightning jumps by Schultz *et al.* (2017) shows that the changes in microphysics occur less than 15 minutes before the lightning jump. The main differences in microphysics between lightning jumps and other increases in flash rate were the change in $10\,\mathrm{m\,s^{-1}}$ updraft volume and the change in peak updraft speed. The mixed phase graupel mass was

not significantly different between lightning jumps and non-jump increases, though the graupel mass did generally increase with the flash rate.

1.4.4 Thunderstorms in the UK

Comparatively, very little research into thunderstorm dynamics has been undertaken in the UK. The charging mechanisms for thunderstorm electrification are, of course, the same as anywhere else in the world. However, the storms themselves are often distinct from the much more active thunderstorms studied in the US or the tropics. For example, Illingworth and Lees (1991) suggest that lightning strikes occur in the nearest 3 km to the storm's reflectivity maximum. This opposes the lightning holes often observed around a hail core in the US (e.g. Krehbiel *et al.*, 2000; Emersic *et al.*, 2011; DiGangi *et al.*, 2016). The reason for this is simply the magnitude of updraft observed in each storm. In the UK a weaker updraft cannot support large hail and therefore the highest reflectivity region consists of graupel, allowing charge to be generated there.

1.5 Lightning

Lightning is generally classified by the location of each end of the flash and the polarity of the charge neutralised by the flash. The most common type of lightning is Intra-Cloud (IC). These have no associated polarity (unlike Cloud-to-ground flashes) as the charge will be moved from one region of the cloud to another. This means there is no net change of charge due to IC lightning in the isolated cloud system, though there will still be charge change along the channel as charge is deposited from one place in the storm to another. The other common type of lightning is Cloud-to-Ground (CG), this can be classified into either positive or negative depending on the sign of the charge transferred to the ground. It is also further classified into upward or downward depending on if the initial channel propagates from the ground to the cloud or the cloud to the ground. For CG flashes, these classifications are not always included, if they are not included it is assumed that

the lightning is a downward, negative flash as these are the most common type. More rarely lightning can also occur between separate storms (inter-cloud flash) or between the storm and clear air (cloud-to-air flash).

The lightning flash itself is a very complex phenomenon involving several steps, all of which are not fully understood, the stages involved in a negative cloud-ground flash are shown in Figure 1.4. The flash involves: an initial breakdown, a stepped leader, the attachment process, a return stroke, dart leaders and finally further return strokes. These steps will not all be covered here, as not all are relevant to the model that is developed in this work.

1.5.1 The initial breakdown

The initial breakdown is the process in which air becomes electrically conducting, allowing for the formation of the lightning channel.

While air is conducting in the fair weather atmosphere, due to the presence of ions generated by galactic cosmic rays or radioactivity near the Earth's surface, the resistance is far too high to allow for the magnitude of current observed in lightning strokes. The electric field breakdown threshold of clean air is where the electric field magnitude is great enough that the molecules in air are separated into positive and negative ions, allowing for a current to flow. However, the magnitude of electric field needed is around $2\,\mathrm{MV\,m^{-1}}$, which is an order of magnitude higher than the large scale electric fields observed in the atmosphere (e.g. Marshall and Rust, 1991). This suggests that there is a way of locally enhancing the electric field to allow for the electrical breakdown of air. Rison *et al.* (2016) present evidence of fast positive breakdowns initiating narrow bipolar events and IC flashes, they describe a fast positive breakdown as "a volumetrically distributed system of positive streamers or streamer-like activity" and they suggest that this could be the mechanism by which all flashes are initiated.

During the fast positive breakdown, many streamers occur simultaneously. Rison *et al.* (2016) conclude that the streamers could be initiated by corona from hydrometeors in locally concentrated regions of high electric field. Although no

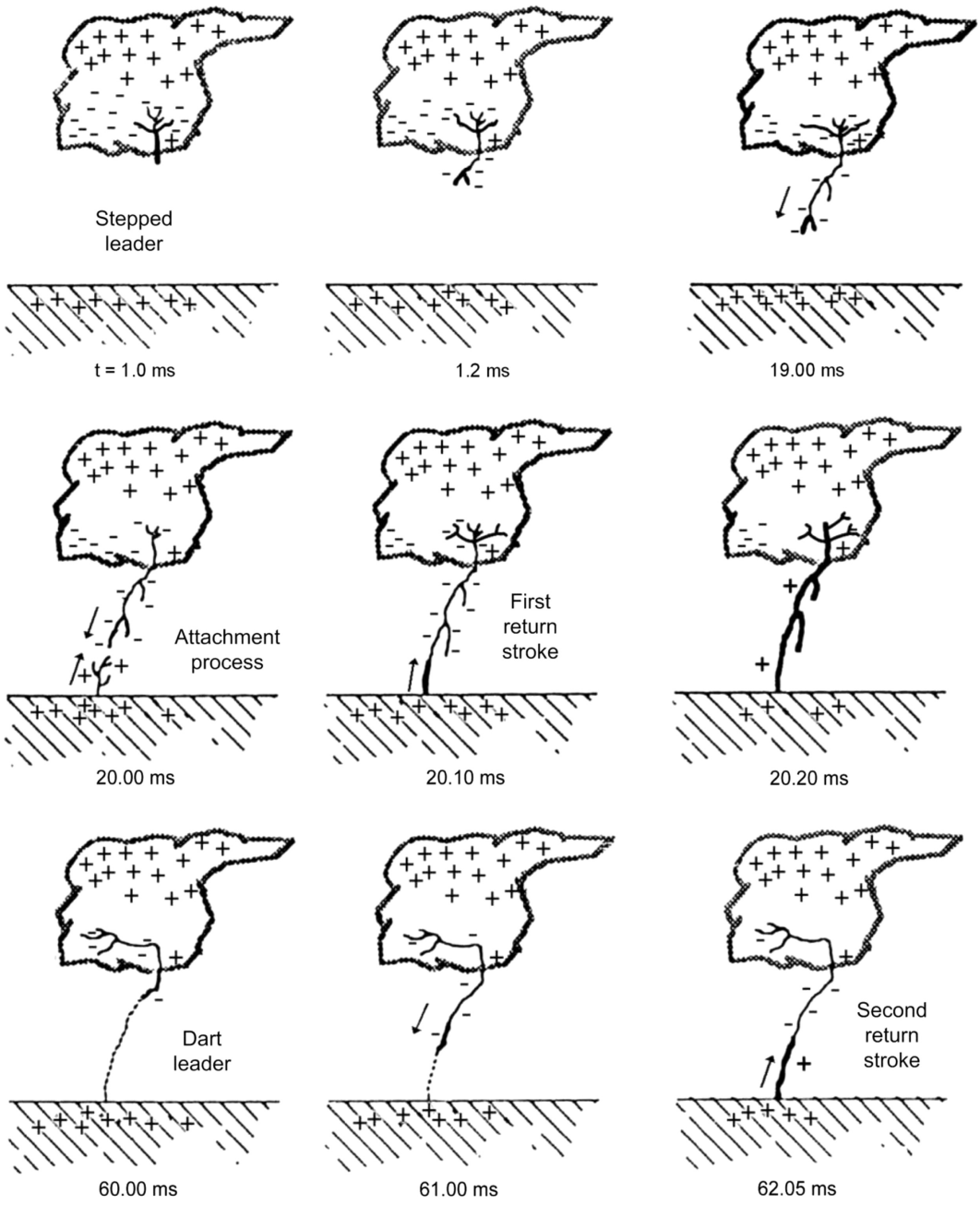

Figure 1.4: A diagram showing the stages of a negative CG flash, from the stepped leader to a return stroke. The timescale is given from the initial breakdown in the cloud. Modified from Dwyer and Uman (2014) with permission from Elsevier.

such regions of high electric field have been observed, it is possible that they could have been missed by in-situ measurements. Rutjes *et al.* (2019) offer an alternative reason for the initiation of numerous, simultaneous streamers. The impact of highly energetic cosmic rays on atmospheric air molecules creates a cascade of other particles. Though only the centre of these cascades contain sufficient high energy

electron densities to cause streamer initiation, the probability analysis of Rutjes *et al.* (2019) suggest that this is possible, given the observations of Rison *et al.* (2016).

Whichever of these methods is responsible for the initial breakdown occurs frequently enough to not obviously restrict the lightning flash rate. The maximum large scale electric field observed in the atmosphere never nears the breakdown field for clean air, it is generally measured to be on the order of $100\,\mathrm{kV\,m^{-1}}$ (Stolzenburg *et al.*, 2007).

1.5.2 Lightning channel

The lightning channel is the element of the lightning flash process that the least is known about. The high speed and altitude of the steps involved means that studying the channel is difficult, instead proxies or analogues such as rocket-triggered lightning or long sparks are often studied.

Once the air has become conducting due to the breakdown processes discussed above, a bidirectionally propagating channel develops (Montanya *et al.*, 2015). One end of the channel propagates into a region of positive charge and the other into a region of negative charge. In the case of a CG flash these two channels will both be approximately vertical and in opposite directions. The groundward propagating channel is the most studied as it is more visible for investigation using high speed cameras and ground based instruments.

For a negative CG flash, the channel initially propagates as a negative stepped leader. The channel moves in discrete steps of 5 - 10 m (Hill *et al.*, 2011). As it does so, negative charge is deposited along the length of the channel; a large deposit of charge is carried in the leader tip, intensifying the electric field ahead of the leader (Carlson *et al.*, 2009). Once the stepped leader tip approaches the ground, a positively charged upward leader is triggered from the surface by the large electric field, caused by the leader tip (Rakov and Uman, 2003). The two leaders attach and the positive leader propagates up the channel neutralising the negative charge as it goes, effectively moving negative charge from the cloud to

the ground. Charge is neutralised in three stages, first the charge carried by the leader tip is neutralised when it reaches the positive leader; next, the charge on the channel is neutralised by the return stroke; and finally, the charge carried by the continuing current that can briefly flow along the channel is neutralised. Charge neutralised by the continuing current is mainly drawn from the top of the lightning channel (Rakov and Uman, 2003).

The channel remains for a period of tens of milliseconds after the return stroke has reached the cloud. The decaying channel is still conducting which allows for further strokes to propagate down the channel. These strokes generally travel around two orders of magnitude faster than the initial stepped leader and often have no branching (Rakov and Uman, 2003), as such they are called dart leaders. The charge carried by the dart leader is again deposited along the channel and again neutralised by the return stroke. There are typically 2-4 subsequent dart leaders and return stokes, though there can be more than 20 dart leaders reusing a channel. Collectively, the initial stepped leader, return stroke, any dart leaders and further subsequent return strokes are called a lightning flash.

There are more processes involved and many of the processes making up a flash are not fully understood, however these are outside the scope of this work.

1.6 Lightning in numerical models

Prior to high resolution, convection permitting and convection resolving, NWP models lightning forecasts were parameterised, if included at all. There are many ways of parameterising lightning; a number of studies are shown in Table 1.1 together with the primary variables used. Most methods currently in operation use large scale convective proxies or, if included within a high resolution model, features connected to the intensity of the convection and the generation of charge.

1.6.1 Lightning parameterisations

Because global circulation models can often have resolutions in tens of kilometers they cannot resolve the mechanisms that generate convection or the convection itself (often on a scale of about 10 km). However, convective parameterisations can provide useful parameters to help predict lightning flash rates. For example, the cloud top height (e.g. Price and Rind, 1992). This is related to the updraft intensity, which also has a large impact on charge generation and separation. Other approaches involve using convective precipitation (e.g. Romps *et al.*, 2014) or any combination of various instability metrics, such as Convective Available Potential Energy (CAPE) and convective inhibition, the lifting condensation level, the level of free convection or the equilibrium level.

Study	Variables used
Price and Rind (1992)	Convective cloud top height
McCaul *et al.* (2009)	Graupel flux and total ice mass
Barthe *et al.* (2010)	Ice mass flux product
Yair *et al.* (2010)	Updraft velocity and ice mass mixing ratios
Romps *et al.* (2014)	Precipitation rate and CAPE
Finney *et al.* (2014)	Upwards cloud ice flux
Lopez (2016)	CAPE, ice and cloud condensate flux, and cloud base height

Table 1.1: Example studies developing model parameterisations for diagnosing lightning flashes or lightning flash rate together with the model variables used in the parameterisation.

Lopez (2016) developed a new parameterisation for the ECMWF's integrated forecasting system. This parameterisation was based on several linked parameters. They used CAPE, the vertical profiles of ice upward flux and cloud condensate within the convective region, and the convective cloud base height. This parameterisation was found to match satellite observations well at both a global and continental scale.

Lightning parameterisations for coarser resolution models such as these remain important for climate modelling. Recently Finney *et al.* (2018) investigated the impact the choice of lightning parameterisation makes to predictions of how flash rates will respond to climate change. They found that the parameterisation had a large effect on the result. The sign of the response of flash rates to a strong global warming scenario changed from positive (i.e. flash rate increasing with a warming climate) using a cloud top height parameterisation to negative when using a ice flux based parameterisation. This shows that achieving an accurate lightning parameterisation for coarse models is still important even with the increase in convection permitting models for short-term forecasting.

In higher resolution, convection permitting, models the availability of more related parameters such as ice fluxes or graupel mass allows for more detailed parameterisations. McCaul *et al.* (2009) based their parameterisation on the upwards flux of graupel and the total ice mass within a model column. These parameters are both strongly correlated with the generation of charge. This parameterisation is widely used, both operationally and as a benchmark to compare against (e.g. Wilkinson and Bornemann, 2014; Fierro *et al.*, 2013).

Non-operationally, electrification schemes have been added to research weather models (e.g. Helsdon *et al.*, 1992; Fierro *et al.*, 2013; Barthe *et al.*, 2012). These schemes usually involve modelling charge generation and separation using either the inductive charging or NIC mechanisms. The specific methods used are discussed in more detail in section 3.2

1.7 Lightning observations

There are two main categories of radio wave based lightning detection networks in use today, very low frequency and very high frequency detection networks. These generally work on a similar basis, detecting electromagnetic emissions from lightning flashes and triangulating the location through time-of-arrival analysis at multiple receiving stations. Other methods of lightning detection involve optical systems on

satellites and counting thunderstorm days.

1.7.1 VLF lightning detection

Very Low Frequency (VLF) lightning detection works by using the radiation emitted by the powerful return stroke. The pattern of VLF radiation emitted from this stroke is analysed and correlated between all receiving stations that have detected it. If four or more stations detect the same pattern the location is determined from the time of arrival for each station. This method of detecting lightning is easy to implement at low cost. The receivers do not need to be close together as VLF waves can propagate large distances through the atmosphere, using the ionosphere as a waveguide. However, because VLF radiation is mainly emitted by the return stroke of a CG flash the detection efficiency of VLF based systems is generally poor for IC flashes, which do not have such powerful strokes.

1.7.2 VHF lightning detection

Very High Frequency (VHF) lightning detection, or Lightning Mapping Array (LMA) systems rely on the VHF radiation emitted by each step of the lightning channel. The pattern recognition and time of arrival detection steps of analysing the radiation work similarly to the VLF systems, however in this case the location is found in three dimensions. In order to detect the VHF radiation and accurately map it in 3D the receivers must have a direct line-of-sight to the lightning channel. This means that a large number of receivers are required to allow for multiple receivers to observe every area within a domain: even if the line-of-sight required is generally to locations several kilometers above the surface. The main advantage of this type of system is the high detection efficiency of IC flashes, even if some steps of the channel are missed it is almost impossible to miss an entire flash. The other advantage is the high resolution information; each step of the channel is mapped out, allowing for inference of charge regions within a thunderstorm and for detailed observations of lightning channel progression and branching (e.g. Hare *et al.*, 2019).

1.7.3 Satellite observations

A third method of observing lightning uses satellite-borne sensors to detect flashes of lightning (e.g. Goodman *et al.*, 2013). These cameras detect the light emitted from lightning flashes and as such are particularly effective at night (Rudlosky *et al.*, 2017), though the detection efficiency in the day is still high. Detectors can be on both low-orbiting (e.g. the Lightning Imaging Sensor on TRMM) or geostationary satellites (e.g. the Global Lightning Mapper on GEOS-16). The clear problem with low Earth orbiting satellites is that there is poor temporal sampling, regions are only observed for a short period of time each pass of the satellite. Geostationary observations are much more consistent, in that they constantly observe the same region. However, they are unable to observe higher latitudes, such as the UK.

Chapter 2

Data and Methods

2.1 Lightning observations

2.1.1 Arrival Time Difference Network

Arrival Time Difference Network (ATDNet) is a long-range, VLF Lightning Location System (LLS) and as such is worse at detecting IC lightning than CG lightning. The radio waves emitted by IC lightning are typically much weaker than those from CG flashes (Enno *et al.*, 2016). The detection efficiency for the network was reported by Enno *et al.* (2016) as 89% for CG flashes and 24% for IC flashes. This was found through comparison with an LMA over southern France. LMAs are the closest system to observing 100% of lightning within the area they operate (though that is usually a small area). As the south of France is on the edge of the scope of the central ATDNet range, it is likely that the detection efficiency in the UK is slightly greater than that of the south of France. There are a larger number of sensors across the UK (four sensors in the British Isles) with a further three sensors across the rest of western Europe.

ATDNet data is reported with an error in the measurement of the ground location of the flash. This is typically between 1 and 3 km within the UK.

2.1.2 Earth Network Total Lightning Network

The Earth Networks Total Lightning Network (ENTLN) is a time of arrival total lightning detection network operating primarily in the USA. It uses wideband sensors to detect both IC and CG flashes, the latter are identified by the presence of a return stroke (Liu *et al.*, 2014).

Recently Zhu *et al.* (2017) found that the network detected 99% of natural CG lightning flashes observed from the Lightning Observatory in Gainesville (LOG), in Florida and 100% of rocket triggered CG flashes. However, these detection efficiencies were only for CG flashes and only tested flashes in Florida, where the sensor network is particularly dense. Across the wider continental United States, Lapierre *et al.* (2019) tested the ENTLN observations against the Global Lightning Mapper (GLM), this includes IC and CG flashes and gives a broader geographic breakdown of the detection efficiency. Lapierre *et al.* (2019) found that the detection efficiency of the ENTLN was high across Florida, all of the pixels showed efficiencies of 80-90% or 90-100%. This is mostly in agreement with Zhu *et al.* (2017), though evidently lower than the 100% recorded against the rocket trigger lightning. In Oklahoma and Kansas, where the lightning observations used in this work are primarily located, the detection efficiency is more variable but is still mostly in the 70-80% range or higher.

2.2 Radar Observations

Radar data are used to provide context for the intensity of the thunderstorms and to demonstrate the quality of the convective forecast. The radar data used are composites from both the UK and the US and rainfall derived from both of these networks.

The UK composite is created from the Met Office's operational radar network of 15 C-band radars. The horizontal resolution is 1 km and the vertical resolution is 500 m. The temporal resolution is 5 minutes.

The rainfall composite for the UK is derived from the radar reflectivity following the method of Harrison and Kitchen (2009). In this method radar observations undergo correction for quality control errors, such as beam blocking or clutter. Rainfall is then derived from reflectivity based on a Z-R relationship of $Z = 200R^{1.6}$ and adjusted based on rain gauge observations and orography.

The rainfall composite for the US is derived in a similar way to the UK composite

(Fulton *et al.*, 1998). The radar reflectivity used is from the US Nexrad network of 159 S-band radars. This refelctivity is quality controlled before Z-R relationships are applied. The Z-R relationship used in this product is generally $Z = 300R^{1.4}$, however, in more tropical locations the relationship: $Z = 250R^{1.2}$ is used instead. The rain rate is capped to prevent unreasonably large rain rates from hail cores. The value of the cap varies from 75-150 mm h^{-1} depending on the location. As in the UK product, rain gauge data are used to adjust the rainfall product.

2.3 The Met Office Unified Model (MetUM)

The MetUM is an operational numerical weather prediction model developed by the UK Met Office. The model is versatile and can be used from high resolution city-scale modelling of London to global climate modelling, it can also include interactions with related processes, such as vegetation, ocean or chemistry. Currently the model is run operationally by the Met Office as a global model with a resolution of 10 km and regionally over the UK with a central resolution of 1.5 km. It is also used operationally by several other countries.

2.3.1 Model framework

The MetUM is run with a dynamical core described in detail by Davies *et al.* (2005): the equations of motion are solved on Arakawa C-grid with a terrain-following, height-based vertical coordinate, discretized to a Charney–Phillips grid. All prognostic variables, except density, are advected using a Semi-Lagrangian scheme. Time stepping is done using a predictor-corrector, semi-implicit scheme.

The MetUM high resolution operational model for the UK is called the UK Variable resolution model (UKV). This is run with a resolution of 1.5 km in the central domain, extending to 4 km at the edges. The 70 vertical levels are arranged to increase in separation quadratically with height and extend to 40 km above the surface. The boundary conditions are provided by the global model. For the most part the UKV is the same as the global version of the model, however, because the

UKV is a convection permitting model, the convection scheme is turned off and convection is simulated by the model explicitly. In this work a combination of the UKV and separate 1.5 km resolution simulations will be used.

The performance of the MetUM in representing convection has been studied by Stein *et al.* (2014) and Hanley *et al.* (2015) through comparison with radar observations of convective cells. Stein *et al.* (2014) found that the 1.5 km resolution runs produced convection that was too wide and too intense as compared to the observations. In particular the width of the storm core (reflectivity above 20 dBZ) in deep convection was a factor of two to three times greater than the observations, depending on the configuration of microphysics used. Hanley *et al.* (2015) found that in the UKV, in shower cases too few small cells and too many larger, more intense cells were produced. In examining the grid length effect on convection, Hanley *et al.* (2015) found that if the grid length was reduced the convection forecast did not necessarily improve. Instead higher resolution simulations produced too many small intense cells in cases of larger, deeper convection.

2.3.2 The modified Wilson and Ballard microphysics scheme

The microphysics scheme of the MetUM is based on the work of Wilson and Ballard (1999). The original Wilson and Ballard (1999) scheme used three prognostic mixing ratios to characterise water in the atmosphere: vapour, liquid droplets, and ice. Rain was diagnosed each timestep and was all precipitated out of the model each timestep. Interactions between these species were based on physical processes, either parameterised using empirical fits to observations, or theoretically derived.

The current microphysics scheme has added to this rain as a prognostic variable, and the option of the splitting of ice into crystals and aggregates. Additionally graupel has also been included as a prognostic variable. In total therefore, the MetUM can be run with six prognostic variables that characterise how water behaves in the atmosphere.

The microphysics scheme is a single-moment bulk scheme. The particle size distribution for a particle of diameter D per unit volume is assumed to be a gamma

distribution:

$$n\left(D\right) = n_0 D^{\alpha} e^{-\lambda D}, \tag{2.1}$$

where α is the constant shape parameter which varies with hydrometeor species and n_0 (units of $\mathrm{m}^{-(\alpha+4)}$) is the intercept parameter and is a function of the slope parameter λ (units m^{-1})

$$n_0 = n_a \lambda^{n_b}, \tag{2.2}$$

where n_a (units $\mathrm{m}^{-(\alpha+4+\mathrm{n_b})}$) and n_b are constants that vary with the hydrometeor species.

Equation 2.1 describes the number of particles at a certain diameter, the intercept parameter (n_0) influences the total concentration of the particles, the shape parameter (α) influences the particle diameter at which the peak of the distribution occurs together with the magnitude of the peak, and the slope parameter (λ) influences how broad the distribution is.

These three parameters vary depending on the hydrometeor species. For ice crystals, aggregates and rain α is 0. For ice crystals and aggregates the parameter n_b is also 0, while n_a is a function of temperature, meaning that n_0 only depends on temperature and not on λ.

The interactions between the species have also been expanded to encompass the additions to the hydrometeors. The possible transfer mechanisms between hydrometeors are shown in Table 2.1.

These processes occur in the model in the same order that they are listed in Table 2.1; the processes are calculated within a grid column and start at the top of the column, working downwards.

The model experiments were run with the combined aggregate and ice crystal hydrometeor species, as this is the operational configuration of the MetUM.

The microphysics scheme also includes calculations for the calculation of radar

Process	Source	Sink	Charge transferred
Homogeneous nucleation of ice	q_{cl} and q_R	q_{cfc}	–
Heterogeneous nucleation of ice	q_{cl} and q	q_{cfc}	–
Deposition onto cloud ice	q_{cl} and q	q_{cfc} and q_{cfa}	–
Autoconversion of crystals to aggregates	q_{cfc}	q_{cfa}	–
Collection of crystals by aggregates	q_{cfc}	q_{cfa}	–
Riming of cloud ice	q_{cl}	q_{cfc} and q_{cfa}	–
Autoconversion of snow to graupel	q_{cfa}	q_g	✓
Riming of graupel	q_{cl}	q_g	–
Collection of rain by cloud ice	q_R and q_{cfc} and q_{cfa}	q_g	✓
Evaporation of cloud ice	q_{cfc} and q_{cfa}	q	✓
Melting of cloud ice	q_{cfc} and q_{cfa}	q	✓
Melting of graupel	q_g	q_R	✓
Evaporation of rain	q_R	q	✓
Accretion of droplets on raindrops	q_{cl}	q_R	–
Autoconvertion of cloud water to rain	q_{cl}	q_R	–

Table 2.1: The hydrometeor mass transfer processes that occur in the MetUM microphysics, processes are shown in the order they occur in the model. q is the vapour mixing ration, q_{cl} is the cloud liquid (droplets) mixing ratio, q_{cfc} is the ice crystal mixing ratio, q_{cfa} is the aggregate mixing ratio, q_R is the rain mixing ratio, and q_g is the graupel mixing ratio. When crystal and aggregates are not separated, processes with a source of sink term of q_{cfc} or q_{cfa} will occur under the generic cloud ice term. The final column shows whether a process allows for the transfer of charge in the electrification scheme developed in Section 3.3.1

reflectivity. This is done in the same manner as Stein *et al.* (2014). The method assumes that there is no attenuation, the bright band has no effect, and that all particles are Rayleigh Scattering. Linear radar reflectivity Z_{lin} is calculated as:

$$Z_{lin} = \hat{Q} \int_0^{\inf} |M(D)|^2 n(D) \, dD, \tag{2.3}$$

where $M(D)$ is the mass of a particle of diameter D, $n(D)$ is given by equation 2.1, and

$$\hat{Q} = 10^{18} \frac{|K|^2}{0.93} \left(\frac{6}{\pi \rho} \right)^2. \tag{2.4}$$

From this the radar reflectivity can also be calculated:

$$Z = 10 \log_{10} (Z_{lin}). \tag{2.5}$$

A minimum reflectivity of $-40\,\mathrm{dBZ}$ is applied across the domain as the log of $0\,\mathrm{mm^6 m^{-3}}$ cannot be calculated.

2.3.3 The thunderstorm electrification scheme

The current operational thunderstorm electrification and lightning scheme is based on the work of McCaul *et al.* (2009). The routine takes place immediately after the microphysics routines. The method initially restricts the location of the calculation to storm points, where the grid column graupel water path is greater than $200\,\mathrm{g m^{-2}}$. The scheme calculates a flash rate based on the mixed-phase graupel flux and the total ice water path. The total flash rate is calculated as:

$$F_r = 0.95 r_1 + 0.05 r_2, \tag{2.6}$$

where r_1 is the product of the graupel mass and the updraft at the $-15\,^\circ\mathrm{C}$ level,

$$r_1 = k_1 w q_g [-15\,^\circ\mathrm{C}] \tag{2.7}$$

and r_2 is the total ice water path,

$$r_2 = k_2 \left(GWP + TIWP \right). \tag{2.8}$$

$TIWP$ includes both crystals and aggregates if in use, or cloud ice if not.

The constants k_1 and k_2 are specified as 0.042 and 0.2 respectively in McCaul *et al.* (2009) and default to these values within the MetUM, though they are available as input and so can be changed.

Once the flash rate is calculated and integrated over a timestep any whole numbers of flashes are output as flashes, any remaining fractions are advected as "flash potential", thereby allowing for the build up of single flashes in thunderstorms with flash rates lower than one flash per timestep. This advected flash potential is added to the flash potential calculated at the current timestep before flashes are determined.

The method used in this work is modified slightly from the method used operationally. In the McCaul *et al.* (2009) study (hereafter MC09) the model output data are fit to observations using a 2 km grid length. This is unchanged in the operational MetUM. This appears to be an error in the code and so to correct it, the parameterisation output used here is re-scaled to the grid length used in the model experiments.

2.3.4 Model experiments

The model runs in Chapters 4 and 5 were done using the nested suite within the MetUM, in this a high resolution domain is nested within the global domain. The model runs were initiated at least 12 hours before the analysis period allowing for the development of convection. The nested domain used a resolution of 1.5 km to match the interior of the domain of the UKV model. The microphysics scheme was run using the single ice species configuration to mimic the operational model.

Chapter 3

Details and results of the explicit electrification scheme

3.1 Introduction and Motivation

Explicitly forecasting lightning flash rates is a relatively new problem in numerical weather prediction. As lightning is a phenomenon most often observed in convective storms, to forecast lightning well requires accurately forecast convection. As NWP models move increasingly to convection permitting resolutions, forecasts of lightning are becoming more common and more viable. However, the verification of lightning forecasts remains difficult. If the forecast of convection that a lightning parameterisation depends on is inaccurate the lightning forecast will also be inaccurate. Therefore, to effectively evaluate a lightning forecast parameterisation it should be examined independently of the convective forecast. One option for doing this is to compare simple, operationally viable parameterisations to a more complex and physically based, explicit electrification model. Because of the complexity of atmospheric electricity, especially the formation of the lightning channel and the need for computationally expensive algorithms (the electric field solver uses a similar algorithm to the most computationally expensive part of NWP models) in an electrification model, an electrification model cannot feasibly be run operationally. To do so would require making other parts of the forecast worse and lightning forecasting is not considered as important as correctly forecasting precipitation or other variables. The usefulness in an explicit electrification model is in assuming (or verifying) that it is more representative of real physical lightning and charge processes given the model's representation of convection. This allows us to use it to evaluate

simpler parameterisations without having the verification penalty from incorrectly forecast convection.

3.2 Literature Review

3.2.1 Non-Inductive Charging Parameterisations

Based on the studies detailed in Section 1.6.1 a number of parameterisations of the charge separated in collisions between graupel and ice aggregates have been developed. These parameterisations are by necessity generally complicated, because the changes in charge magnitude and sign are non-linear and piecewise with respect to both temperature and LWC.

One of the most important studies is Mansell *et al.* (2005), in this a number of parameterisations based on different laboratory studies, are developed and evaluated. The first three schemes are based on Takahashi (1978), Ziegler *et al.* (1991) and Saunders *et al.* (1991). The next two use Rime Accretion Rate (RAR) rather than LWC or Effective Water (EW) and are based on the work of Saunders and Peck (1998) and Brooks *et al.* (1997). The results of similar model experiments (i.e. constant inductive charging and constant ice crystal concentration which were also changed by Mansell *et al.* (2005)) show that the RAR schemes initially produced reversed-polarity thunderstorms, then changing to a standard tripole as the storm developed. The Ziegler scheme produced many more lightning flashes than the other schemes. Mansell *et al.* (2005) concluded that the RAR-based schemes were much more likely to produce inverted-polarity charge structures and are more sensitive to the microphysical conditions.

The inductive charging method and ion capture are also included within the study of Mansell *et al.* (2005), but were found to have a minor role in thunderstorm electrification compared to NIC.

3.2.2 Lightning Discharge Schemes

The final aspect of a lightning parameterisation is to discharge lightning strikes. This process is not only the main objective of the scheme, but is also necessary to remove charge from the model, where otherwise charge could accumulate indefinitely.

There is a wide range of models of individual lightning strikes. At one end are very computationally expensive methods that require frequent updates to the electric field and explicitly model branching (e.g. Mansell *et al.*, 2002; Maslowski and Rakov, 2006; Iudin *et al.*, 2017; Mansell *et al.*, 2010). At the other end are bulk schemes that discharge lightning from thresholds of charge or electric field (e.g. Fierro *et al.*, 2013; Lynn *et al.*, 2012). These simpler methods provide much less information about the lightning strike. In particular, the bulk methods cannot differentiate between positive and negative lightning or between intra-cloud, inter-cloud or cloud-to-ground lightning.

Rawlins (1982) first modelled a cumulonimbus with a charging scheme added. If the electric field reached a threshold of 500 $\mathrm{kVm^{-1}}$, the charge in the entire domain was reduced by 70% (an arbitrary choice). The charge was reduced by this percentage in each hydrometeor species, meaning that more charge was neutralised than the reduction in net charge suggested. That is if 70% of charge is removed in each hydrometeor category then the total charge is reduced by 70% rather than just the net charge being reduced by 70%.

Helsdon *et al.* (1992) introduced an intracloud lightning parameterisation to their two-dimensional cloud model (Helsdon and Farley, 1987). This parameterisation calculated the lightning channel from the electric field, using a flat threshold of $400\,\mathrm{kVm^{-1}}$. This parameterisation has paved the way for much of the succeeding work. The lightning channel was propagated bidirectionally, parallel and anti-parallel to the ambient electric field. Helsdon *et al.* (1992) do acknowledge that the use of the ambient electric field rather than the local electric field at the leader tip is a limitation of the study. Including the leader tip electric field could potentially aid the propagation of the lightning channel through lower electric field areas leading to

a higher proportion of CG lightning. Helsdon *et al.* (1992) also introduced a novel way of neutralising charge. Based on the work of Kasemir (1960) they assumed that the overall channel charge should remain neutral. In order to facilitate the neutrality on a grid with a lightning channel defined by the propagation criteria, Helsdon *et al.* (1992) included four extra grid points at the ends of the lightning channel where the positive and negative charge may be balanced. Either positive or negatively charged ions were added to balance the charges. These ions could be collected by hydrometeors in future timesteps.

MacGorman *et al.* (2001) made several notable improvements to this scheme. They introduce a random selection of the initiation point for lightning strikes, from points above a threshold, to account for sub-grid scale variations in the electric field. They also vary the initiation threshold with height. More significantly they allow the lightning channel to propagate through areas of low electric field but high charge density. This was done to better represent the lightning structure observed by Macgorman *et al.* (1981) where layers of acoustic (thunder) sources are used to infer charge regions and to represent that the local electric field from a lightning channel can cause the flash to have a large horizontal extent throughout these charge regions.

Mansell *et al.* (2002) produced a more extensive branching lightning parameterisation, based on a stochastic dielectric breakdown model (Wiesmann and Zeller, 1986). Their method calculates the electric field contribution from the channel leader tip and selects new channel points from the net electric field. The electric potential for the entire domain must be recalculated every time a point is added to the channel to account for the effect of the channel on the potential. Furthermore, Mansell *et al.* (2002) recalculate the charge distribution on the channel every fifth added point to check for (and impose if necessary) charge neutrality along the channel. These calculations are computationally expensive, particularly in parallelised models where the communications between processors needed to calculate the potential are a bottleneck.

Barthe *et al.* (2012) used a scheme similar to that of MacGorman *et al.* (2001),

but included some of the branching aspects from Mansell *et al.* (2002). The scheme uses the initial electric field to initiate a lightning strike, then propagates bidirectional leaders until the electric field falls below a propagation threshold, similarly to previous schemes. However, because the scheme of Barthe *et al.* (2012) is specifically intended to be used in a parallel structure the lightning strike is kept to a single vertical column. This prevents the possibility of the channel travelling into a neighbouring processor. It does sacrifice some of the structure of a lightning strike captured by MacGorman *et al.* (2001). To allow for horizontal extent, after the strike channel is calculated branches are simulated from the channel.

A recent model of lightning development was created by Iudin *et al.* (2017). As with previous lightning channel models, this is a cloud scale model (i.e. a 12x12x12 km domain) but with a finer resolution than many others of 250 m. In this study the charge centres are prescribed rather than being linked to microphysical processes. The charge structure prescribed is a tripole with an additional negative screening layer at the top of the thunderstorm.

The method of Iudin *et al.* (2017) improves on other previous methods by predicting the conductivity, internal electric field and current of the lightning channel. The inclusion of these parameters allows for a physical representation of the movement of charge within a lightning channel and therefore allows for a changing electric field at the leader tip. Because of this propagation of charge throughout the channel, this method models lightning strikes reaching the ground.

3.3 Method and data

3.3.1 Microphysical Charging Parameterisation

The charging scheme has been implemented within the Met Office's Unified Model (MetUM) as described in Section 2.3. It is only allowed to run if the model is at convection-permitting resolution and graupel is included as a prognostic variable. A list of all the diagnostic and prognostic variables included within the MetUM

from the development of this scheme is given in Appendix A.

3.3.1.1 Charge generation

The charge generated within the model is found using a parameterisation of the Non-Inductive Charging (NIC) method. The magnitude and sign of the charge to each particle depends on the size of the two particles, and the temperature and liquid water content of the background atmosphere. The inductive charging method, ion capture and charge leakage all have a role to play in thunderstorm charge generation and dissipation, however their roles are secondary to that of NIC (e.g Mansell *et al.*, 2005) and so, for the sake of simplicity, are not included here.

Because the NIC method relies on collisions between graupel and cloud ice in a similar way to many of the other microphysical processes, the formulation of the charge generation routines is similar to the other particle collision processes. The equation for the rate of charge generation is given by:

$$\frac{dQ}{dt} = \int_0^\infty \int_0^\infty E_{ig} \frac{\pi}{4\rho} \left(D_i + D_g\right)^2 \left|V_i\left(D_i\right) - V_g\left(D_g\right)\right| \delta q \, n_i\left(D_i\right) n_g\left(D_g\right) dD_i dD_g, \quad (3.1)$$

where Q is the charge on graupel (the negative of charge on ice aggregates) per kg of dry air, E_{ig} is the collision-separation efficiency for graupel and ice aggregates, ρ is the density of dry air, D is the diameter of diameter of a particle, V is the fall speed of a particle, n is the number density of a particle, the subscripts i and g refer to cloud ice and graupel respectively and δq is the charge separated per graupel-aggregate collision (the convention used here is that δq represents the charge transferred to a graupel particle in a graupel-aggregate collision, the charge on the aggregate will be equal and opposite).

This equation describes how the rate of charge generation is dependant on the charge transferred per collision, the collision-separation efficiency, and on the rate of collisions between ice particles and graupel, through the collisional area of the particles ($\frac{\pi}{4}\left(D_i + D_g\right)^2$), the differential fall speed of the particles ($\left|V_i\left(D_i\right) - V_g\left(D_g\right)\right|$)

and the number of each particle ($n_i(D_i)n_g(D_g)$).

The collision-separation efficiency is currently being treated as a tunable parameter. This is due to the difficulty in accurately and simply including the parameter within the scheme. Collision-separation efficiency is composed of the product of two terms: the collision efficiency (this is the likelihood that two particles will collide given that one is within the collision area of the other) and the separation efficiency (this is the likelihood that two particles will separate after a collision). A collision-separation efficiency term should itself include a number of variables such as temperature and LWC as a measure of the "stickiness" of the particles as well as collision angle, shape factor, and velocity (e.g. two slow moving dendrites are more likely to coalesce than two graupel striking a glancing blow).

There are a number of methods to parameterise the amount of charge that is transferred in a graupel and cloud ice collision (δq). Some of these methods are used and evaluated by Mansell *et al.* (2005). From the results of this study and how applicable each scheme is to the microphysics of the UM, a decision was made to use the method based on Saunders and Peck (1998), which relies on a number of empirical relationships built through the work of Saunders and Peck (1998); Saunders *et al.* (1991); Jayaratne and Saunders (1985); Jayaratne *et al.* (1983). This results in an empirical relationship of charge, dependant on the size of the ice particles, the speed of the collision between cloud ice and graupel and the rate at which supercooled water is being collected by the graupel particle:

$$\delta q = B D_i^a \left(V_g - V_i\right)^b q_{\pm}\left(RAR\right), \tag{3.2}$$

where B, a and b are constants shown in Table 3.1. The term $q_{\pm}(RAR)$ is a function dependent on the Rime Accretion Rate (RAR). Practically this equation means that within the model, the charge transferred between colliding graupel and cloud ice is dependant on the size of the cloud ice particle, the speed of the collision and the rate at which the particles are growing at. The rate at which the particles are growing at is included via the RAR, which is the liquid water content multiplied by the collision-collection efficiency and the mass-mean fall speed of the graupel, i.e.:

$$RAR = LWC\ E_{collect}\ V_g. \tag{3.3}$$

If $RAR > RAR_{crit}$

$$q_+(RAR) = 6.74(RAR - RAR_{crit}), \tag{3.4}$$

if $0.1\,\mathrm{g\,m^{-2}\,s^{-1}} < RAR < RAR_{crit}$

$$q_-(RAR) = 3.9\,(RAR_{crit} - 0.1)\left(4\left[\frac{RAR - (RAR_{crit} + 0.1)\,/2}{RAR_{crit} - 0.1}\right]^2 - 1\right), \tag{3.5}$$

if $0.1\,\mathrm{g\,m^{-2}\,s^{-1}} > RAR$

$$q_\pm\,(RAR) = 0 \tag{3.6}$$

where:

$$RAR_{crit} = \begin{cases} s(T) \ : \ T > -23.7\,^\circ\mathrm{C} \\ k(T) \ : \ -23.7 \geq T > -40.0\,^\circ\mathrm{C} \\ 0 \ : \ T \leq -40.0\,^\circ\mathrm{C} \end{cases} \tag{3.7}$$

where

$$\begin{aligned} s(T) = 1.0 &+ 7.9262 \times 10^{-2}\,T + 4.4847 \times 10^{-2}\,T^2 + 7.4754 \times 10^{-3}\,T^3 \\ &+ 5.4686 \times 10^{-4}\,T^4 + 1.6737 \times 10^{-5}\,T^5 + 1.7613 \times 10^{-7}\,T^6 \end{aligned} \tag{3.8}$$

and

$$k(T) = 3.4\left[1.0 - \left(\frac{|T + 23.7|}{-23.7 + 40.0}\right)^3\right]. \tag{3.9}$$

The temperature variable used in equations 3.7 - 3.9 is in Celsius.

Practically these equations govern the sign and magnitude of the charge transferred to the graupel and how it depends on the temperature and RAR. The polynomial functions in equations 3.8 and 3.9 create the sign change shown in the curve

Charge Sign	Crystal Size, μm	B	a	b
+	<155	4.9×10^{13}	3.76	2.5
+	155-452	4.0×10^{6}	1.9	2.5
+	>452	52.8	0.44	2.5
-	<253	5.24×10^{8}	2.54	2.8
-	>253	24	0.5	2.8

Table 3.1: Values of coefficients for equation 3.2

in Figure 3.1. At temperatures lower than $-40\,°C$ it is too cold for liquid water to exist and so charging cannot occur.

Following the method of Mansell *et al.* (2005), the charge transferred by collision term is limited to a maximum magnitude of 50 fC. This is to prevent unrealistically large charge generation and unrealistically large lightning flash rates. The model is sensitive to this term, however the term was consistently limited to 50 fC throughout all the runs as suggested by Mansell *et al.* (2005) and as suggested by the measurements of maximum charge on hydrometeors in section 1.4.1.

The charge calculated in equation 3.1 is added to the grid-box total charge on graupel (from the previous timestep) and subtracted from the grid-box total charge on aggregates (from the previous timestep) within each grid-box.

Both aggregates and graupel can be charged positively or negatively within a thunderstorm; this is reflected in the charge parameterisation. As can be seen in equations 3.4, 3.5, 3.8 and 3.9 the sign of the charge is a function of RAR and temperature. The critical RAR and sign of charge transferred to graupel is shown in Figure 3.1, indicating that graupel can charge positively or negatively throughout the depth of the cloud. Positive charging is more likely at warmer temperatures and therefore lower in the cloud, but still require relatively high RARs. This means graupel is more likely to charge positively at the earlier stages of thunderstorm development while there are higher water contents.

3.3.1.2 Charge separation

In order to achieve a net charge within a grid-box and therefore a charge distribution to calculate the electric field, the charge on the graupel must be separated from the

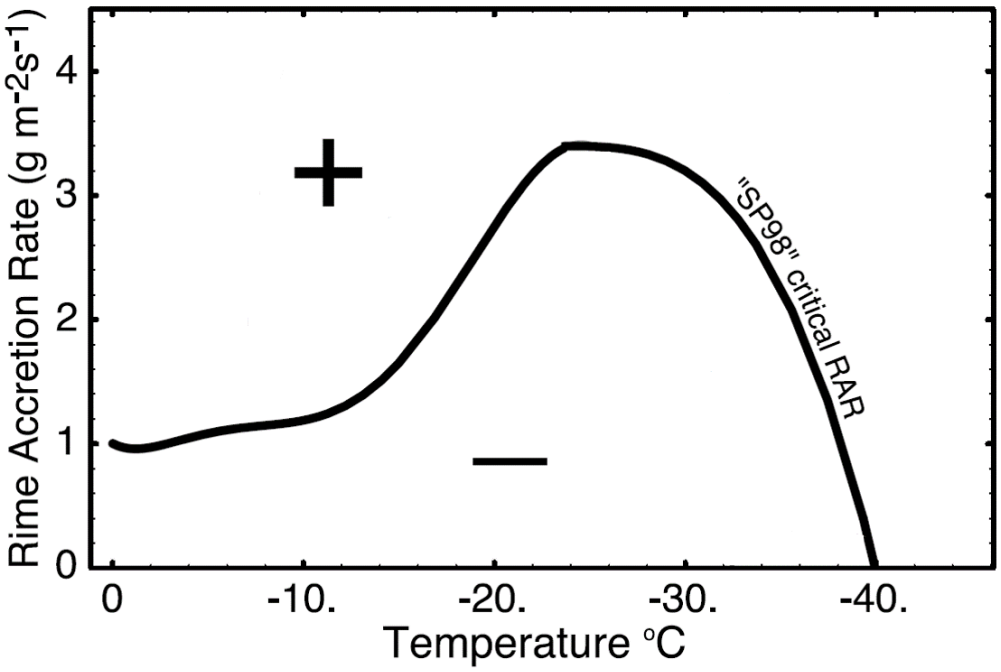

Figure 3.1: Plot of the critical RAR curve used in the parameterisation of charge transfer based on Saunders and Peck (1998). Graupel charges positively above the curve and negatively below the curve. Adapted from Mansell *et al.* (2005)

equal and opposite charge on the cloud ice. The primary method of this is through gravitational sorting. The fall speed of graupel is greater than that of cloud ice for similar sized particles. The charge is moved together with the hydrometeor mass in the existing subroutine in the UM that handles gravitational settling of hydrometeor species. Charge is moved between grid-boxes within a column in an equal proportion to the fraction of hydrometeor mass mixing ratio that is transported. Charge that falls to the surface is simply removed from the scheme.

3.3.1.3 Charge transfer between hydrometeors

Physically, when attached to a hydrometeor, charge should remain with that particular hydrometeor no matter the state of the hydrometeor. As such, charge is also transferred between hydrometeor species. Similarly to the charge separation method charge is added and removed to a hydrometeor category proportionally to the mass mixing ratio transferred. The mass mixing ratio transferred is calculated in existing subroutines in the UM large scale precipitation scheme. Charge is trans-

ferred between two hydrometeor species that can contain charge (these are graupel, cloud ice and rain), for example the collection of ice by raindrops to form graupel will transfer charge from both the ice and raindrop species to graupel. If only one charged hydrometeor species is included in the process then charge is removed where appropriate, but is never added (a full list of the processes that can transfer charge is given in Table 2.1). For example in the evaporation of rain charge is removed proportionally to the ratio: mass of rain evaporated to rain mass. However in the growth of aggregates from deposition no charge change occurs, as there is currently no representation of space charge capture or charge stored on cloud water vapour.

3.3.1.4 Advection of charge

The charges are stored as prognostic variables, this means that they are advected each timestep. The charges are advected with the moist variables (i.e. the hydrometeors themselves). Within each timestep, the advection takes place after all the other processes, meaning that the charge that is advected has already been transformed between hydrometeor species and had any excess charge removed by lightning strikes.

3.3.2 Electric Field Solver

The electric field is solved from a distribution of charges found from the microphysical charging step. First the Poisson equation for electrostatics is solved for the electric potential (Φ).

$$\nabla^2 \Phi = -\frac{\rho_c}{\epsilon}, \tag{3.10}$$

where ρ_c is the charge density and ϵ is the electrical permittivity of air, taken to be 8.8592×10^{-12} F/m The electric field is then found from the gradient of the electric potential:

$$\boldsymbol{E} = -\nabla \Phi \tag{3.11}$$

The electric potential is solved using the BiConjugate Gradient Stabilized (BiCGStab) method. This method solves a system of linear equations $\boldsymbol{Ax} = \boldsymbol{b}$, where $\boldsymbol{A}$ is a sparse matrix signifying the grid points surrounding the grid point at which the electric potential is being calculated. This is effectively a discretisation of the laplacian term in equation 3.10. The terms $\boldsymbol{x}$ and $\boldsymbol{b}$ are vectors, with $\boldsymbol{b}$ being the charge density points, i.e. the right hand side in equation 3.10. These methods never solve a full matrix-matrix operation, but instead use matrix-vector operations, where $\boldsymbol{Ax}$ can be solved using $\boldsymbol{A}$ as a function. Such methods are very applicable to the system being solved here, where (in 3d) the matrix is only non-zero on seven diagonals (i.e. on a finite element grid the electric potential depends only on itself and the two adjacent points in the x,y and z directions).

The BiCGStab method is based on the BiConjugate Gradient method (BiCG), itself based on the Conjugate Gradient (CG) method. This family of methods find a residual from the original equation and then each subsequent iteration. They then calculate search directions from the residual and some constants to update the iterate.

The BiCGStab method was chosen here as it was already implemented within the UM to solve the Helmholtz equation and could therefore be relatively simply converted to solve equation 3.10. The method has advantages over simpler methods, it can solve non-symmetrical linear systems and is numerically stable. This method is slightly more computationally expensive than the CG method. The matrix formed from eq. 3.10 is symmetric positive definite and so could be solved using the CG method (or indeed a number of simpler methods). However, having the time saving of having the BiCGStab scheme mostly already coded within the model outweighs the potential benefits of computational efficiency. Figure 3.2 shows the pseudo-code for the BiCGStab method, taken from Barrett *et al.* (1994). From this code only the matrix-vector operation step needed to be changed within the UM code.

Although Figure 3.2 suggests that the method uses a preconditioner, because the matrix being solved is relatively simple (i.e. it is sparse, tridiagonal and positive definite) it is not necessary to precondition. Therefore, for the sake of simplicity,

Compute $r^{(0)} = b - Ax^{(0)}$ for some initial guess $x^{(0)}$
Choose $\tilde{r}$ (for example, $\tilde{r} = r^{(0)}$)
for $i = 1, 2, \ldots$
  $\rho_{i-1} = \tilde{r}^T r^{(i-1)}$
  if $\rho_{i-1} = 0$ **method fails**
  if $i = 1$
    $p^{(i)} = r^{(i-1)}$
  else
    $\beta_{i-1} = (\rho_{i-1}/\rho_{i-2})(\alpha_{i-1}/\omega_{i-1})$
    $p^{(i)} = r^{(i-1)} + \beta_{i-1}(p^{(i-1)} - \omega_{i-1}v^{(i-1)})$
  endif
  solve $M\hat{p} = p^{(i)}$
  $v^{(i)} = A\hat{p}$
  $\alpha_i = \rho_{i-1}/\tilde{r}^T v^{(i)}$
  $s = r^{(i-1)} - \alpha_i v^{(i)}$
  check norm of s; if small enough: set $x^{(i)} = x^{(i-1)} + \alpha_i \hat{p}$ and stop
  solve $M\hat{s} = s$
  $t = A\hat{s}$
  $\omega_i = t^T s / t^T t$
  $x^{(i)} = x^{(i-1)} + \alpha_i \hat{p} + \omega_i \hat{s}$
  $r^{(i)} = s - \omega_i t$
  check convergence; continue if necessary
  for continuation it is necessary that $\omega_i \neq 0$
end

Figure 3.2: Pseudo-code for the preconditioned biconjugate gradient stabilized method of solving a system of linear equations $\boldsymbol{Ax} = \boldsymbol{b}$ with a preconditioner $\boldsymbol{M}$. Taken from Barrett *et al.* (1994)

the choice has been made not to precondition the matrix.

3.3.3 Lightning Discharge Method

The lightning discharge method is based on that of Barthe *et al.* (2012), which uses thresholds of electric field to initiate and then propagate lightning strikes. An electric field threshold is the only factor considered here as the other factors impacting lightning initiation (discussed in Section 1.5.1) are too complex to be included.

The first threshold is the initiation threshold, which locates grid-points at which the electric field magnitude is large enough to cause electric breakdown of air and

therefore initiate a lightning strike. The threshold is taken from Marshall *et al.* (1995) and given by:

$$E_{thresh} = 167000 \times 1.208 \exp\left(-\frac{z}{8400}\right) \tag{3.12}$$

where z is the height above sea level in m and E_{thresh} is given in $\mathrm{V\,m^{-1}}$. The threshold is empirically based, using measurements of the maximum electric field within thunderstorms, it decreases exponentially with height as the conductivity of air increases with height through the depth of atmosphere at which thunderstorms occur.

The second threshold is the propagation threshold. This is used to determine whether the lightning channel can propagate through a grid-box. It is fixed at $15\,\mathrm{kV\,m^{-1}}$ (Barthe *et al.*, 2012). Following the example of MacGorman *et al.* (2001) lightning is also allowed to propagate through regions of charge magnitude greater than 0.5 nC. Besides being more physically accurate, this also helped to prevent a grid-box with high charge but low electric field from causing an unreasonably large number of lightning strikes by initiating lightning strikes in the next grid-box.

The initiation point is chosen as the point with the greatest magnitude electric field relative to the initiation threshold (i.e. where $|E|/E_{thresh}$ is largest) within the column (so long as the electric field magnitude is greater than the initiation threshold). From this point the lightning channel is propagated in the z direction. For simplicity, each lightning strike is only allowed to propagate in the z direction within a column, to prevent the possibility of a lightning strike propagating into a neighbouring processor which is non-trivial to handle in the UM. The strike is propagated in both directions vertically, approximating a bi-directional leader (Helsdon *et al.*, 1992). Propagation continues in a direction until the two consecutive grid points do not fulfill the propagation criteria set above, or if the channel reaches the top or bottom of the domain. Once propagation in both directions has been stopped the lightning strike is classified as either a CG or IC strike. It is classified as a CG flash if the lightning channel has reached the surface. Otherwise the strike is classified as an IC flash.

In order to mimic the neutralisation of charge along the lightning channel, charge is removed from all grid-boxes that the lightning channel propagated through. Charge is removed from all hydrometeor categories, the magnitude of charge is 30% of the net charge within the grid-box (Ziegler and MacGorman, 1994; Fierro *et al.*, 2013). The charge is neutralised on hydrometeor species of the same charge as the net charge of the grid-box. If more than one hydrometeor species of the correct sign is present, the magnitude of charge removed from each species is proportional to the magnitude of charge already on the species.

Charge is also removed from grid-boxes horizontally level with the lightning channel within an arbitrary radius of 2 km (i.e. only directly adjacent grid-boxes within the 1.5 km model), this attempts to represent the neutralisation of charge in the branched channel of a lightning stroke. The proportion and method of removing charge from the outlying grid-boxes is exactly the same as for the grid-boxes on the lightning channel.

It is expected, though not enforced, that this should remove approximately equivalent amounts of positive and negative charge in the case of an IC flash, to mimic the transfer of charge from the positive to negative charge regions (or vice versa). It is assumed that charge primarily of one polarity is removed, in the case of a CG flash (Borovsky, 1995).

Once the charge has been removed from the hydrometeor categories, the lightning channel location and amount of neutralised charge are stored for output as diagnostics.

If any lightning strikes have been generated within a timestep, and therefore the charge distribution been modified, the process from the calculation of the electric field is then repeated with the updated charge values as shown in Figure 3.3. If, after the electric field recalculation, the electric field magnitude remains greater than the initiation threshold anywhere in the domain the lightning discharge processes are also repeated, otherwise the scheme stops here. To prevent the possibility of the code being stuck in an infinite loop, if the loop is repeated more than 15 times within a timestep the code is forced to move on.

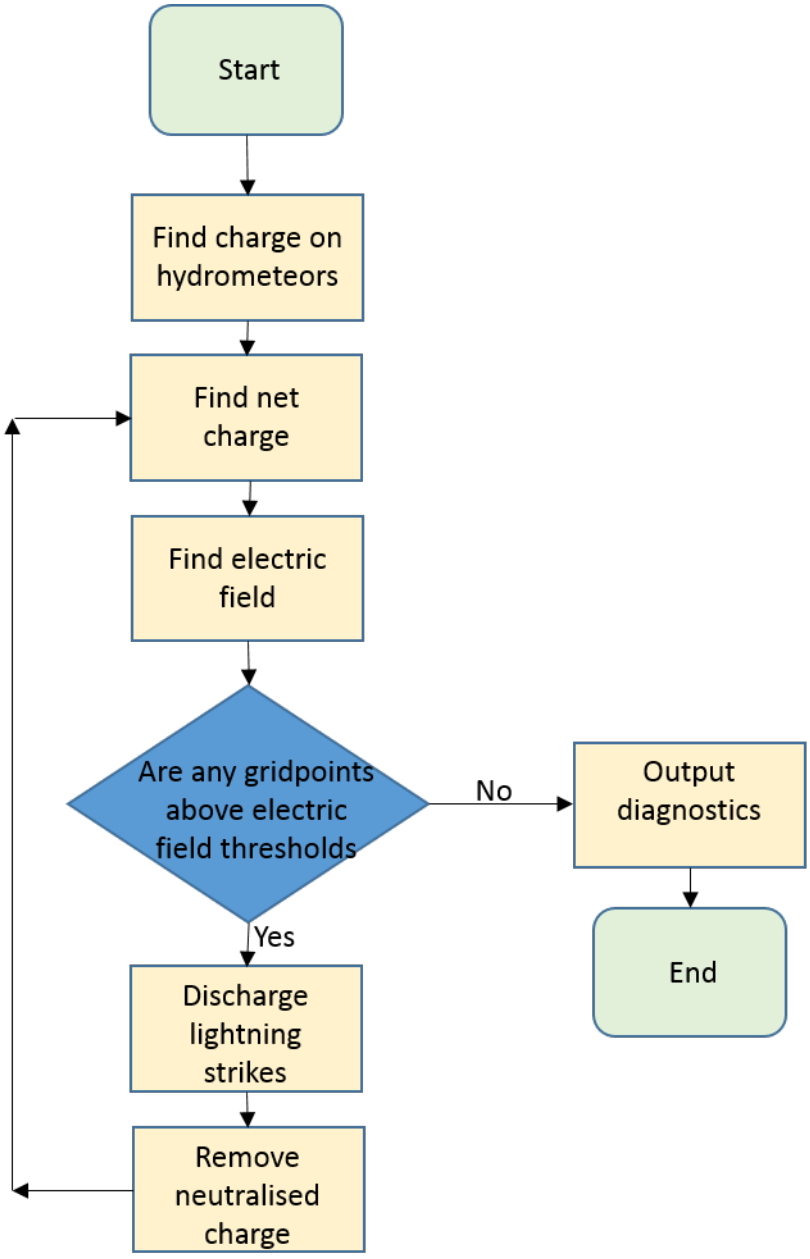

Figure 3.3: Flowchart showing the order of processes within the lightning scheme. The routine is called during the large scale precipitation scheme, before hydrometeor mass transfer is calculated.

3.3.4 Description of case studies

3.3.4.1 2017/08/31 - Scattered convection

The scheme is first tested on a case-study in the UK. This test case was a day of widespread, scattered convection across the south of the UK. A trough crossed

across the south of the country between approximately 0600 and 1800. This lead to strong convection and a number of lightning strikes in the Irish Sea at 0600, the convection moved east with the trough, culminating in more organised convection over East Anglia (see the right hand column of Figure 4.1 and Figure 4.2b). Convection was capped by a small isothermal layer at 450 hPa ($\sim$ 6 km).

The UKV model was run here using the nested grids. The inner domain was a 1.5 km resolution grid of size 622x810 with 70 vertical levels at a variable resolution and centred around 54.18°N, -4.01°E . The boundary conditions were provided by a global driving model with a resolution of 40 km at mid-latitudes. Other than the addition of the electrification scheme on the inner domain, the model was run as if in operational use and was only run with initial conditions.

The model uses a modified Wilson and Ballard (1999) microphysics scheme, this is a bulk scheme with four hydrometeor categories as well as cloud ice and cloud water.

3.3.4.2 2017/05/16 - Supercells

In order to better understand how the scheme works in a more vigorous convective environment, the second case study examined here is a Great Plains supercell case. This was a day with low to mid-level shear and high (approximately 3000-3500 Jkg^{-1}) CAPE. The dryline was set up across the Texas-Oklahoma panhandle, extending into Kansas and Mexico. There was a southerly surface wind, backing to south-westerly in the mid-levels. Convective initiation over Oklahoma and Kansas began around 1800 UTC and intensified to supercell structures by 2200 UTC (see the right hand column of Figure 4.5 and Figure 4.6b). There were 30 tornado reports on this day throughout the Great Plains.

The UM was again run using a nested grid. In this case the model was set up in almost the same configuration as in Section 3.3.4.1. The differences being the grid was centred around 36.98N, 97.98W, and of size 1000x800 points.

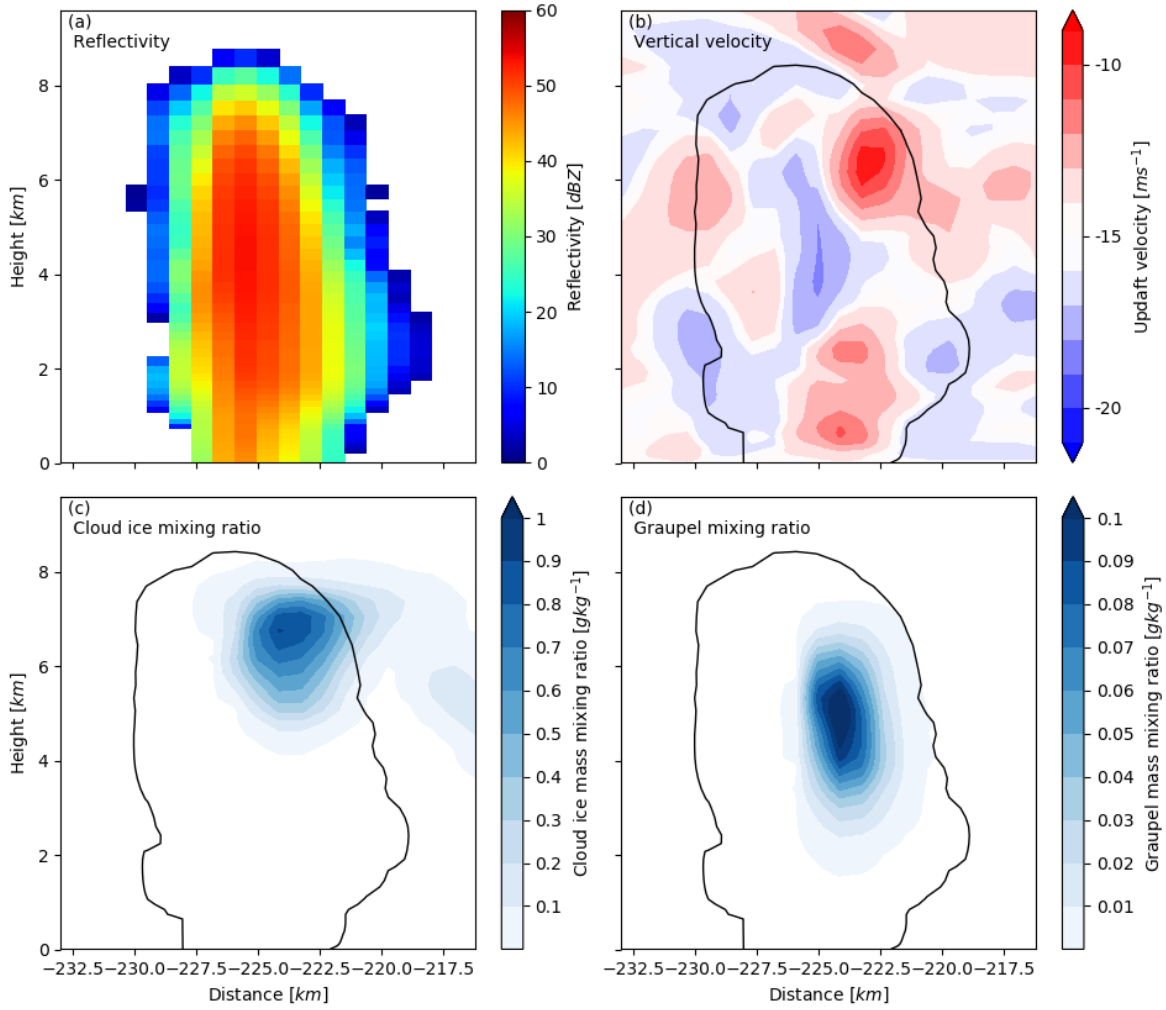

Figure 3.4: A vertical cross-section of a thunderstorm at 03:40. (a) shows the modelled radar reflectivity. (b) shows the updraft velocity. (c) shows the cloud ice mass mixing ratio. (d) shows the graupel mass mixing ratio. In (b), (c) and (d), the outline indicated by the solid black line is the 5 dBZ contour.

3.4 Results

3.4.1 31st August 2017 - Scattered convection

A closer examination of some of the key interactions and variables is shown in Figures 3.4 to 3.6. The reflectivity shown in Figure 3.4a demonstrates that this thunderstorm, though not very vertically developed and lacking an anvil, had a strong storm core with high reflectivity extending up to around 7 km. The updraft velocity in Figure 3.4b shows that the main updraft is on right hand side of the

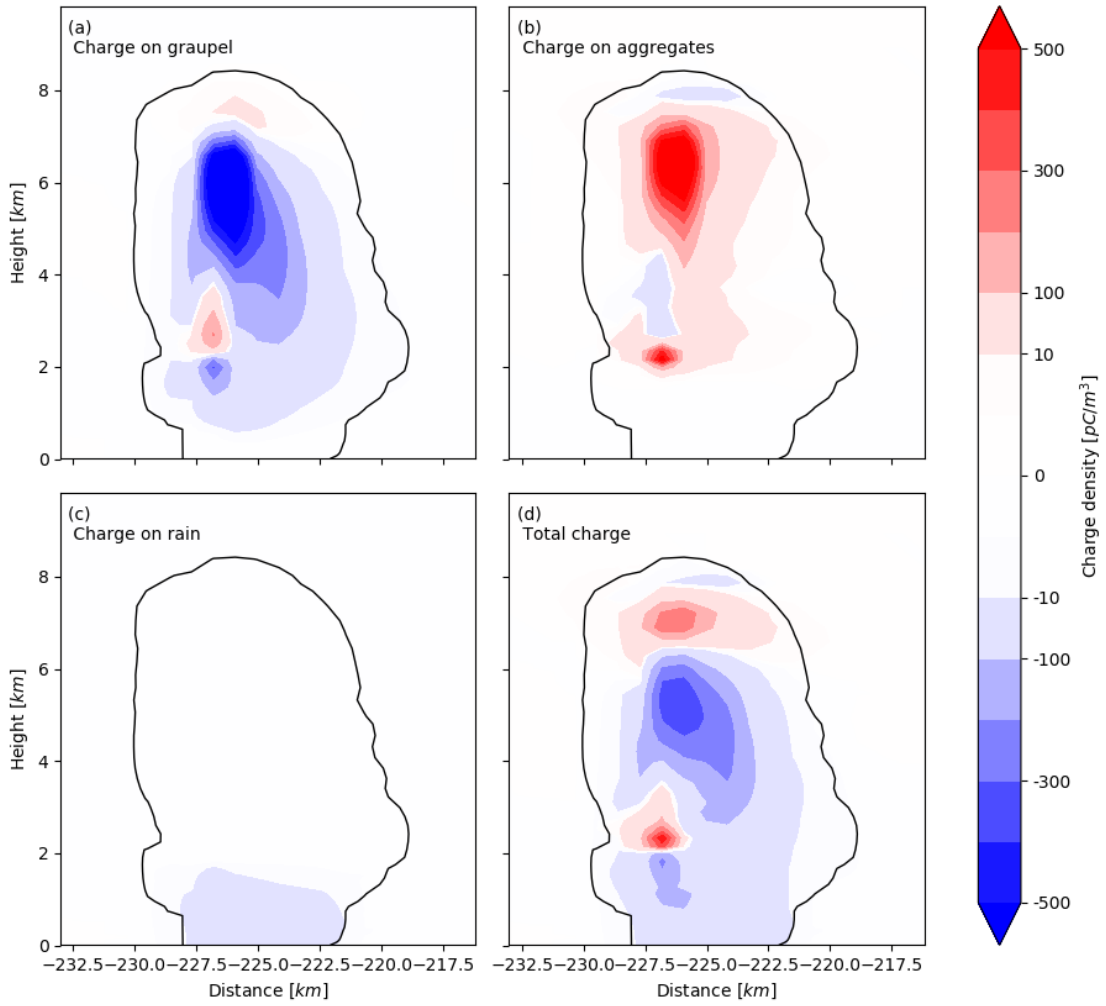

Figure 3.5: A vertical cross-section of a thunderstorm at 03:40 showing the modelled charge. (a) shows the charge density stored on graupel, (b) shows the charge density stores on aggregates, (c) shows the charge density stored on rain (not cloud droplets), and (d) shows the sum of the previous three, i.e. the net charge density. In each plot, the outline indicated by the solid black line is the 5 dBZ reflectivity contour. The charge shown is the charge after charge from lightning flashes has been neutralised.

cross-section and while the updraft does not quite extend through the depth of the storm, there is a strong, positive region of vertical motion at around 6 km altitude. This is in the same region as the region of cloud ice in Figure 3.4c, and slightly above the region of graupel in Figure 3.4d. As the mass mixing ratios and the updraft velocity are taken from the end of the time step (as opposed to the charge values in Figure 3.5, which are taken from part way through the time step) this shows that the updraft is strong enough to loft cloud ice but does not have as great

an impact on graupel.

The charge structure of this particular thunderstorm (fig. 3.5d) is slightly more complex than the traditional tripole. There is a tripole-like structure, with a main negative charge layer, an upper positive charge layer, and a small lower positive charge layer. However, there is the addition of a large (but weak) area of negative charge at the lower east side of the storm.

The region of greatest charge generation is located at around 6 km altitude in Figure 3.6a, this appears to be responsible for the upper positive charge region and the main negative charge region. A second region with a high rate of charge generation at 2.5 km appears to generate the lower dipole in Figure 3.5d. The monotonicity of the charge generation is not typical of other studies (i.e. Fierro *et al.*, 2013; Barthe *et al.*, 2012), however the generation of a relatively well structured dipole here raises the question of whether a smaller and simpler charge generation region is just as realistic.

The negative and positive charges are largely carried exclusively by the graupel (fig. 3.5a) and aggregates (fig. 3.5b) respectively, as suggested by the NIC theory and gravitational separation. There is a large overlap between the two hydrometeor species' charge centres. In this case the charge carried on graupel is larger than that carried on aggregates, creating a larger negative charge centre than upper positive charge centre. Both graupel and aggregates melt at the melting layer to transfer their charge to raindrops, this creates the charge layer shown in Figure 3.5c. This layer is slightly negative, again through the stronger negative charge on graupel.

The maximum charge magnitude in Figure 3.5d is less than half the maximum magnitudes of Fierro *et al.* (2013). This is expected and indeed desirable, because the cloud structure here is much smaller and weaker than in Fierro *et al.* (2013) and therefore the charge magnitude and structure is also expected to be smaller. The electric field shown in 3.6b is the electric field after the lightning discharge had occurred, as such the magnitudes are lower than that required to generate lightning. The highest magnitudes are, as expected, in the regions between positive and negative charge. It should be noted that if sufficiently small spacial distances

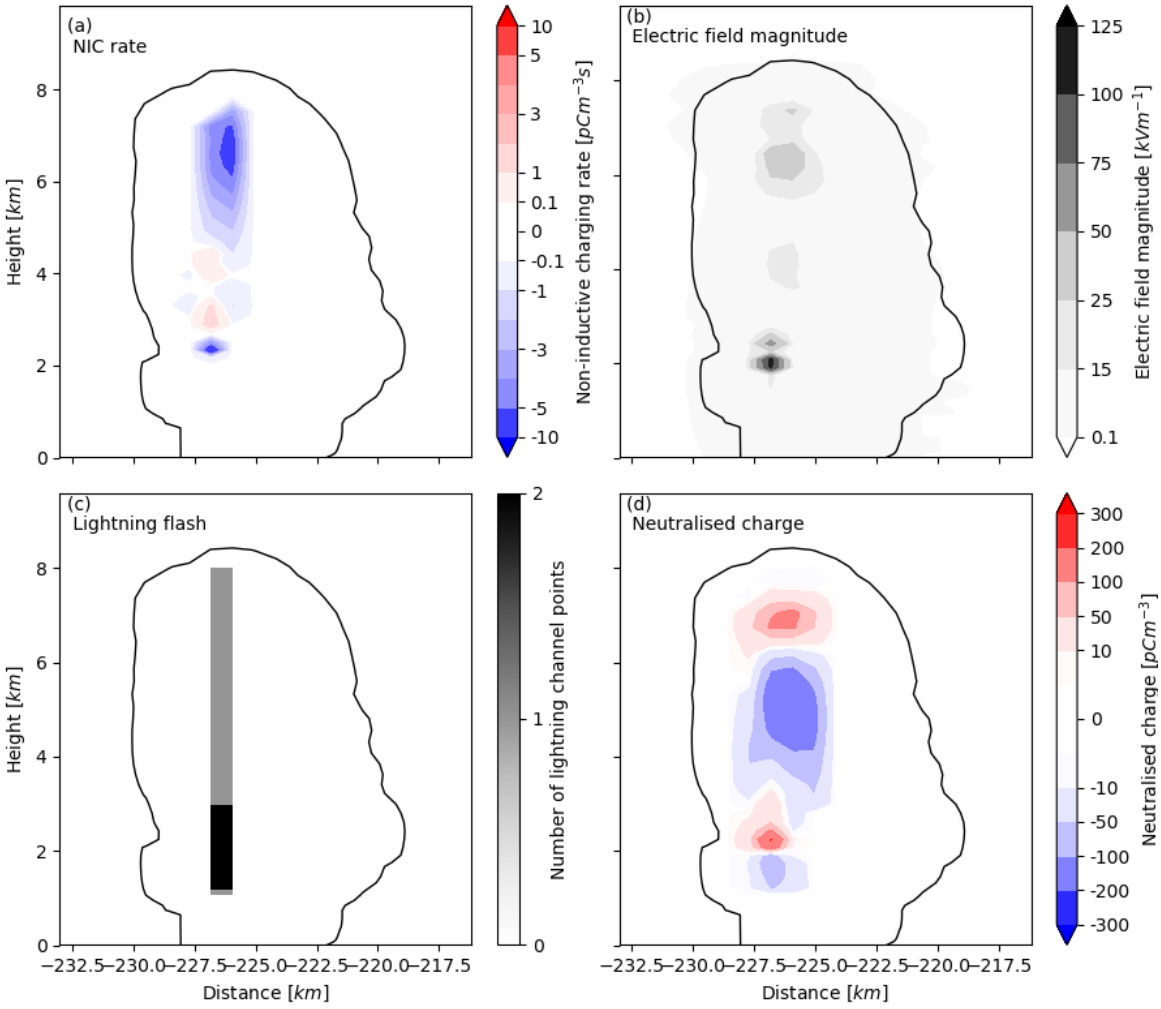

Figure 3.6: A vertical cross-section of a thunderstorm at 03:40 showing the modelled charge. (a) shows the non-inductive charging rate for graupel, (b) shows the electric field magnitude after lightning strikes have been discharged, (c) shows the lightning flash channels, and (d) shows the charge neutralised after the lightning flashes have been discharged. In each plot, the outline indicated by the solid black line is the 5 dBZ contour.

are present between charge centres a strong electric field can still be generated, as demonstrated at −227.5 km and 2000 m.

From Figure 3.6c it can be seen that there were two lightning strikes from this storm in this particular time step. Both of these were intra-cloud flashes, the first of these was a relatively large flash from around 1 km to 8 km above the surface. The second is a much smaller flash extending only between the lower positive and the small low negative charge regions. The charge is neutralised in the entire depth

of the storm because of the larger lightning strike. The neutralised charge fits fairly well to the area of higher electric field because of the inclusion of the neighbouring grid columns.

3.4.2 16th May 2017 - Supercells

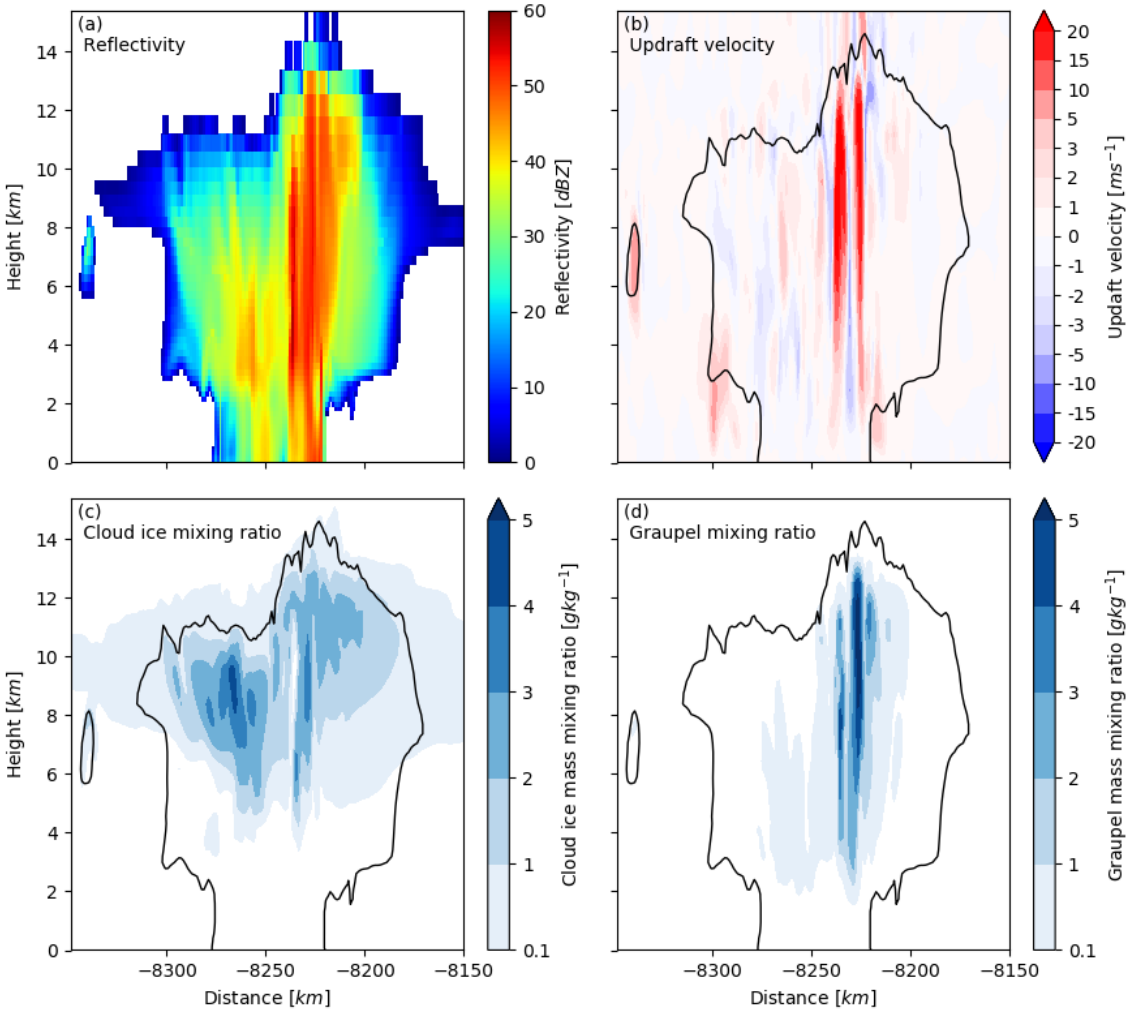

Figure 3.7: A vertical cross-section through a convective line at 22:50. (a) shows the modelled radar reflectivity. (b) shows the updraft velocity. (c) shows the cloud ice mass mixing ratio. (d) shows the graupel mass mixing ratio. In (b), (c) and (d), the outline indicated by the solid black line is the 5 dBZ contour.

This storm is clearly much stronger and larger than the UK example. The storm here (Fig. 3.7a) extends to above 14 km in altitude and the width is an order of magnitude greater than the UK storm (Fig. 3.4a). The magnitude of the reflectivity

in the storm core is, at its maximum, similar between the two cases, however in the US case the volume of the high reflectivity region is much greater. The updraft region in this storm is also very strong, reaching velocities in excess of $20\,\mathrm{m\,s^{-1}}$. The updrafts extend throughout the depth of the storm and their impact can be seen in Figure 3.7d, where the graupel is lofted almost to the top of the storm. Figure 3.7c shows that the cloud ice is suspended at the top of the storm by the widespread ascending air between 6 and 10 km altitude in Figure 3.7b.

The charge structure shown in Figure 3.8 is complex, possibly due to the width of the storm on show. Broadly the structure could be interpreted as an inverted tripole. There is, at around 12 km, a weak negative charge layer caused by negatively charged aggregates being lifted to the top of the storm. Below this, at around 10 km, there is a strong positive charge layer that extends across the width of the 25 dBZ area in Figure 3.7. The western side of the storm is simpler in charge structure, with there only being a large negative charge region extending from the upper positive region to the surface. On the eastern side of the storm however, the structure is much more complex. There are several negative charge regions towards the bottom of the storm, but there is also a large region of positive charge that reaches the surface, creating a horizontal dipole at -8230 km. It is worth noting that this horizontal dipole does not create a particularly large electric field magnitude (fig. 3.9b), especially when compared to the electric field caused by the much smaller vertical dipole at -8250 km and 4 km.

The complex structure of the net charge density is due to a similar structure in the NIC rate, shown in Figure 3.9a. The charging is not strictly ordered (as one may expect) vertically. There does appear to be more negative charging at the 10 km level than at the 4 km level. But positive charging occurs throughout the storm. Notably the charge on the west of the storm in Figure 3.8d has no source from NIC in Figure 3.9a, and must therefore be caused by charging from previous timesteps.

The charge on aggregates appears to accumulate charge towards the top of the storm, both of the upper charge centres are primarily due to the charge on aggregates. Further, the charge in the west of the storm does not extend to the

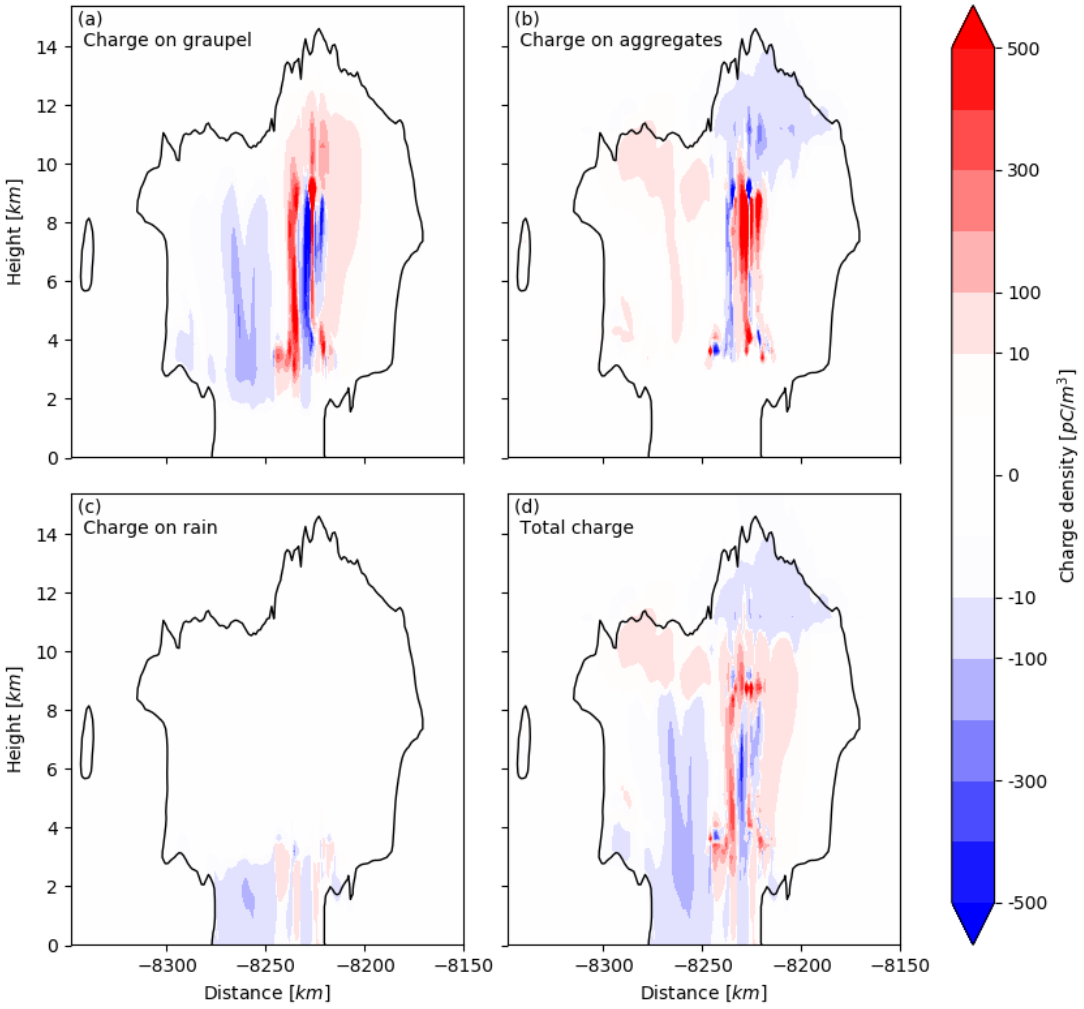

Figure 3.8: A vertical cross-section of a thunderstorm at 22:50 showing the modelled charge. (a) shows the charge density stored on graupel, (b) shows the charge density stores on aggregates, (c) shows the charge density stored on rain (not cloud droplets), and (d) shows the sum of the previous three, i.e. the net charge density. In each plot, the outline indicated by the solid black line is the 5 dBZ contour. The charge shown is the charge after charge from lightning flashes has been neutralised.

melting layer, suggesting that the aggregates are evaporated before reaching the melting layer, thereby removing the charge.

The charge on graupel extends through much more of the storm, in particular the negative region on the west of the storm. This is possibly due to the graupel evaporating less quickly and therefore maintaining its charge, together with the higher fall speed of graupel. The mainly positive charge on the east of the storm is caused by the two strong columns of positive charging.

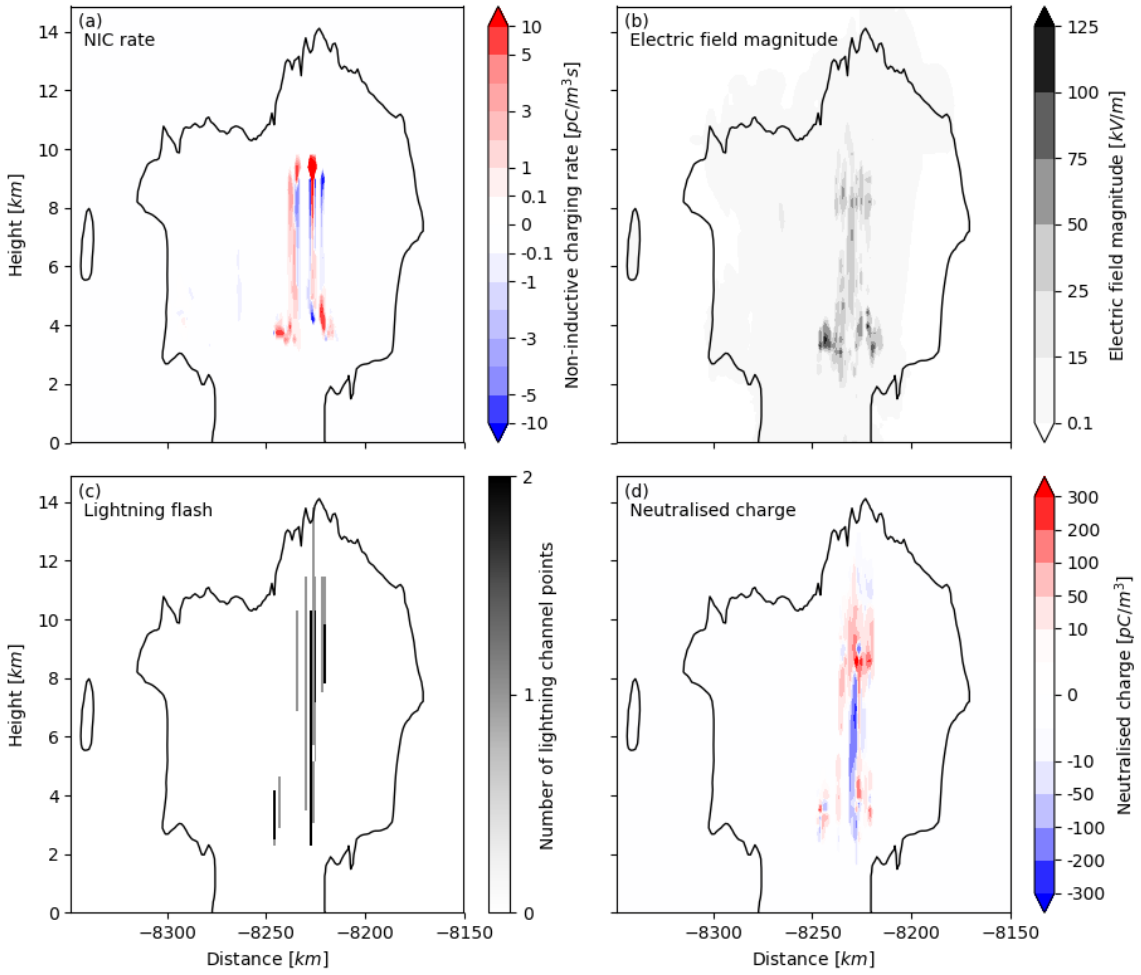

Figure 3.9: A vertical cross-section of a thunderstorm at 22:50 showing the modelled charge. (a) shows the non-inductive charging rate for graupel, (b) shows the electric field magnitude after lightning strikes have been discharged, (c) shows the lightning flash channels, and (d) shows the charge neutralised after the lightning flashes have been discharged. In each plot, the outline indicated by the solid black line is the 5 dBZ contour.

Similarly to the case in Section 3.4.1 the magnitude of charge held on graupel is greater than that on aggregates and therefore the sign of the total charge is often dictated by the sign of the graupel charge. Between 2 and 3 km above the surface both graupel and aggregates melt and transfer all charge to raindrops (shown in fig. 3.8c).

The number of lightning flashes (fig. 3.9c) here is clearly much larger than in Section 3.4.1. There are a number of grid columns where there are more than one lightning flash. Most of the these columns the lightning flashes occur essentially

overlaid (although the first channel is generally longer than the second). However at −8230 km there is a case where two flashes are generated within the same column without overlapping. As in Section 3.4.1 none of the flashes here reach the surface. For this reason, it is suspected that the propagation electric field threshold does not allow the lightning channel to often reach the ground (similarly to Mansell *et al.*, 2002). This is likely due to the fact that the internal charge of the lightning leader tip allows for an increased electric field ahead of the leader, thereby allowing the leader to propagate to the surface. The study of Iudin *et al.* (2017) models the internal current of the channel and allows lightning to reach the surface. Because CG flashes in the electrification scheme do not reach the ground and are then not classified as CG flashes, the categorisation of flashes in the scheme is artificially skewed towards IC flashes. Therefore, to avoid this impacting the results, only total lightning is examined in comparing the lightning output to observations.

3.5 Conclusions

An explicit thunderstorm electrification scheme has been developed, based largely on the work of Fierro *et al.* (2013) and Barthe *et al.* (2012). This electrification scheme has been implemented in the MetUM. The scheme uses graupel - cloud ice collisions to generate charge, based on the NIC theory. The charge that is generated is separated within the model through transformations to other hydrometeor species and through gravitational separation. The resulting charge density distribution can be used to calculate the domain electric field. The magnitude of the electric field can then be used to find grid columns where lightning flashes could be discharged. Two thresholds are used to discharge lightning, an initiation threshold and a propagation threshold. This allows for the creation of a lightning channel. Charge is neutralised along this channel and in the immediately neighbouring grid-points. The routine is repeated as shown in Figure 3.3 to allow for the discharge of multiple lightning flashes within the same timestep.

The charge structure produced by the electrification scheme shown in Figure

3.5d appears to be a realistic charge structure compared to the structure described in Section 1.4.1. The magnitude of the charge centres appears realistic and the scheme appears to produce lightning in the correct regions compared to the electric field.

Chapter 4

Verification and comparison of lightning parameterisations within the UM

4.1 Introduction

In Chapter 3 a new explicit electrification scheme was presented and the output demonstrated using a small single cell thunderstorm. In this chapter, the electrification scheme is compared against observations and against the existing MC09 based parameterisation. Three skill scores used in the study of Wilkinson (2017) are also used here to examine the accuracy of the intensity, coverage and location of the lightning forecast from both methods.

The aims of this comparison are to investigate the accuracy of the new electrification scheme in a situation where the model forecast of convection is reasonably accurate. And to compare the MC09 parameterisation to the new electrification scheme, in order to examine where the MC09 parameterisation could be improved.

4.2 Method and Data

4.2.1 Verification of scheme

The scheme can be verified from the lightning flash output using the same method as Wilkinson (2017). The verification of the scheme uses two different case studies in order to examine how the scheme performs in different scenarios.

This verification method uses several skill scores to measure different aspects of the forecast. The ones that will be used in this analysis are the Quasi-Symmetric

Distance Score (QSDS), to measure the accuracy of the location of lighting flashes; the intensity score, to measure the accuracy of the number of flashes; and the Symmetric Extreme Dependency Score (SEDS) originally from Hogan *et al.* (2009), to measure the accuracy of areal coverage of the flashes.

The QSDS is a measure of the location of the forecast compared to observations. The score is based on the distance D_{dis}. This is the average of the mean distances between forecasts and the nearest lightning observation, and the mean distances between observations and the nearest forecast lightning flash. The QSDS is on a scale from -1 to 1 where -1 represents the furthest possible distance from observations to forecasts, 0 represents a completely hedged forecast (i.e. lightning forecast in every grid-point) and 1 represents a perfect forecasts.

SEDS is a measure of the accuracy of the areal coverage of the forecast (i.e. how widespread lightning flashes are in the forecast compared to the observation). It is given by the equation:

$$SEDS = \frac{\ln\left[(a+b)/n\right] + \left[(a+c)/n\right]}{\ln\left(a/n\right)} - 1 \tag{4.1}$$

where a, b, c and n are correct forecasts, false alarms, misses, and the total number of predictions and events respectively.

Wilkinson (2017) used this score because it has a perfect score of 1 and a completely hedged score of 0, and because it is self-consistent with increasing numbers of observations in a domain. The score uses the whole domain contingency table scores (i.e. hits, misses, false alarms, and correct rejections). This examines the number of grid points that correctly forecast lightning compared to the observations on the same grid. It does not provide any information on how far the forecasts are from the observations or on the number of lightning flashes within a grid-box compared to observations. For example a single grid-box with 20 forecast lightning flashes 100 km from an observed lightning flash will be scored equivalently to the forecast being exactly correct. One other possible disadvantage of using the SEDS is that missed forecasts and false alarms are treated with the same weighting. While forecasting hazardous events it is often preferable to have very few to no missed forecasts, even

if it means a comparatively high number of false alarms. However, as here the score is not being used to evaluate forecast skill, just to compare observations and two methods of forecasting lightning it is better to evenly weight misses and false alarms.

The intensity score is more intuitive, it is simply

$$I = \frac{T_F - T_O}{T_F + T_O} \tag{4.2}$$

where T_F and T_O are the total number of forecast and observed lightning flashes respectively. This gives a score of 0 for a perfect forecast, the score will approach 1 for over-forecasting and -1 for under-forecasting.

4.2.2 Lightning data

The US lightning data used here is from the Earth Network's Total Lightning Network (ENTLN), the data gives the location and timing of observed lightning flashes. The method of lightning detection is explained in Section 1.7.1. The detection efficiency is discussed in Section 2.1.2. The UK lightning data are from the ATDNet, the detection efficiency is discussed in Section 2.1.1. In order to compare the observations with the model output, the observations are gridded to the model grids and accumulated to match the timing of the model output.

4.3 Results

In this section the electrification is examined in more detail across two case studies, one in the UK and one in the US. Both days were chosen at least in part because, to the eye, the MetUM produced accurate forecasts, thereby allowing the analysis and comparison of the electrification scheme with the observations, without the convection forecast having too much impact.

4.3.1 UK Case - 31th August 2017

The first case study where the new lightning parameterisation will be tested is the same case used in section 3.3.4.1. This day was largely a day of scattered convection. The convection lasted all day and was initiated by a small trough that slowly crossed the UK from west to east. Towards the end of the day the convection became more organised, resulting in several smaller squall lines across East Anglia.

Independent radar observations (not pictured), collected with Chilbolton Advanced Meteorological Radar, show that the isolated convection in the early afternoon reached altitudes of around 7 km.

The representation, by the model, of the convection in the morning appears accurate (Fig. 4.1a), even down to small details such as the scattered rain throughout the English Channel. The main area of convection in the Irish Sea is largely in the correct location and at the correct intensity. At 1200 Z the model output (Fig. 4.1c) again accurately represents the observations (Fig. 4.1d). The widespread isolated convection locations of the storms is well captured across England and Wales. The first signs of the forecast not performing so well (although still not particularly inaccurate) are the lack of clustering of storms in Figure 4.1e. In the observations (Fig. 4.1f) the storms over the east coast and East Anglia have begun to organise into large multicell systems. This is not captured by the model, which continues to maintain isolated single cell convection. Because of this the intensity of the rainfall (and therefore convection) in the model is lower than that of the observations.

Figure 4.2 shows the model lightning flash output compared to the ATDNet observations binned to the same grid. It is immediately obvious that there are some deficiencies with the new electrification scheme. The total number of flashes output from the scheme are around four times greater than the flashes observed by ATDNet. This is also displayed in the intensity score in Figure 4.3a, where most of the hours examined show an intensity score above 0, though most hours are much lower than the MC09 parameterisation. It is known that, within the ATDNet, the detection of IC flashes in particular are under counted, this means that an individual flash comparison of the forecast and observations is not appropriate. However,

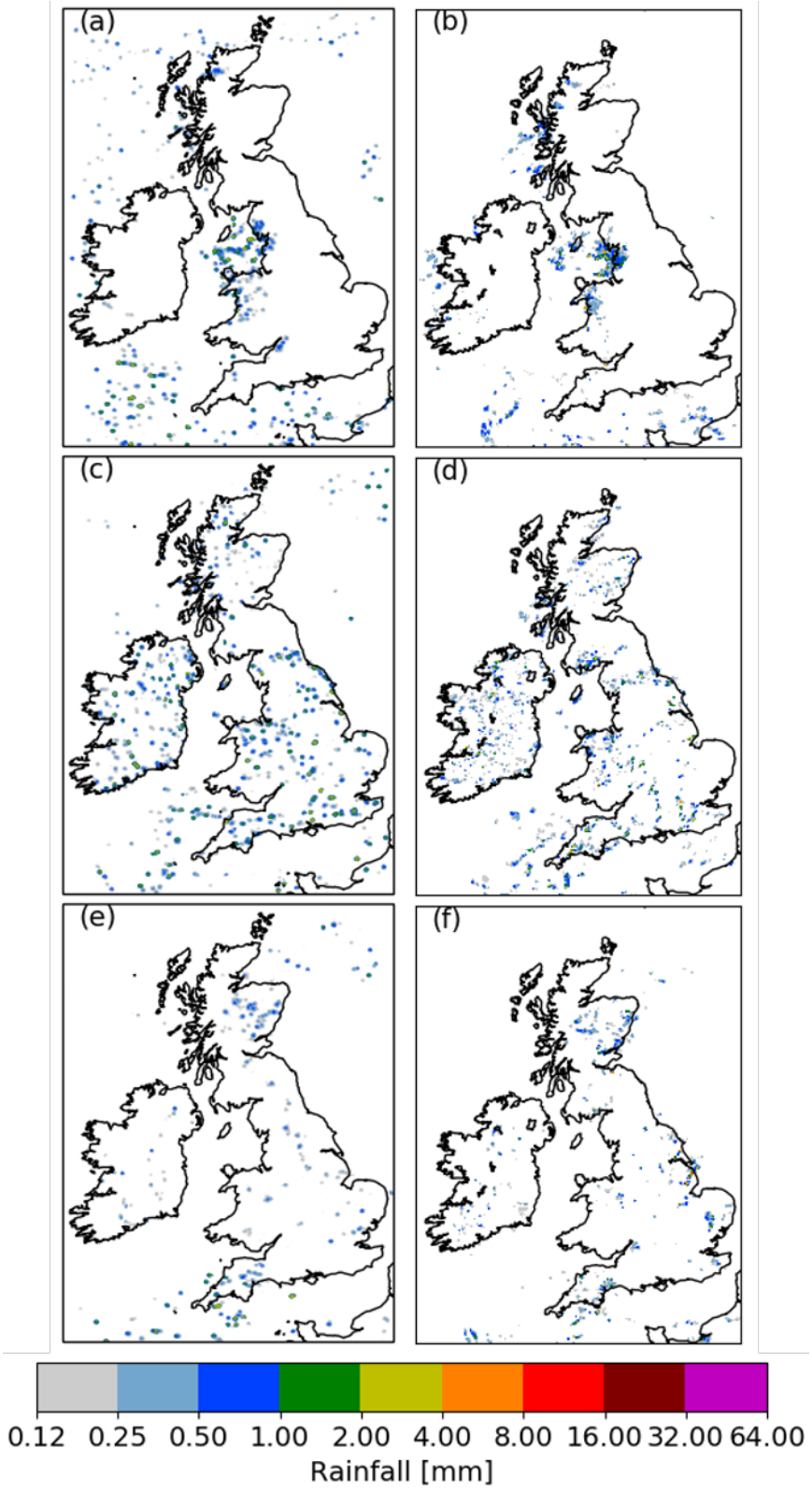

Figure 4.1: Rainfall over the UK for the 31st August 2017. The model output 5 minute accumulated rainfall is shown in the left column at times (a) 0600, (c) 1200, and (e) 1800. The observations of 5 minute accumulated rainfall are shown in the right column at times (b) 0555, (d) 1200, and (f) 1800

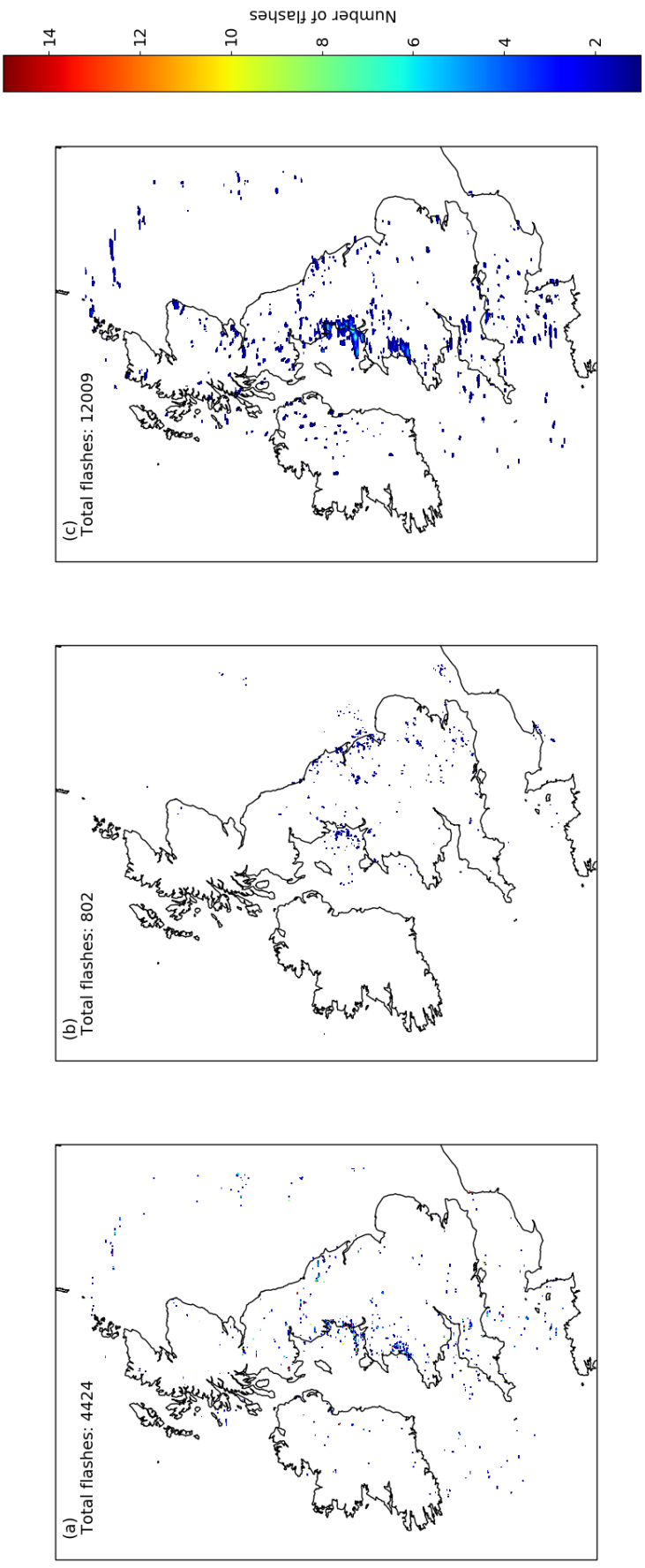

Figure 4.2: Accumulated lightning flashes over the entire day of 31st August 2017. (a) shows the total lightning output from the new electrification scheme detailed in section 4.3. (b) shows the ATDNet observations binned to match the model grid in (a). (c) shows the total lightning output from the MC09 parameterisation.

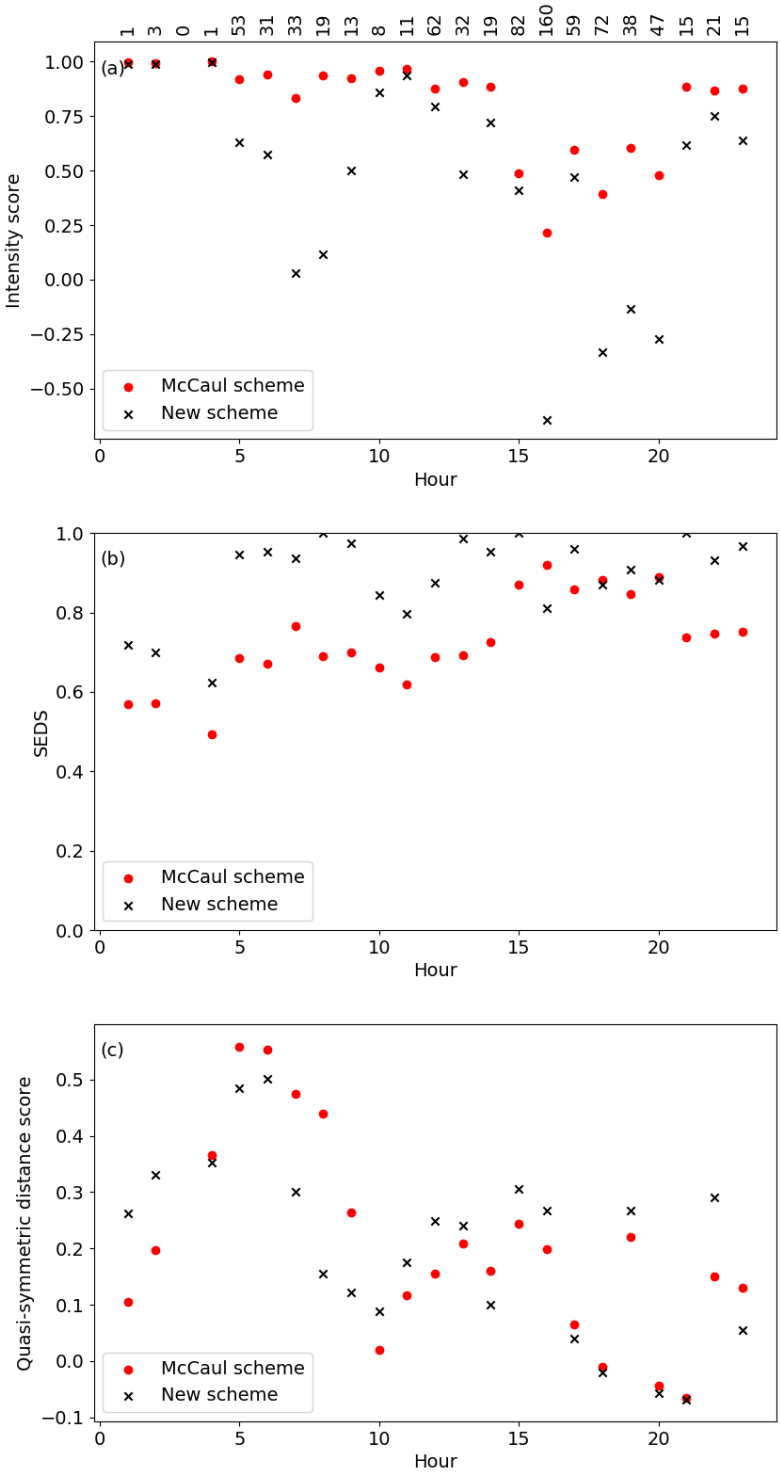

Figure 4.3: Verification statistics for hourly lightning flashes across 31st August 2017. (a) shows the intensity score for the new parameterisation and for the MC09 scheme, 0 indicates a perfect score (b) shows the SEDS for the new parameterisation and for the MC09 scheme, 1 indicates a perfect score, (c) shows the Quasi-Symmetric distance score for the new parameterisation and for the MC09 scheme, 1 indicates a perfect score. The numbers above the top plot indicate the hourly observed lightning flashes.

some information can certainly be gained examining the differences between the observations and each forecast. The detection efficiency could account for some of (but not all) the difference in intensity between the electrification scheme and observations. Is is also notable that the electrification scheme lightning output is more clustered than the observations. In some grid-boxes there are as many as 15 flashes, whereas the observations never record more than 5 flashes within a grid-box. Even with these higher intensity grid-boxes the model generally does a good job of capturing the scattered nature of the lightning observations. The SEDS in Figure 4.3b shows the electrification scheme consistently has a SEDS near 1 and never falls below 0.6, indicating there is consistently skill in the forecast. The skill in coverage is somewhat linked to the skill in intensity. At times where the intensity score is high (meaning a poor forecast), the SEDS often decreases. For example from 0100Z until 0400Z, where the intensity score is at its highest (mainly due to the small amount of observed lightning) the SEDS is at its lowest. Conversely at 0700Z and 0800Z, where the intensity score is close to 0, the SEDS is close to 1, indicating high skill. The model output clearly does not just follow regions of high reflectivity or high precipitation rate. Across the Irish Sea there are many grid-boxes with only one or two flashes in the box and no lightning around them.

An issue with the model output is the lack of lightning across the east of the UK. This is demonstrative of the difficulty already mentioned in verifying lightning forecasts. The missed convection shown by Figure 4.1e is the reason that lightning flashes observed here were missed by the model. This difficulty with forecasting lightning in the correct location is displayed in Figure 4.3c. There is little diference between the skill of the two forecasting methods in terms of location. This suggests that the lightning location forecast skill may rely more on the skill of the convective forecast than the forecast method. For example, early in the day the convection forecast skill appears to be good and the lightning location forecast is similarly skillful, particularly around 0500Z. However as Figure 4.1 shows the intense convection later in the day is not present in the model. This appears to be reflected in the location forecast, where the skill reduces throughout the day in both the MC09

parameterisation and the new electrification scheme.

4.3.1.1 Flash density and rain rate

In Figures 4.2 and 4.3 it can be seen that the MC09 parameterisation predicts lightning over too great an area in comparison with the relatively sparse nature of the observations. In contrast the coverage of the new electrification scheme appears to match well the observations and only predicts lightning in a comparatively small number of grid-boxes. In order to investigate why this might be the case the hourly total lightning flashes within a grid box were binned for ranges of hourly rainfall accumulation. The median, 75th, 90th, 95th and 99th percentiles for each bin were plotted in Figure 4.4.

Because the lightning in this case is for the most part sparsely distributed, the 90th percentile, for both the observations and the new scheme, shows no lightning for almost all of the rain bands. The MC09 parameterisation, however shows 0.1-0.2 lightning flashes consistently at rain rates between 2 and 10 $\mathrm{mm\,h^{-1}}$, this explains why the MC09 parameterisation shows much more widespread lightning in Figure 4.2 than either the new scheme or the observations. It can also be seen that the MC09 parameterisation is much less variable at the 99th percentile than the new scheme. There are, however a number of high peaks in the 99th percentile of the new scheme, this is possibly due to the more complex interactions between cloud ice and graupel that are required to produce lightning in the new scheme. That is, a high rain rate does not necessarily imply the co-location of graupel and cloud ice in the same way that a high rain rate generally implies a high TIWP.

4.3.2 US Case - 16th May 2017

The second case study is a much more convective case, as demonstrated in Figure 3.7. This case is described in Section 3.3.4.2

The main convection of the day began around 2000Z. It can be seen in Figure 4.5a that the convection has been initiated by 1800Z. At 2100Z the difference in

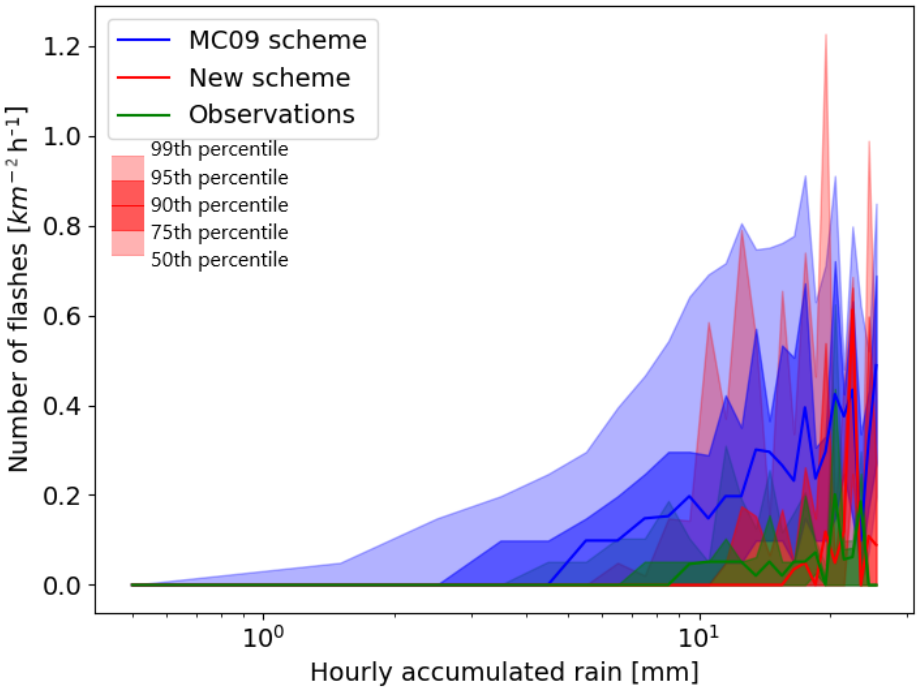

Figure 4.4: Hourly lightning accumulation binned by grid-box hourly rainfall accumulation. The median, 75th, 90th, 95th and 99th percentiles of lightning accumulation are shown for each given rainfall accumulation. Data are from the UK case study of 31st August 2017.

timing between the model and observations is much more clear. The convective line seen in Figure 4.5c is already well developed and organised. The main band of convection in Figure 4.5e and f appear similar in location, extent and intensity. The smaller, more isolated storms behind the convective line, however, are not captured by the model. While the lines look similar at midnight, the model convection is beginning to dissipate, while the observed rainfall is still at its peak. The modelled convection across Oklahoma and Texas is already much weaker than in the previous hours and the intensity of the storms in this region is lower than that of the storms in the observations.

The lightning output from the model is shown in Figure 4.6a for the new scheme, 4.6c for the MC09 parameterisation and 4.6b for the corresponding observations. In this case the MC09 parameterisation is closer to the observations than the new scheme is. The new scheme, in fact, predicts more lightning than the MC09 param-

eterisation in contrast to the results in Section 4.3.1. However, even though it does slightly over-predict the lightning here, the total lightning forecast is proportionally more accurate than the forecast in Figure 4.2. The intensity score shown in Figure 4.7a shows a similar picture throughout the forecast period. The MC09 consistently shows lower intensity scores than the new electrification scheme with the notable exception of the period between 100 Z and 500 Z on the 17th, where the new electrification scheme greatly under-predicts the number of flashes. Also as mentioned in section 2.1.2 the detection efficiency of ENTLN in this region can be as low as 80% within the domain, this means that the actual number of flashes could be closer to the new scheme output, or even possibly exceed the total flashes from the new scheme. On a large scale, the new scheme also shows too little coverage of flashes compared to the observations. This is particularly true throughout the period from 100 Z and 500 Z on the 17th where the intensity scores are particularly low. The final six hours of the forecast however show an improved SEDS. The overall coverage could, in part, be prescribed to the convection output of the model, which, as seen in Figure 4.5 does not capture the larger area of mid-intensity rainfall.

Similarly to section 4.3.1 the location of the lightning flashes depends largely on the convective forecast, and because the storms in the case are not marginal, but instead are producing a large amount of lightning, there is not much variation in the QSDS score in Figure 4.7c between the MC09 parameterisation and the new electrification scheme. There are only a small number of time periods where there is much difference between the two schemes and these are usually when either there are not many observations or one of the schemes is not producing much lightning. As a whole the forecast of the lightning location becomes less accurate steadily through the last three hours of the forecast. Although not shown in Figure 4.5 the convection at this time appears poorly represented, although missing radar observations make this uncertain to verify.

The intensity of lightning within individual pixels in Figure 4.6a is often too intense. Figure 4.7a shows that this is often the case through the entire domain, particularly at 2000Z and from 0500Z on the 17th until the end of the run. Not

only are the saturated areas in the figure more widespread than those in Figure 4.6b, but the maximum number of flashes in a pixel is twice as much as observed. Conversely the maximum number of flashes in a pixel in the MC09 parameterisation is too small, but there is too wide an area of mid-intensity flashes.

The coverage of both the new scheme and the MC09 parameterisation are both uniformly high, with the exception of the first five hours of the 17th in the new scheme, where the intensity score is very low. This is in no small part due to the accuracy of the convective forecast in this case. It can be seen earlier in the forecast where the model was initiating the convection early the SEDS drops for both forecast methods. It is interesting that the MC09 parameterisation has a much better coverage here. It is possible that in storms much more similar to the storms it was originally developed for the scheme performs better.

4.3.2.1 Flash density and rain rate

Although the coverage scores in Figure 4.7 are much better than those in Figure 4.3, it is still valuable to examine the flash rate for given rain rates, as was done for the UK case. It can be seen that the new scheme vastly over-predicts lightning at high rain rates, with even the 50th percentile above 10 flashes per grid-box per hour. This is not the case throughout the entire range of rain rates. Until a rain rate of around $1\,\mathrm{mm\,h^{-1}}$ the new scheme predicts the fewest lightning flashes, it is only around $8\,\mathrm{mm\,h^{-1}}$ that the new scheme begins to increase in flash rate much more rapidly than the observations. The MC09 parameterisation remains very self consistent here, as in the UK case. The high flash rate at the 75th and above percentiles for the very largest rain rates is the reason that the MC09 scheme was accurate in predicting the total number of lightning flashes. This is however not realistic: given the stochastic nature of lightning flashes, it should be expected (and is demonstrated in Figure 4.8) that there is a high variability in the number of flashes for a given rain rate.

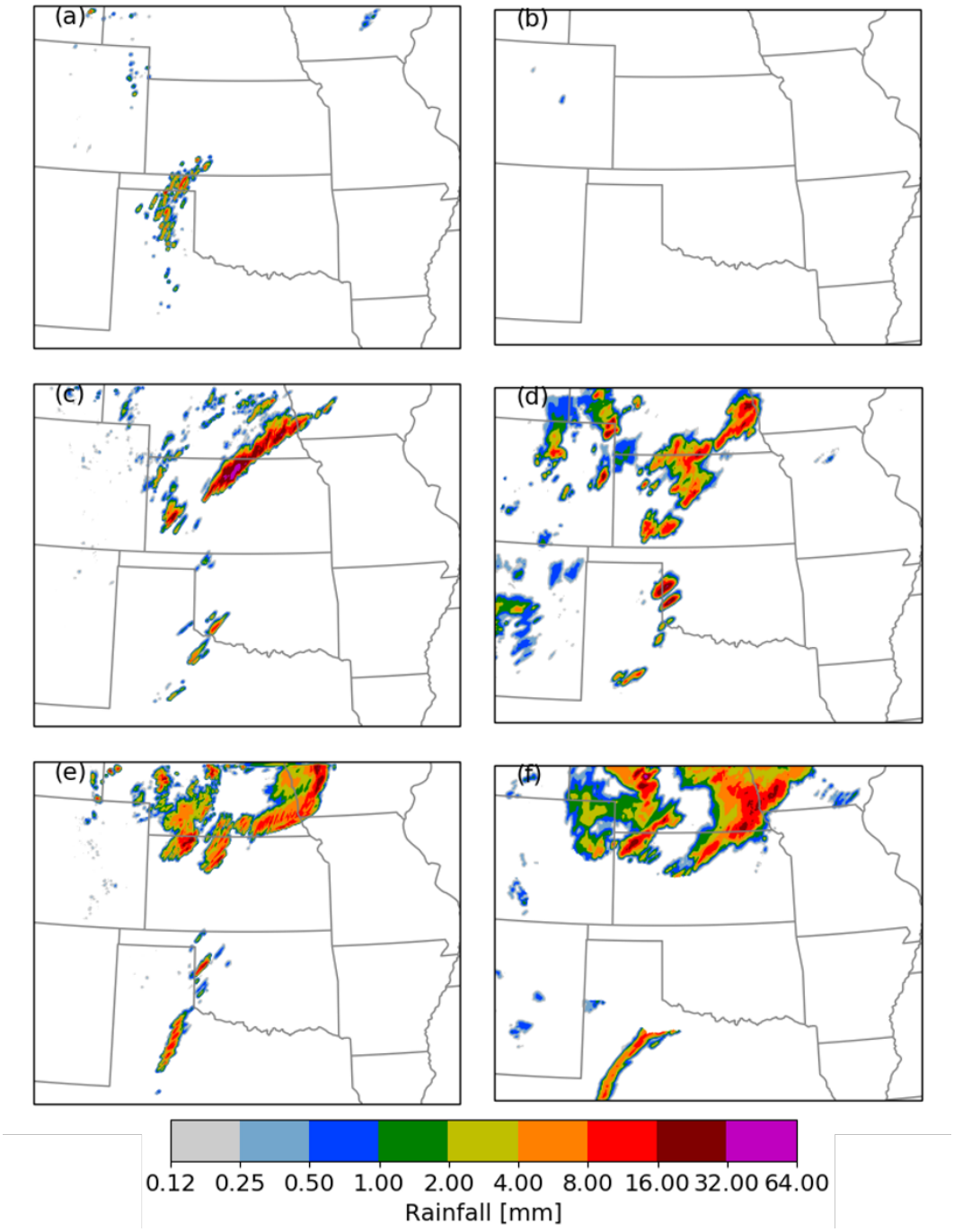

Figure 4.5: Rainfall maps of Oklahoma and Kansas for the 16th and 17th May 2017. The model output hourly accumulated rainfall is shown in the left column at times (a) 1800Z on the 16th, (c) 0000Z, and (e) 0300Z on the 17th. The radar derived observations of hourly accumulated rainfall are shown in the right column at the same times.

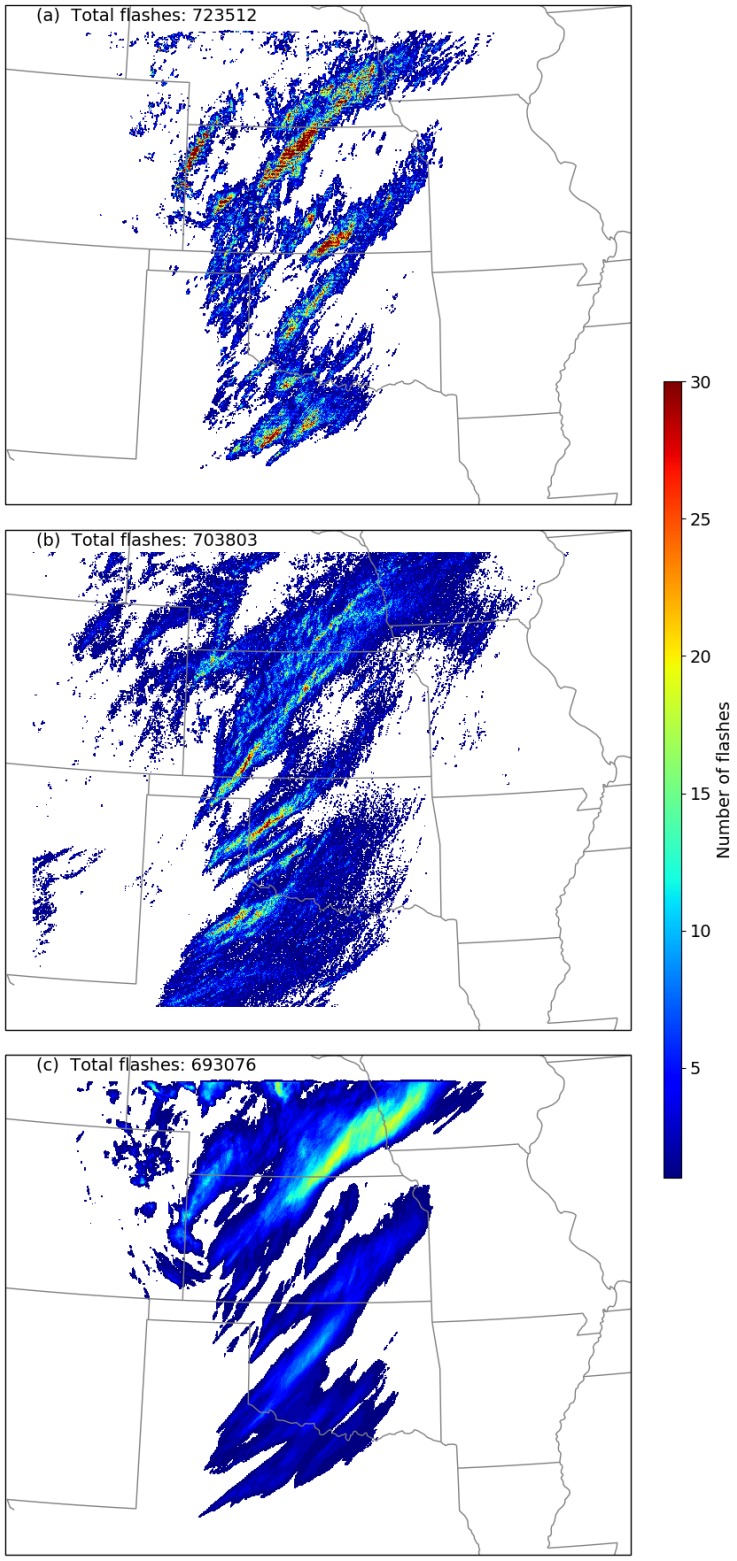

Figure 4.6: Accumulated lightning flashes from 12Z 16th May to 12Z 17th May 2017. (a) shows the total lightning output from the new electrification scheme. (b) shows the ENTLN observations binned to match the model grid in (a). (c) shows the total lightning output from the MC09 parameterisation.

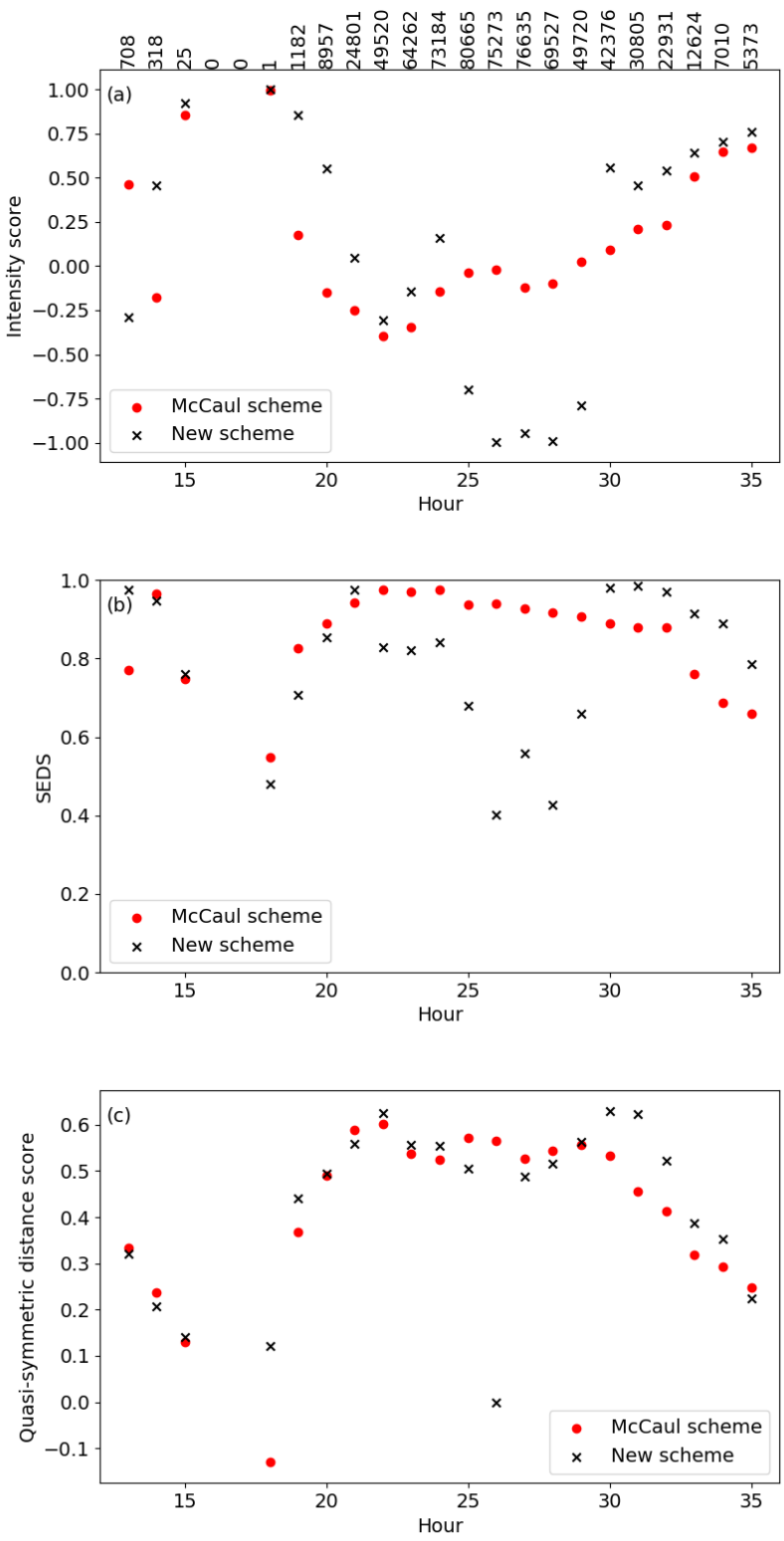

Figure 4.7: As Fig. 4.3 but for the US case of 16-17th May 2017.

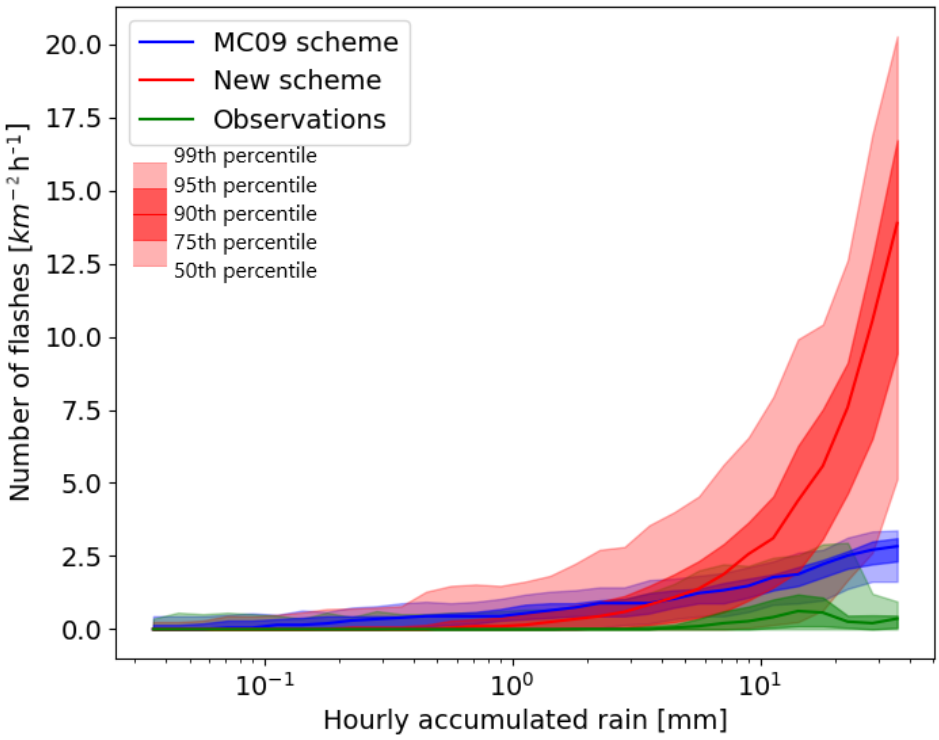

Figure 4.8: Hourly lightning accumulation binned by grid-box hourly rainfall accumulation. The median, 75th, 90th, 95th and 99th percentiles of lightning accumulation are shown for each given rainfall accumulation. Data are from the US case study of 16-17th May 2017.

4.4 McCaul parameterisation changes

Prior to finishing this thesis it was found that there were several errors in the implementation of the MC09 parameterisation within the MetUM. These were related to confusion over several unconventional units used within the McCaul *et al.* (2009) study. Rather than the output of the flash rate given by Equation 2.6 being given in units of s^{-1} or min^{-1}, the units were $5min^{-1}$. Further the units of graupel mass mixing ratio used for r_1 appear to be $g\,kg^{-1}$ rather than $kg\,kg^{-1}$ (although the TIWP for r_2 does appear to be in units of $kg\,kg^{-1}$). These changes were expected to increase the role of the r_1 term and decrease the role of the r_2 term. It was anticipated that through implementing these changes the MC09 parameterisation should produce more lightning in the earlier stages of the thunderstorm lifetime and

reduce the total lightning and the lightning coverage.

Given that these errors were found relatively late there was not time to repeat all the analysis here with the updated parameterisation. However, the updated MC09 scheme forecast for the UK case study is shown in Figure 4.9. The updated MC09 scheme forecast for the US case study is shown in Figure 4.10.

The corrected MC09 parameterisation in Figure 4.9c produced a much improved forecast in the UK case study, in terms of total forecast lightning. However, the reduction of lightning appears uniform across the domain. This means that the areas with least lightning no longer produce any lightning, thereby causing a lack of lightning from small single cell storms, particularly in the north east of England. Overall, while this forecast is much more accurate in terms of the total number of lightning flashes forecast, it may not be as informative from an operational standpoint as it misrepresents the threat of lightning from the single cell convection.

Similarly for the US case study, shown in Figure 4.10c, the number of total lightning flashes have reduced greatly. In this case the reduction in lightning has made the forecast much worse, both in terms of lightning intensity and coverage. It also does not appear to have much improved the appearance of the lightning forecast: the number of flashes still appears to be contoured, suggesting that the correction to the r_1 term from Equation 2.6 does not greatly change the manner in which the parameterisation produces lightning.

4.5 Discussion

The new electrification scheme works well in the UK case study of the 31st August 2017, despite the tunable parameter, the collision-separation efficiency, being tuned in the US case study. The scheme also visually appears to be more physically representative of the pattern of lightning in Figures 4.2 and 4.6; this is studied in greater depth in chapter 6.

The major deficiency of the new scheme in the UK case is the over-forecasting of lightning in individual grid boxes. This gives a coverage that appears similar

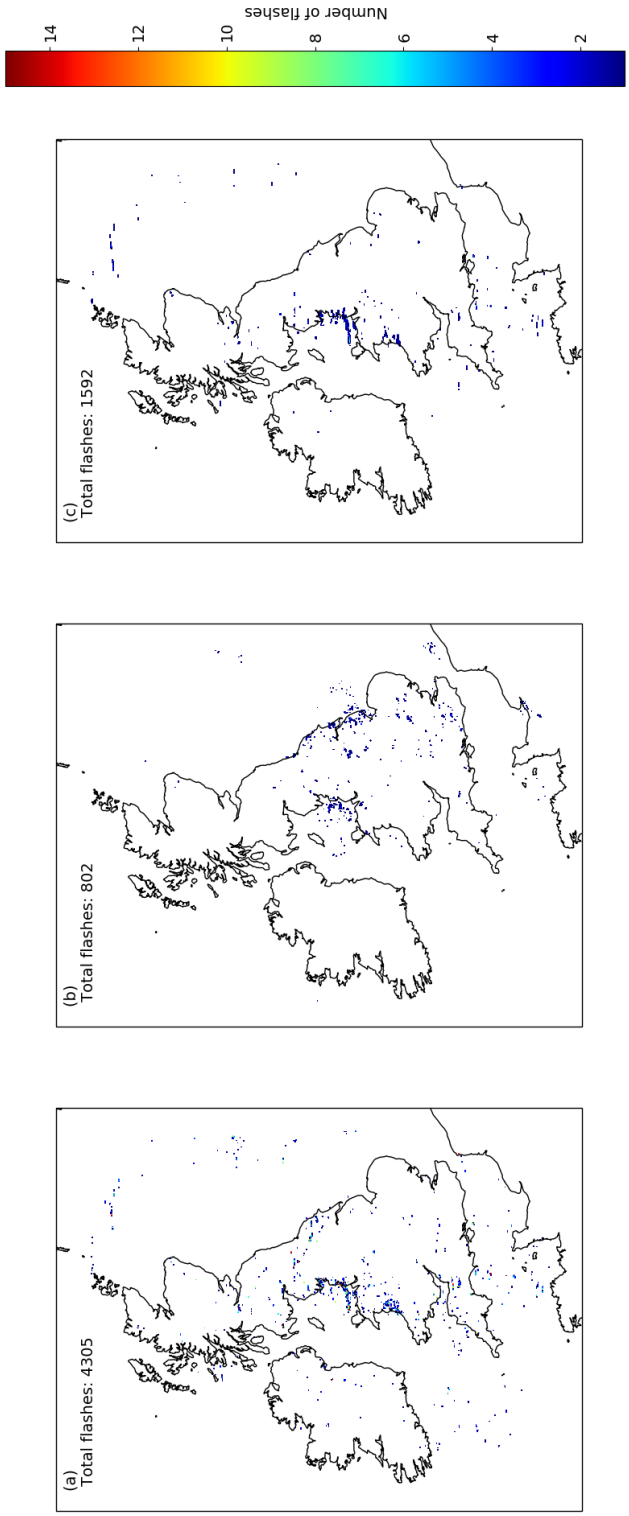

Figure 4.9: As Figure 4.2, but (c) shows the total flash output from the updated MC09 parameterisation.

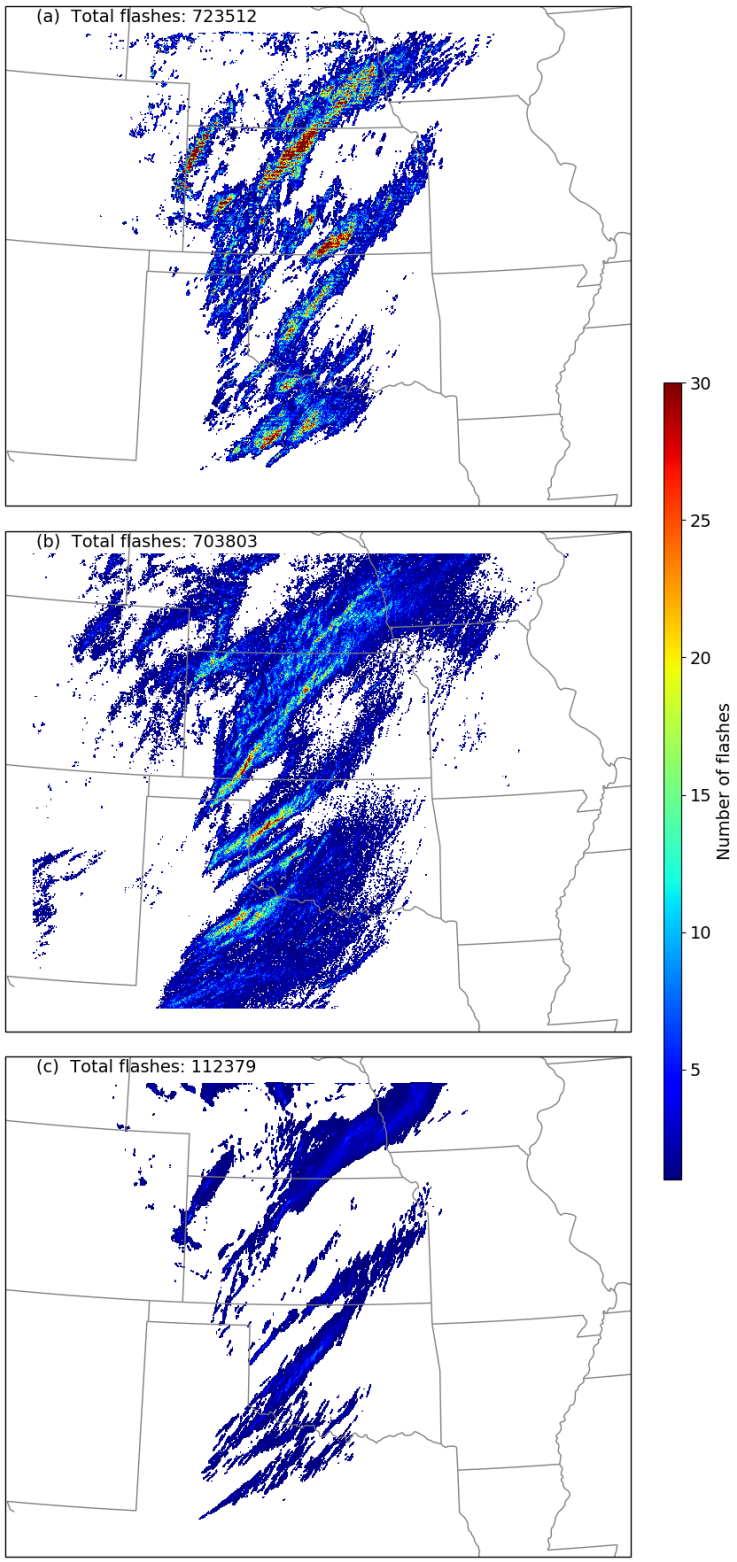

Figure 4.10: As Figure 4.6, but (c) shows the total flash output from the updated MC09 parameterisation.

to that of the observations while simultaneously over-forecasting the intensity of the lightning. This over-forecasting is also obvious in Figure 4.6 where the high intensity regions of >20 flashes per grid-box extend over too large an area. This leads to a similar problem as observed in the UK case, where the total lightning flash number is over-forecast while the coverage, in this case, is smaller than the observations.

In Figure 4.8 the cause of the high number of grid points with a high flash intensity appears to be due to the scheme over-forecasting lightning in high rainfall rates. In Figure 4.4 the behaviour of the new electrification scheme at high rain rates is difficult to discern, given the small number of data points, however it appears that the 95th percentile in particular follows an upward trend similar to that in Figure 4.8. A major difference between the two figures is that the MC09 curve remains above that of the new scheme in the UK whereas in the US it forecasts fewer flashes at rain rates higher than about $4\,\mathrm{mm\,h^{-1}}$.

The MC09 parameterisation over-forecasts the lightning total in the UK while producing a good forecast based on the same method in the US. This suggests that there may be a difference in convection and how this relates to lightning in the UK and the US that is not well captured by the MC09 parameterisation. It is possible that if the proportion of graupel in the TIWP in the US case study is higher than that in the UK case study, this could lead to the forecast in the US being more accurate based only on the TIWP.

4.5.1 Collision-separation efficiency

For two particles (in the case here a graupel particle and a cloud ice particle) within one another's collision kernel, there are three possible options of interaction, shown in equation 4.3.

$$E_{coalescence} + E_{separation} + (1 - E_{collision}) = 1 \tag{4.3}$$

Where $E_{coalescence}$ is the collision-coalescence efficiency, $E_{separation}$ is the collision-

separation efficiency and $E_{collision}$ is the collision efficiency.

The first term indicates that two particles collide and coalesce, becoming one particle. The second term indicates that two particles collide and separate, this is term of interest here. The third term indicates that the smaller particle is carried around the larger by the streamlines, without any collision occurring. The probability of the three options must sum to 1.

The collision-separation efficiency is comprised of an implicit collision efficiency, multiplied by the probability of, given a colliding ice particle and graupel, the separation of the two particles. This efficiency has not been studied extensively due to the fact that for the majority of microphysical processes the outcome is no different to if the particles had not collided. Similar to the collision-coalescence efficiency, this parameter should itself have dependencies on temperature and particle size and shape. However, given that no studies quantify these relationships, the decision was made to make this parameter tunable.

The collision-separation efficiency has been set to 0.3 as a consequence of testing the scheme and comparing the results to the ENTLN observations. It was most convenient to compare the total number of lightning flashes across the US domain for entire day, as the location and coverage of flashes did not appear to change greatly between the lightning producing values of collision-separation efficiency. The US domain was chosen because of the greater number of lightning flashes and the better detection efficiency of the ENTLN over the ATDNet. The results of the sensitivity analysis are shown in table 4.1. It can be seen that the number of lightning flashes varies hugely with the collision-separation efficiency. The relationship is approximately linear.

Because the detection efficiency of the ENTLN can be as low as 70-80% within the domain (though it is usually higher), the validation of a specific value of the collision-separation efficiency is not appropriate. However, it is still appropriate to tune the scheme to an approximate value of the collision-separation efficiency, or to a range of values. In this case (given that the observations are likely too small) either 0.3 or 0.35 (or any value between) could have reasonably be used. The value

of 0.3 has been chosen because it gives a more reasonable number of total flashes for the case in section 4.3.1.

Separation Efficiency	Number of flashes	Difference from observations
0.15	271,985	-431,818
0.20	425,404	-278,399
0.25	573,172	-130,631
0.30	723,512	19,709
0.35	859,980	156,177
0.40	984,754	280,951

Table 4.1: Sensitivity analysis for four values of the separation efficiency. The number of flashes refers to the total flashes throughout the entire domain from 12Z 16th May to 12Z 17th May 2017.

The large perturbation of the lightning flashes for a given rain rate in Figure 4.8 could potentially be the lack of representation of hail within the UM. It is well known that lightning flashes avoid the updraft region of large thunderstorms where hail is formed (see Section 1.4.2). It is thought that this is due to the lack of charging that occurs with hail undergoing wet growth. Wet growth of hail or graupel is when there is sufficient warming of the surface of the ice particle, due to heat from the latent heat of freezing, that any further water collected by the particle does not immediately freeze; thereby creating a layer of liquid on the surface of the particle. When this occurs, it is likely that the collision-separation efficiency decreases causing hail and ice aggregate particles to collide and coalesce rather than charge being separated. Because of this process, even when there are large rain rates within storms with strong updrafts there may not be as much charge created and lightning as expected. This process is not represented within the UM, rather hail particles are treated as large graupel particles and within the new electrification scheme the collision-separation efficiency is held constant, regardless of the graupel mass or growth rate. This allows very large amounts of charge to be created within this situation causing a high lightning flash rate, where one may not be observed in real life.

This also explains the reason that a similar perturbation of the number of lightning flashes is not seen in the UK case. In the UK the updraft velocities are smaller

creating less graupel. This means that the same lightning holes are not generally observed in the UK and that the model does not have the run-away increase in lightning flashes.

This suggests that a representation of the separation efficiency as a function of the graupel mass could be an appropriate way to reduce the charge generated in thunderstorm cores with large amounts of hail.

4.6 Conclusions

A scattered convection case study in the UK and a supercell convection case study in the US were examined in both the new scheme and the MC09 parameterisation. The new scheme performed well in terms of total flashes in both case studies. The MC09 parameterisation, while accurately predicting the number of lightning flashes in the US case, over-forecast the flashes in the UK case by an order of magnitude. In terms of coverage, in the UK case in particular the new scheme better fits the coverage of the lightning according to the SEDS, showing that it better matched the scattered nature of the observations. As opposed to the MC09 parameterisation which appear to mostly forecast lightning in regions of high precipitation. The lightning flash pattern was much more widespread in the US case and so both parameterisations did generally well at forecasting the coverage. The MC09 parameterisation tended to create more widespread areas of medium intensity flash rates and not generate any areas with high flash rate intensity. The new scheme on the other hand generated a small number of locations with many more flashes than were ever observed in a single grid box. The forecast of the locations of lightning differed very little between the two methods, the location accuracy was much better in the US case than in the UK case, though in both cases the accuracy decreased towards the end of the day.

The MC09 parameterisation was incorrectly implemented within the MetUM. When the corrections were applied to both terms in Equation 2.6 the total number forecast for the UK was much improved. In the US case study, however, the forecast reduced greatly, causing that forecast to degrade in quality. The coverage of both

forecasts also appeared to be worse with the changes implemented.

It is suggested that the high intensity flash rates produced by the new scheme could be due to poor representation of hail and the wet growth of graupel within the model. Hail and graupel, while undergoing wet growth, have a collision-separation efficiency of 0, i.e. every ice particle that collides with a wet hail or graupel particle will coalesce to it. Because this is not represented by the new scheme, the locations with the highest graupel mass mixing ratio (which is likely where the wet growth is occurring) may have artificially inflated flash rates.

Chapter 5

Rapid intensification of single cell thunderstorms in the UK

5.1 Introduction

Within the UK, marginal storms are developed single cell convective storms that either produce a small number of lightning strikes, or produce no lightning themselves but appear similar to storms that do produce lightning. Therefore, marginal thunderstorms can be difficult to identify early in their lifetime, before they produce lightning. However, these marginal thunderstorms can still be destructive, for example Elsom *et al.* (2016) report that the first lightning strikes from a short-lived thunderstorm killed two men near the peak of Pen-y-fan in Wales. On days with marginal storms, therefore, it is especially important to accurately predict which storms will and will not produce lightning and to predict when storms might become electrically active.

Numerous studies have examined multicellular thunderstorms (e.g. Carey and Rutledge, 1996, 1998; Bruning *et al.*, 2007) or mesoscale convective systems (e.g. Cifelli *et al.*, 2002; Ely *et al.*, 2008; Wang and Liao, 2006) in the US or tropical regions and some have studied lightning in supercells (e.g. Stough *et al.*, 2017; Wiens *et al.*, 2005) or within tropical cyclones (e.g. Cecil *et al.*, 2002; Lyons and Keen, 1994; Black and Hallett, 1999). There have, however, been comparatively few studies on simple single cell thunderstorms (e.g. Dye *et al.*, 1986). Single cell thunderstorms should be the simplest version of convection as there are no influences on a storm and its structure from competing storm cores and updrafts. It is hoped that observations of single cell storms will be informative for and applicable to more

complex convection.

Previous studies examining the onset of lightning using radar data have focused on reflectivity at certain isotherms (see table 1 in Mosier *et al.*, 2011). However, frequently, thunderstorms in the UK do not reach these high levels of intensity even when electrically active. Indeed, in the UK, lightning can be observed in thunderstorms with a maximum reflectivity of less than 40 dBZ. These low reflectivity thunderstorms mean that the thresholds referenced in Mosier *et al.* (2011) would regularly not capture the onset of lightning.

This less intense nature of the convection in the UK leads to weaker updrafts and to less graupel routinely present in the convective clouds, and therefore fewer electrified storms. This is exemplified by the storm tracks and lightning strikes shown in Figure 5.1. There is only one storm which produces more than 10 lightning strikes over its lifetime. Instead, the majority of the storms produce 1 or 2 strikes, while some storms that initially appear similar to the lightning producing storms, produce no lightning at all. The difference between the storms that produce a small number of lightning strikes and those that appear similar in track intensity and length but with no lightning presents a challenge to forecast.

While the uncertainty involved in forecasting convection means that the differences between the "low lightning" and "no lightning" convective storms cannot be discerned on forecasting timescales, it is useful to investigate these differences for the possibility of nowcasting applications and also to examine the microphysics that causes one storm to produce lightning but not another. In order to do this, the Met Office radar network was used in conjunction with the Met Office Arrival Time Difference Network lightning observations to examine storms (especially the mixed phase region) prior to their producing lightning. Subsequently, model data from the Met Office UKV model was used to analyse the physical causes and consequences of the observed intensifications.

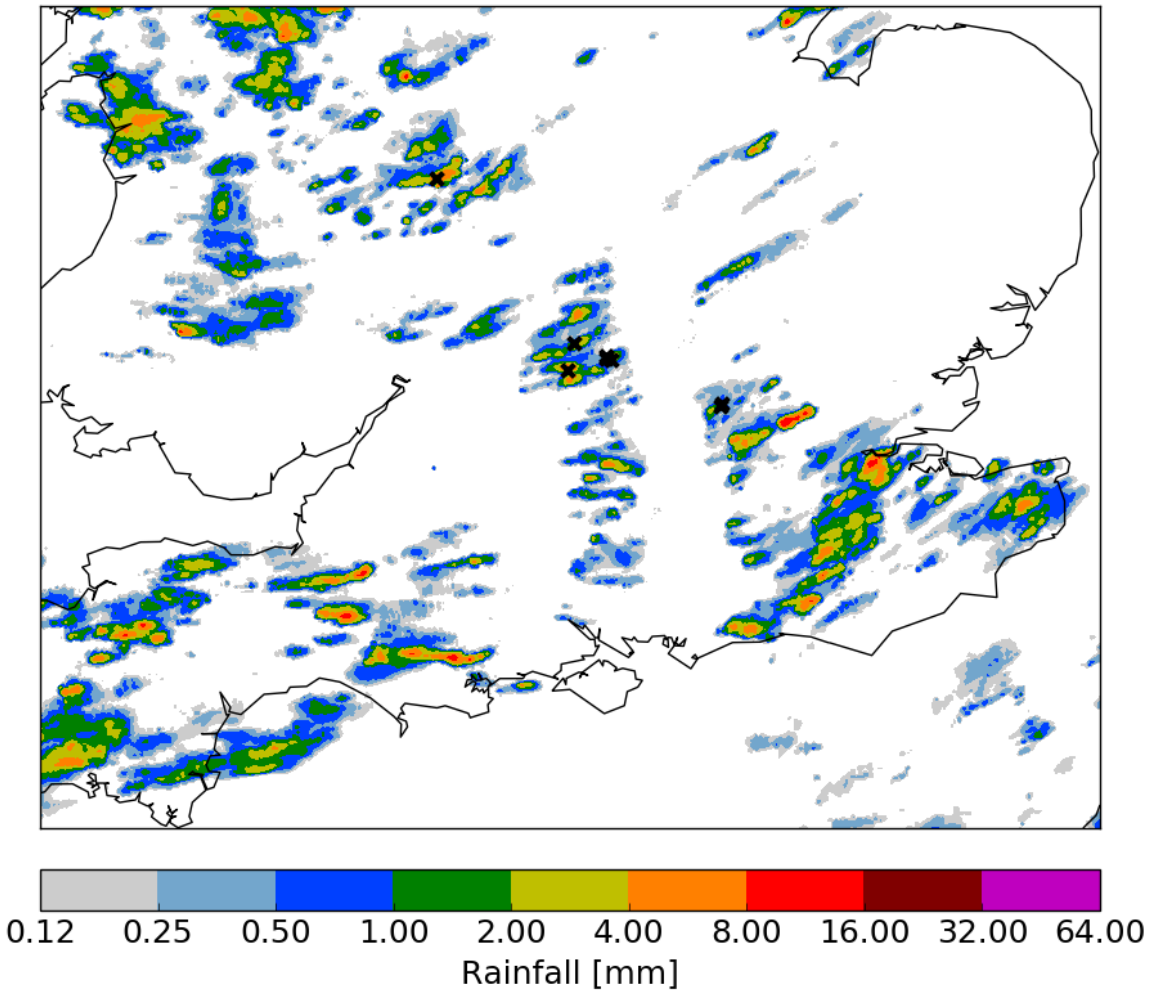

Figure 5.1: The accumulated rainfall from the radar composite on 2017/08/31 from 12:00 - 13:00, black crosses show the location of lightning strikes.

5.2 Data and Method

The domain is focused on the south of the UK (specifically the Heathrow domain from Scovell and Al-Sakka, 2016). This is the part of the UK that most frequently experiences thunderstorms (Cecil *et al.*, 2014). Two days of observations (2012/08/06 and 2017/08/31) are used in total in this analysis.

5.2.1 Radar Composite

The Met Office 3D radar composite is compiled from the 15 operational C-band radars in the Met Office network. It has a 1 km resolution in the horizontal and

500 m resolution in the vertical, extending to an altitude of 12 km (Scovell and Al-Sakka, 2016). Especially across the south of the UK, the coverage of this radar network is comprehensive with as many as 4 radars observing individual pixels. The mosaic has a temporal resolution of five minutes allowing for the representation of the evolution of thunderstorms. Currently the only radar parameter included in the composite is radar reflectivity. The composite was used to track storms (see section 5.2.2) and storm cores and to examine the 3d structure of lightning producing storms.

5.2.2 Storm Tracking

To allow for tracking of storms within the 3d mosaic, the composite was condensed to a 2d composite. Each column was represented by the 75th percentile of reflectivity above 2.5 km. As shown in Figure 5.2a, using the 75th percentile reduces the variability inherent to the maximum value in a column while retaining the relevant information about the most intense parts of the storm. Also the 75th percentile retains information about the storm even if the convection is relatively shallow, whereas the median must have a storm of at least 6 km depth before showing a signal. Ignoring the data below 2.5 km eliminates the potentially misleading intensification of the melting layer (e.g. at 153 km in the top right panel of Figure 5.2) which contains little information about the microphysics of a thunderstorm (Mattos *et al.*, 2016). It can be seen in Figure 5.2 that the more convective (1135 and 1140 UTC) timestamps have a smaller difference between the entire column method (the black line) and the above the melting layer method (the red line) than the more stratiform timestamp (1130 UTC).

Storms were tracked in this 2d composite using the tracking method from Stein *et al.* (2015); in this case the storm edge was defined as the 5 dBZ contour (using the 75th percentile above 2.5 km) and the minimum storm area was 5 km^2. In addition to the 5 dBZ contour to mark the cloud edge, a 25 dBZ contour was used to mark a storm core and used to calculate a storm core area. The storms were then limited to single cell storms in order to reduce the impact of multiple storm cores interacting

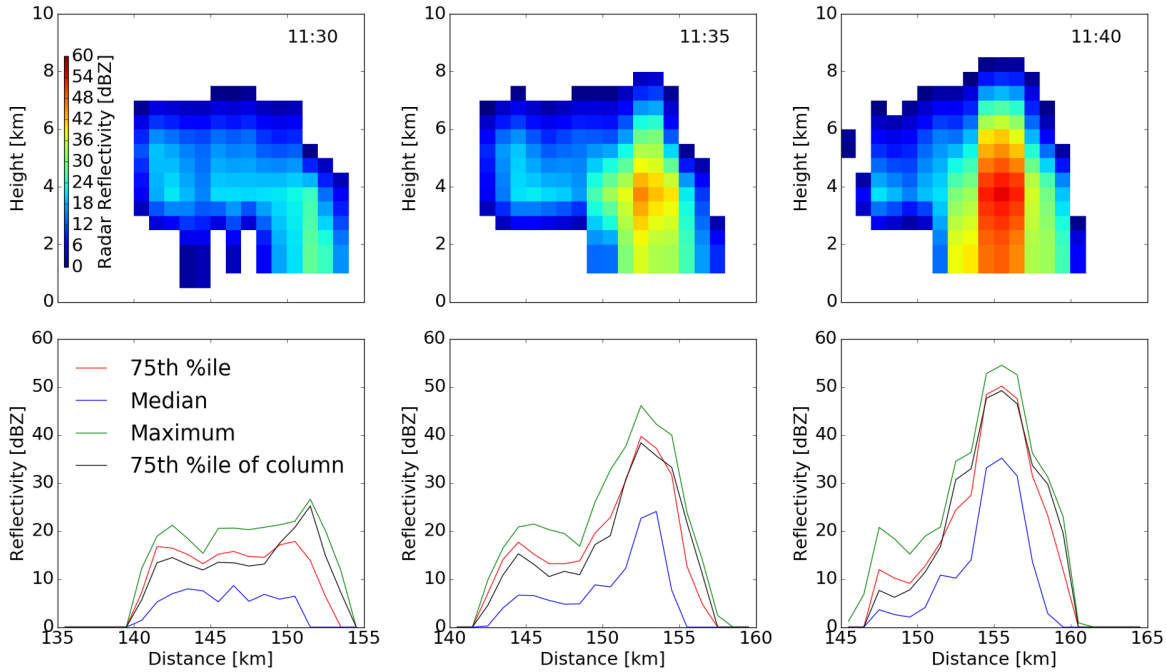

Figure 5.2: Top row shows radar cross sections through the most intense area of a single cell thunderstorm at the times indicated on 2012/08/06. Bottom row shows methods of reducing the cross section to individual points. The median, maximum and 75th percentile (in red) only consider data above 2.5 km (2.5-12 km) whereas the 75th percentile of column (in black) uses the entire column of data (0-12 km).

and thereby confusing the interpretation of the microphysics within the storm.

The lower limit for the storm size was chosen as no storms with an area smaller than 9 km^2 were observed to produce a lightning strike (see Figure 5.3), including this lower limit greatly reduced the number of storms that were tracked. The 5 dBZ contour was chosen arbitrarily as a small enough reflectivity to include all of the cloud information while not including noise. The 25 dBZ contour for the storm core maximized the skill of using the intensification of the storm core to predict lightning. We used two skill scores to test the accuracy of a variety of reflectivity contours to define the storm core, namely the SEDI and the FAR (see section 5.5), the results of which are shown in table 5.1. Of these, for the two days of observations, the 25 dBZ contour proved to be the best predictor (as a compromise of SEDI and FAR) of lightning following an intensification.

Core Threshold	10	15	20	25	30	35
SEDI Score	0.87	0.87	0.88	0.86	0.76	0.70
FAR	0.85	0.80	0.66	0.52	0.25	0.08

Table 5.1: Table showing the SEDI and FAR scores for thresholds to define the storm core

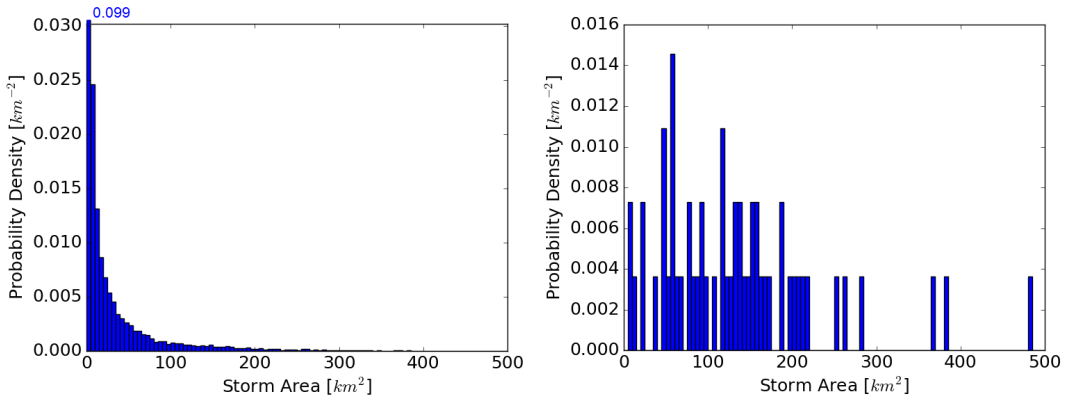

(a) (b)

Figure 5.3: Histograms showing the plan area of single cell storms for (a) all single cell storms (b) lightning producing single cell storms. Bin width is 5 km^2. In (a) the 0-5 km^2 bin extends to a probability density of 0.099 km^{-2}

5.2.3 Lightning Data

ATDNet lightning strikes were co-located with the radar composite using latitude and longitude to match to the Cartesian radar grid, each strike was situated in a gridbox by finding the nearest grid box centre. Lightning strikes that occurred within a storm area and within the previous five minutes (to match the radar interval) were associated with that storm. If a strike could not be co-located with a storm or if, due to its location error (location error is specified for each individual strike, it is typically 1-3 km), a strike was co-located with multiple storms, the strike was discarded and ignored.

5.2.4 Model Data

The UKV is the Met Office convection-permitting implementation of the Unified Model (UM), run operationally over the UK (Tang *et al.*, 2013). The only difference to the model configuration in Section 2.3 is that it is a variable resolution model

with a horizontal grid-length of 1.5 km in the interior, extending to 4 km at the edges. The model can also output forward modeled radar reflectivity as an output diagnostic, this enables the model output to be used in the storm tracking method used above for the radar observations.

For the UKV simulations used here, the model was run with the 04 UTC operational analysis as initial conditions, with lateral boundary conditions provided by the 00 UTC global model forecast. The model was run for 16 hours. The model data used were: forward modelled reflectivity, graupel mass mixing ratio, and vertical wind speed. For these model runs, the electrification scheme was not included in the model, therefore the runs here do not contain any electrical parameters. The data were all output on the native model grid, with a 15 minute temporal resolution.

The radar shows lighter rain rates over larger areas and less intense heavy rain rates than the model. The model output in Figure 5.4 also appears to be more clustered than the observations for the same period in Figure 5.1.

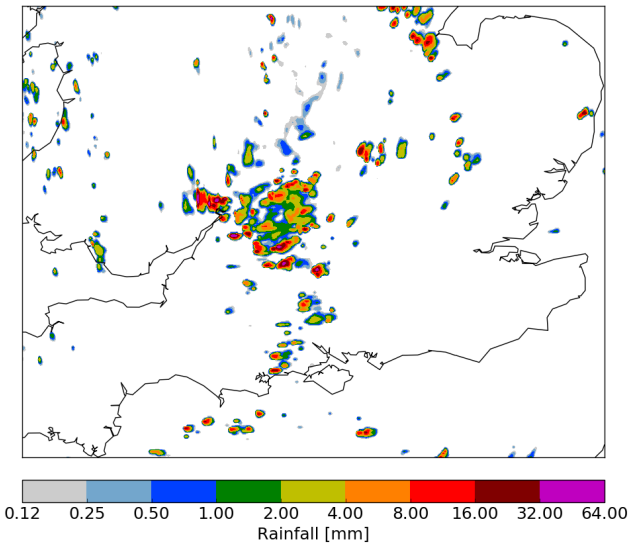

Figure 5.4: The accumulated rainfall from the model on 2017/08/31 from 12:00 - 13:00.

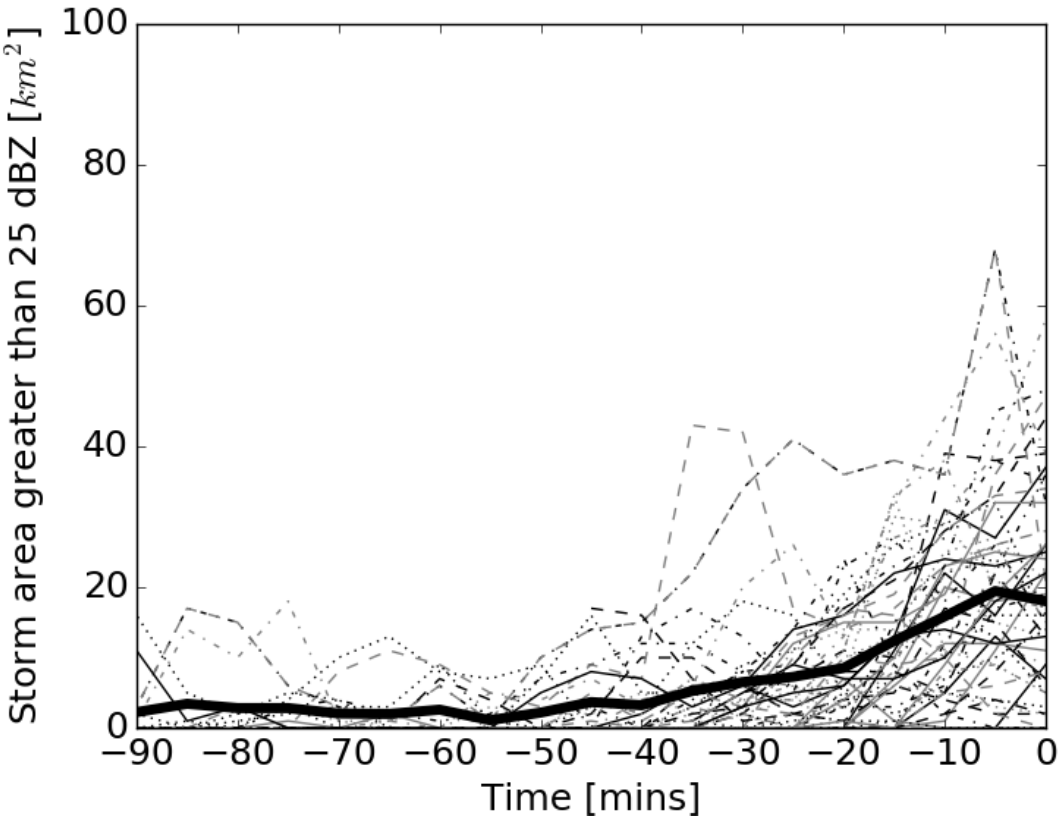

Figure 5.5: Lines showing the increase in storm core area for all single cell thunderstorms in the time before the onset of lightning at time 0, the bold line shows the mean.

5.3 Results

Figure 5.5 shows the area of the storm core prior to the first lightning strike of a storm. Each line represents the evolution of a separate thunderstorm core from first detection until the time of first lightning strike (at time 0). The chart includes 55 single-cell thunderstorms, across two days of thunderstorm activity. Of these thunderstorms, only 3 had no change or a decrease in storm core area before the lightning strike. Each of these three storms had no storm core per our definition and maintained no core until producing lightning. Of the storms that increased in core area 39 out of 52 increased by 10 km^2 or more, the most explosive storm observed increased from a core area of 6 km^2 to 58 km^2 in just 25 minutes. Half the number of storms that intensified before the onset of lightning did so by 10-25 km^2.

As the only radar parameter available within the composite at the time of writing was radar reflectivity, more detailed microphysical information than that already shown could not be obtained from observations. Therefore the Met Office convection permitting UKV model was used to investigate the microphysics. The forward modelled reflectivity that is output from the UKV was compatible with the tracking algorithm used for the radar data, and so the same algorithm was used to track storms in the model.

From the model, these isolated storms were found to undergo a similar rapid intensification. Figure 5.6a shows the evolution of the storm core, from radar observations, until it undergoes a rapid intensification (an increase of $10\,km^2$ in storm core area in 15 minutes or less, see section 5.5), rather than until a lightning strike as in Figure 5.5. There is some overlap between the lines in Figures 5.5 and 5.6a, 34 of the 55 lines in Figure 5.5 are also included in 5.6a together with 37 other intensifying storms. The intensification of the storm core was used, as this measure could be replicated in the model (shown in Figure 5.6b). The two means in Figure 5.6b, while slightly offset in absolute storm core area, show similar increases in core area within the final 15 minutes of the plots. The model plot shows an increase in core area from a mean of $7.6\,km^2$ to a mean of $23.5\,km^2$, within 15 minutes. The observations show an increase in core area from a mean of $3.2\,km^2$ to a mean of $17.4\,km^2$ in 15 minutes, although the majority of this change occurs within the final 5 minutes of the intensification. The range of magnitudes of the intensifications was smaller than that in Figure 5.5, because by definition the intensifications were larger than $10\,km^2$. About 95% and 90% of the intensifications were between 10 and $25\,km^2$ for the radar observations and model respectively.

In Figure 5.6a the mean area of storm core in both panels follows a similar path. The difference in temporal resolution between the observations and the model means that the observations appear to have more variability than the model and appear to intensify slightly later than the model. However the magnitude of the intensification is very similar within the final 15 minutes and the final core area is approximately similar in both the model and the observations. Therefore we now investigate the

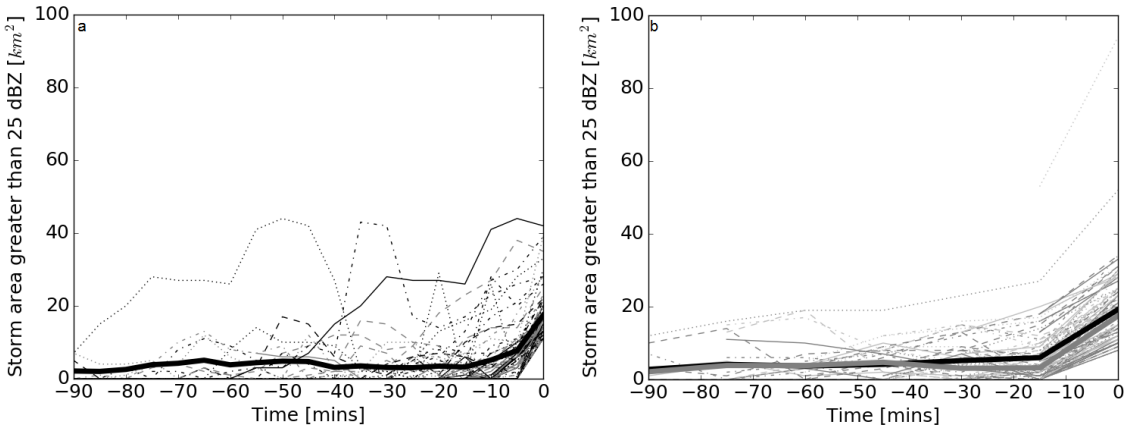

Figure 5.6: Lines showing the storm core area before an intensification (defined as an increase of 10 km2 in storm core area in 15 minutes or less) for (a) radar observations; and (b) the forward modelled radar output from the model. In both plots the black bold line shows the mean, in (b) the grey bold line shows the mean from (a) at the same temporal resolution as the mean in (b).

simulated microphysical properties of the similar modelled intensifications to understand potential physical mechanisms occurring during the observed intensifications and whether the microphysics relates to thunderstorm electrification.

Within the model, the graupel mass, the updraft area greater than 1 ms^{-1} at the melting layer and maximum updraft velocity in the storm core were measured before and after the model intensifications. The differences across the intensification for all parameters were plotted in boxplots in Figure 5.7. Each boxplot shows that approximately 75% of the storms increase in their respective parameter across an intensification. Each boxplot also shows that the distributions are slightly positively skewed. Although in each parameter the lower quartile value is near 0, there is still a portion of the distribution that shows a decrease across an intensification.

The boxplots in Figure 5.7 show, on average, for all of the parameters examined in the model, an increase across an intensification. This follows the expectation that as reflectivity is increased and high reflectivity is observed over a larger area there must be more and/or larger particles present in the cloud. The decreases shown in each variable may relate to the fact that (as shown in Figures 5.5 and 5.6a) not all intensifications lead to the onset of lightning. Figure 5.7b tells us that at least a part of this increase in reflectivity is due to an increase in graupel mass within the

storm core. Linked to this is an increase in both updraft area and peak updraft velocity. These are again linked to the formation of graupel as supercooled liquid (suspended in the mixed-phase region by the updraft) is required to rime ice and thereby create graupel. The riming process can feedback to the updraft through releasing latent heat, thereby increasing buoyancy and the updraft velocity. It can be surmised that during the process of an intensification the increase in updraft area (causing an increase in riming) creates an increase in graupel mass and therefore an observable increase in radar reflectivity.

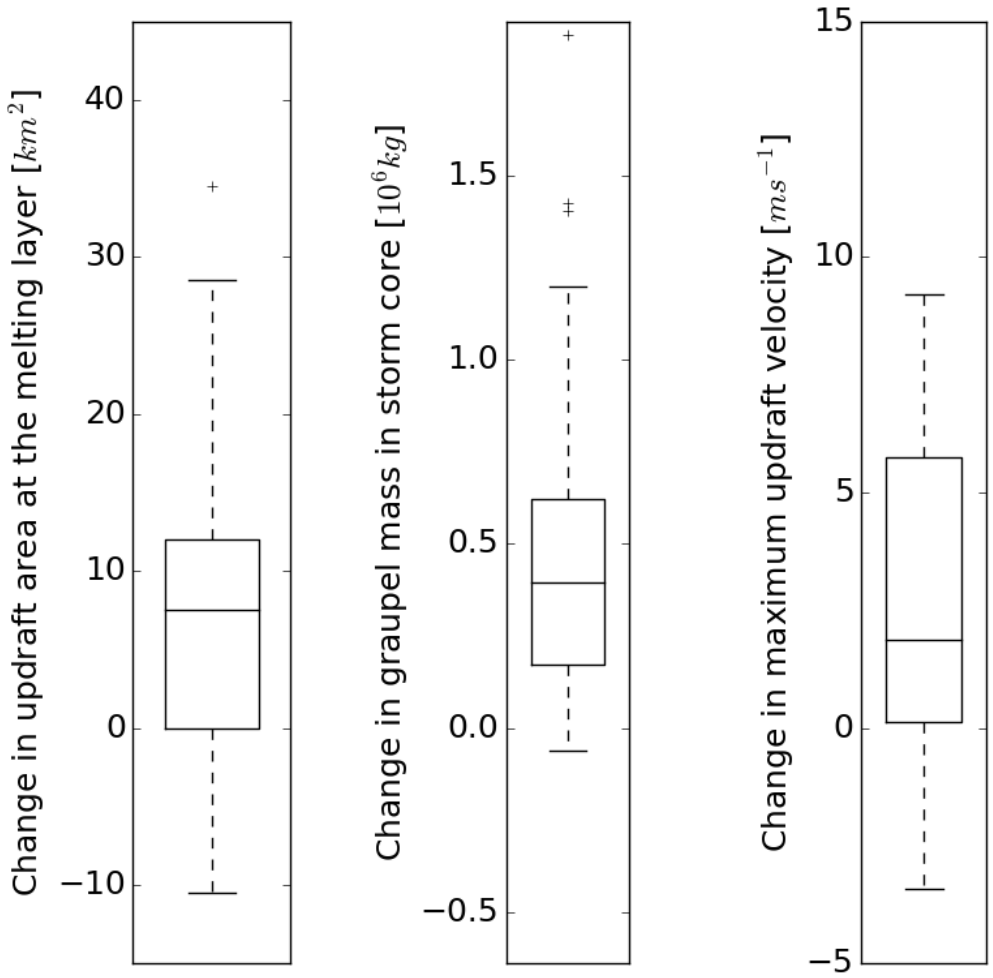

Figure 5.7: Boxplots showing the change in microphysical parameters across the intensifications observed in the model: (a) shows the change in updraft area within the storm at the level of the melting layer (2.5 km); (b) shows the change in graupel mass within the storm core, above the melting layer; (c) shows the change in maximum updraft velocity within the storm core, above the melting layer.

5.4 Discussion

5.4.1 Thunderstorm electrification through rapid intensifications

The rapid intensifications are important for thunderstorm charging in particular because of the increase in graupel mass and maximum updraft velocity shown in Figure 5.7. The graupel is the most obviously necessary as (according to the NIC theory) graupel and ice crystals must be present to separate charge. The increase in graupel mass in the majority of storms allows for the creation and storage of an increased amount of charge within the storm. This is especially important for single cell storms as, frequently, before the storm underwent an intensification the mass of graupel present in the storm was too small to allow enough charge for a lightning strike (see table 5.2, it is estimated that the order of 10^5 kg of graupel is needed to store enough charge to generate a lightning strike). This seems to corroborate the speculation of section 4.5 that graupel mass is a limiting factor of thunderstorm charging in the UK and therefore lightning production within single cell storms.

	Graupel Mass [10^6kg]			Updraft Area at the Melting Layer [km^2]			Maximum Updraft Velocity [ms^{-1}]		
	Start	End	Difference	Start	End	Difference	Start	End	Difference
Min	0.00	0.0006	-0.19	0	0	-8	0.27	1.05	-3.84
Lower Quartile	0.003	0.12	0.07	1	6	0	1.64	4.61	0.0049
Median	0.014	0.30	0.22	4	9	3.5	3.86	6.15	1.44
Upper Quartile	0.097	0.62	0.47	10	15	7.75	5.74	7.81	4.08
Max	2.14	2.22	1.26	30	41	20	12.3	12.6	9.00

Table 5.2: The raw data for Figure 5.7

The updraft velocity is also important for the charging process, not just in the creation of graupel. A strong updraft is necessary to suspend large graupel particles after collisional charging and to separate the graupel and ice crystals through the lofting of ice crystals to the top of the cloud. Further to this, Bruning and MacGorman (2013) speculate that the turbulence created due to the shear at the edge of the updraft can help to cause charge separation through mixing of particles in turbulent eddies. This could be another mechanism by which the increase in

updraft strength shown in Figure 5.7 promotes thunderstorm charging.

Therefore, both an increase in updraft area and in updraft strength are important for storm charging and therefore the onset of lightning. With just a broad weak updraft there may be a large amount of graupel formed, but no strength to suspend it while charge separation occurs and to allow separation of the graupel from the cloud ice. However, equally, if there is just a narrow strong updraft there may not be enough graupel generation to allow for a significant amount of charge to be generated within the storm.

5.4.2 Low or zero lightning convective storms

It is suggested that this intensification process is of such importance in the UK because of the limiting factor that graupel mass appears to present to storm electrification. Figure 5.1 shows that there are storms that produce one or two lightning strikes, and some storms that look similar in reflectivity but produce no lightning. The low lightning convective storms and zero lightning convective storms are a unique challenge to forecast due to their marginality. However the results of this study suggests that there is a possibility to at least nowcast the onset of lightning in these storms with a lead time of up to 30 minutes.

In Figure 5.5 some storms can be observed to exist for 90 minutes before eventually intensifying and then producing lightning, this further suggests that the intensification is vital for storm electrification. However, in Figure 4a there are also many storms that can be observed to intensify in a similar way to the lightning producing storms, without producing lightning (37 of 71 intensifications do not result in lightning). Therefore it is suggested that the intensification (while necessary itself) is not the only process that is required to produce lightning in single cell storms. It is possible that in observing storm intensifications we are only observing one part of the entire lightning generation process (i.e. the generation of the microphysical ingredients necessary for electrification) and missing other steps, such as the charge separation and the triggering of lightning.

5.5 Use of rapid intensifications in nowcasting

As mentioned in section 5.4.2 a possible application of the observed intensification of storms prior to the onset of lightning is in nowcasting. For the majority of storms in Figure 5.5, it appears that a forecast lead time of 10-15 minutes can be obtained using the intensification of the storm core, with as much as 30 minutes being observed on occasion.

Contingency tables such as the example in Table 5.3 are commonly used to express the ability of a binary forecast. From these tables several measures of the accuracy of a forecast can be shown. Often used are the hit rate (H):

$$H = \frac{a}{(a+c)},$$

the false alarm rate (F):

$$F = \frac{b}{(b+d)},$$

the false alarm ratio (FAR):

$$FAR = \frac{b}{(b+a)},$$

and the frequency bias (B):

$$B = \frac{(a+b)}{(a+c)},$$

where a, b, c and d are correct forecasts, false alarms, misses, and correct nulls respectively.

However, many of these measures are not useful for the forecasting of rare events such as lightning. In these forecasts, the correct nulls must be taken into account, however not to the extent that an entirely null forecast would be considered more skilful than actually forecasting (Gilbert, 1884).

With this in mind, Ferro and Stephenson (2011) developed the Symmetric Extremal Dependence Index (SEDI),

$$SEDI = \frac{lnF - lnH + ln\,(1-H) - ln\,(1-F)}{lnF + lnH + ln\,(1-H) + ln\,(1-F)}.$$

This measure has the benefits of converging to a meaningful score as the number of events forecast approaches 0, being difficult to hedge and having a regular range of -1 to 1. However, it still does not take into account any measure of forecast bias, specifically the number of false alarms. As such, two measures are used from this point on, SEDI and FAR. Together these two scores should provide adequate information to judge the performance of the nowcasting metric.

In order to test the usefulness of core intensification as a nowcasting metric, storms were tracked in two days of observations (2012/08/06 and 2017/08/31). The nowcasting metric was trained in these days to optimise the SEDI score for predicting the onset of lightning from storm core intensifications. Both the storm core area required and the time over which it intensified were varied. The training of the metric gave the best measure as an absolute increase of 10 km^2 in storm core area within 15 minutes. The results of using this definition of an intensification are shown in table 5.3.

In the training days this metric could predict a lightning strike within 30 minutes after the intensification in 80.5% of cases. However with this prediction there was also a large number of false alarms, resulting in a false alarm ratio (FAR) of 0.51.

		Observed								
		2012/08/06			2017/08/31			Total		
		Yes	No	Total	Yes	No	Total	Yes	No	Total
Predicted	Yes	17	21	38	12	9	21	29	30	59
	No	2	1900	1902	5	2694	2699	7	4594	4601
	Total	19	1921	1940	17	2703	2720	36	4624	4660
									SEDI	0.94
									FAR	0.51

Table 5.3: Contingency table showing the results of the two training days for the nowcasting application

Having been trained on the two days mentioned above to optimise the SEDI score, the nowcasting metric was then tested on four further days of convection.

Of the testing days that were chosen, three were lightning cases and one a non-lightning case. The three lightning cases were a larger scale convective day, with a mix of organised and short-lived convection (2012/08/25); another day with fair-weather convection (2011/08/07); and a frontal case with embedded convection and convection in the wake of the front (2012/05/14). The other day was a day with convection, but no lightning (2012/06/22). These days were chosen to test the metric in situations different to the original training days and to confirm that the metric does not predict lightning on days where none is present. The results of these tests are recorded in table 5.4.

The results of the testing days did not show the same level of skill as was displayed in the training days. The best SEDI score was on 2011/08/07, the day with fair-weather convection. The SEDI score was 0.81, somewhat lower than the SEDI score of the training days of 0.94, though the FAR was also quite low in this case at 0.38. The day with convection but no lightning was well forecast with no lightning predicted either. The other two days, however, both had much lower SEDI scores at 0.75. Although the FAR in these two days was the same or lower than the training days, the lack of skill in the correct predictions means that the intensification metric does not have useful predictive skill.

Overall there were more missed lightning flashes than correctly predicted flashes on each of the testing days, other than the day with no lightning. In examining the individual missed cases on 25/08/2012 it was found that in many of these cases lightning was produced at very low reflectivity. Figure 5.8 shows storms at the point of the onset of lightning (reflectivity shown uses the same composite as described in section 5.2.2). It can be seen that two of the storms have no reflectivity above 20 dBZ and the final storm has only six gridpoints above 25 dBZ. The very low reflectivity of storms producing lightning was unexpected. The reflectivity threshold used for the intensification could not be updated to improve the predictability for these cases without including a large number of false alarms.

		Observed														
		2011/08/07			2012/05/14			2012/06/22			2012/08/25			Total		
		Yes	No	Total	Yes	No	Total	Yes	No	Total	Yes	No	Total	Yes	No	Total
Predicted	Yes	5	3	8	1	3	4	0	0	0	19	3	22	25	9	36
	No	6	2658	2664	6	1063	1069	0	356	356	33	2387	2420	47	6464	6511
	Total	11	2663	2674	7	1066	1073	0	356	356	52	2390	2442	72	6475	6547
			SEDI	0.81		SEDI	0.75					SEDI	0.75		SEDI	0.74
			FAR	0.38		FAR	0.51					FAR	0.14		FAR	0.26

Table 5.4: Contingency table showing the results of the four test days for the nowcasting application

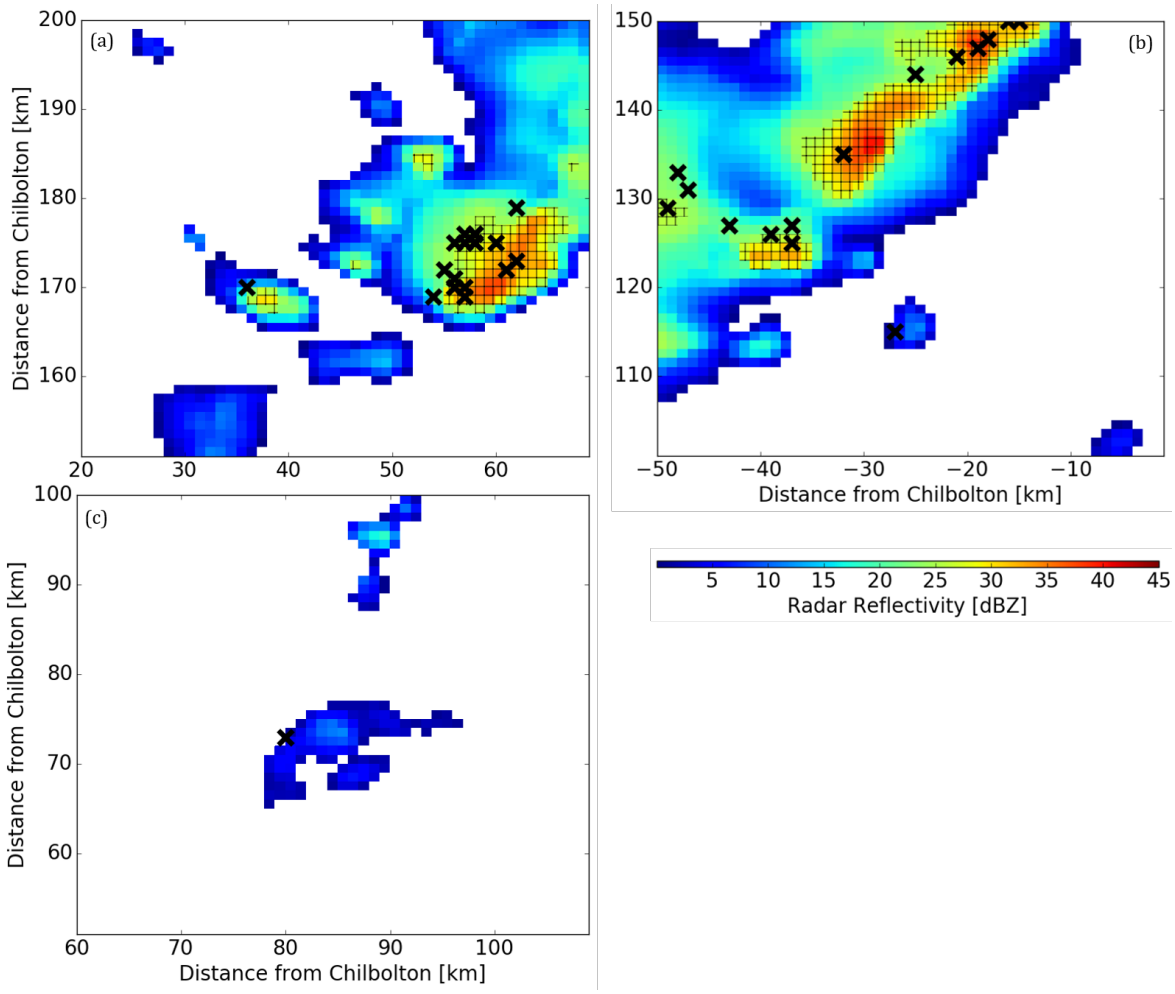

Figure 5.8: Plots showing the onset of lightning in three small thunderstorms. Black crosses show the location of lightning strikes and hashing shows regions with reflectivity above 25 dBZ, i.e. areas designated as a storm core in section 5.2.2. All snapshots are from 25/08/2012 (a) is at 13:30, (b) is at 13:00 and (c) is at 11:40

5.6 Conclusions

This work shows that marginal single cell storms in the UK undergo a rapid intensification and increase in storm core size prior to the onset of lightning. Closer examination of the microphysics of similar intensifications simulated in the Met Office UKV model show that the observed intensifications may be due to an increase in the graupel mass in the storm core, this in turn is likely related to an increase in the updraft area at the melting layer. Further, during the intensification, there is also an increase in the peak updraft velocity which can cause turbulent mixing of graupel and cloud ice and aids the charging and charge separation processes. However,

although almost all observations of lightning from single cell thunderstorms were preceded by an intensification, not all intensifications led to lightning. Therefore, it is assumed that there are other factors involved in the production of lightning from a small convective storm. Further work is needed to identify the other processes that are necessary for lightning production. The use of intensifications as a nowcasting metric appears to have skill in cases of small single cell storms, allowing for the prediction of the onset of lightning up to 30 minutes in advance. However, the metric does not appear to work in other synoptic situations.

Chapter 6

Evolution of thunderstorms from the model lightning output

6.1 Introduction

Another motive for developing an explicit electrification scheme is that it should produce a more realistic representation of thunderstorm lightning timing through a better representation of the evolution of the microphysics associated with electrification. This will allow the use of the electrification scheme in studying other aspects of thunderstorms.

In this section the analysis from section 5.3 is repeated using the storms and lightning data as modelled by both the new electrification scheme and the MC09 parameterisation (the uncorrected version). Because neither method of forecasting lightning feeds back to the rest of the model, the only difference in the thunderstorms in the two data sets is which storms produce lightning and the timing and the timing of the lightning within the storms. The intensity of the storm core will be investigated in the lead up to lightning onset within thunderstorms in the model. The flash rate of single cell thunderstorms from the MC09 parameterisation and the new scheme are also compared to that of observations.

6.2 Results

Figure 6.1 show the same evolution of the storm core before the onset of lightning as is shown in Figure 5.5. The lightning data used for this plot is taken from the forecast of the new electrification scheme. The thick black line is the mean of the

individual lines and the thick grey line is the mean from Figure 5.5. It can be seen that there is an increase in storm core area prior to the onset of lightning, as predicted by the new electrification scheme in modelled storms. It is a shallower increase than the observations, though the magnitude of the overall increase is similar. In the 20 minutes before the onset of lightning, the mean increases from 9.8 km^2 to 16.1 km^2, compared to the increase from 6.7 km^2 to 13.3 km^2 from the observations.

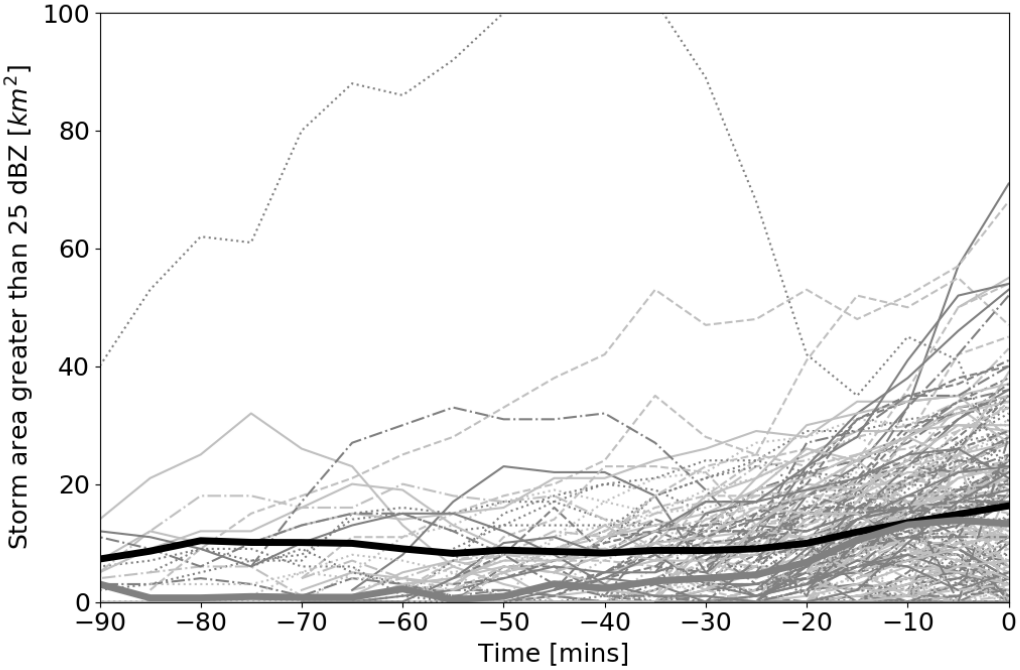

Figure 6.1: Lines showing the increase in storm core area for all single cell thunderstorms in the time before the onset of lightning, as modelled by the new electrification scheme, at time 0. The bold black line shows the mean, the bold grey line shows the mean of the observations from Figure 5.5.

The mean of the core area of the modelled storms is consistently greater than that of the observations throughout the 90 minutes before the onset of lightning. This means that the core area for lightning producing storms is, on average, larger in the model than in the observations.

In contrast, the intensification of the modelled storms prior to the onset of lightning as predicted by the MC09 parameterisation in figure 6.2 closely follow

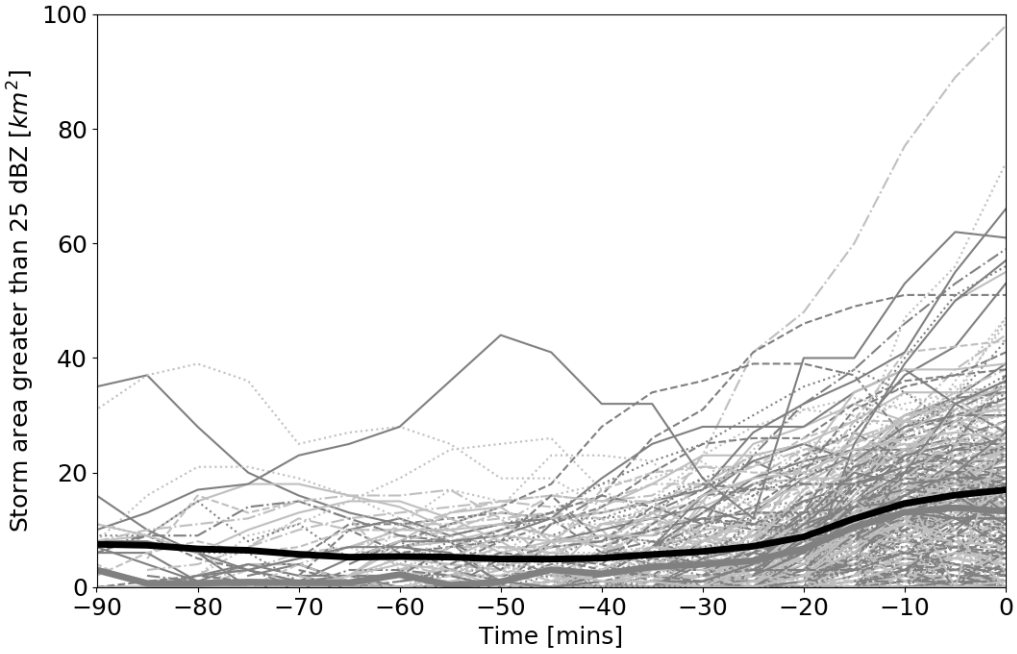

Figure 6.2: As Figure 6.1 but using the lightning data as modelled by the MC09 parameterisation instead.

the mean of the observations. The mean stays quite small through the majority of the graph however, at -20 minutes the storm core begins to increase rapidly in area. The magnitude of the intensification is actually slightly larger than the observations, as the storms in which the MC09 parameterisation predicts lightning continue increasing in core area right up to the onset of lightning, whereas the mean of the observations flattens out at -5 minutes.

This shows that the MC09 parameterisation is predicting the onset of lightning more accurately than the new scheme, and initially suggests that the MC09 parameterisation is therefore representing the storm evolution better than the new scheme. In order to investigate this the boxplots shown in Figure 5.7 have been replicated here. Change in cloud ice mass has been included because, as discussed in section 4.5, ice mass is the primary influence on the production of lightning in the MC09 parameterisation and also has an important role in the new scheme.

The boxplots corresponding to the changes in microphysics in the 15 minutes prior to the onset of lightning in the new scheme are shown in Figure 6.3. These

show generally good agreement with the boxplots shown in Figure 5.7. Both the change in graupel mass and the change in updraft area at 2.5 km altitude are matched well by the new scheme with around 75% of the distribution increasing in both cases and the distributions being positively skewed. The magnitude of the change in updraft area and graupel mass is slightly larger for the new scheme as compared to the observations of the intensifications. There is a large difference in the distribution of the change in maximum updraft velocity. While still being somewhat positively skewed, the median is slightly negative compared to the 25th percentile of the data being positive in the observations. The distribution of the change in ice mass is similar to that of the change in graupel mass, although the magnitude of the change is larger.

The same boxplots but for the MC09 parameterisation in Figure 6.4 show a largely different story. Each of the boxplots for change in updraft area, change in graupel mass, and change in maximum updraft velocity show a distribution which suggests that there is no significant change in any of the parameters in the 15 minutes prior to the onset of lightning. There is a positive change in the ice mass prior to the onset of lightning, as is expected given the method that the parameterisation used to predict lightning. Although even this generally positive change has a large negative tail.

This suggests that, even though the MC09 parameterisation is quite accurately predicting the correct timing of the onset of lightning with respect to the evolution of the storm core, it appears to be doing it for the wrong reasons. The new scheme is better at capturing the changes of storms in the intensifications prior to lightning, even though the storms are not intensifying as much in that scheme.

The individual storm tracks that can be seen in Figure 4.6b seem to suggest that the flash rate of a storm peaks soon after the storm starts producing lightning. This appears to be relatively well reproduced in the new scheme's storm tracks in Figure 4.6a, but the tracks in the MC09 parameterisation in Figure 4.6c seem to show the peak of lightning further on in the storm's lifetime.

In order to investigate if this is indeed the case the flashes produced by the

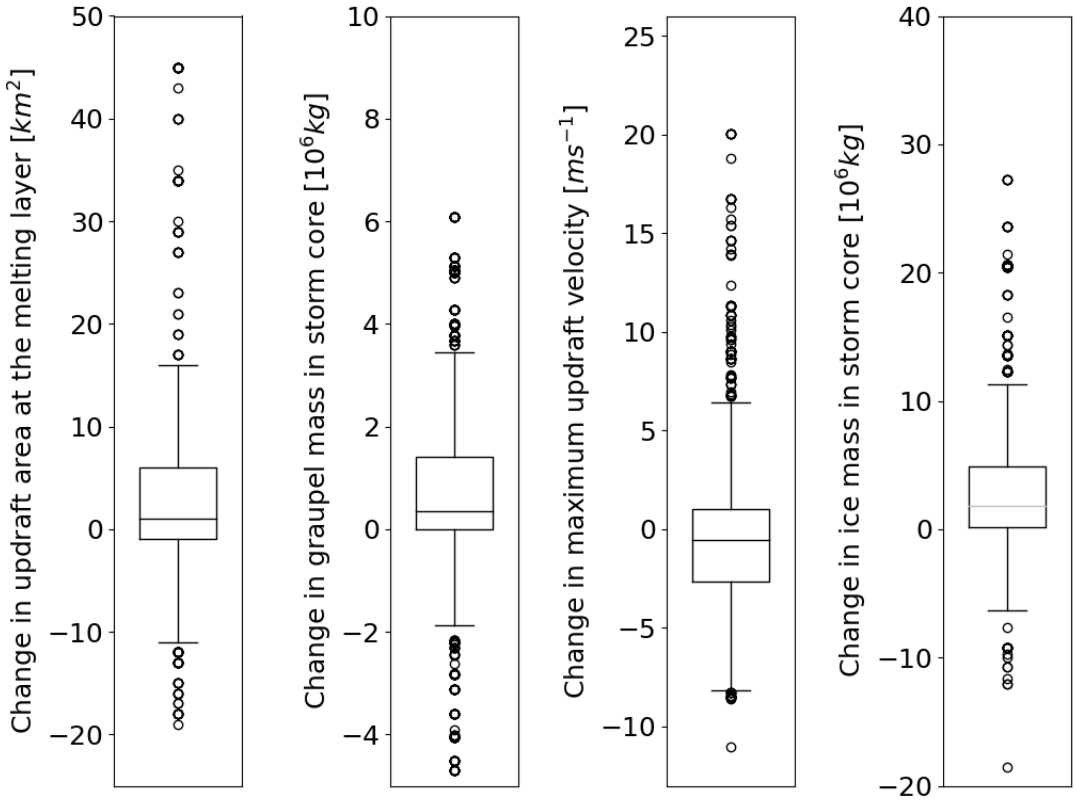

Figure 6.3: Boxplots showing the change in microphysical parameters across the final 15 minutes before the onset of lightning as modelled by the new electrification scheme: (a) shows the change in updraft area within the storm at the level of the melting layer (2.5 km); (b) shows the change in graupel mass within the storm core, above the melting layer; (c) shows the change in maximum updraft velocity within the storm core, above the melting layer; (d) shows the change in total ice mass within the storm core, above the melting layer.

tracked single cell storms were recorded for the duration of the storms' lifetimes. The flash numbers were accumulated every five minutes. The means of all lightning producing single cell storms for the MC09 scheme, the new scheme and the observations are shown in Figure 6.5, where the time on the x-axis starts at the onset of lightning in each storm.

The means of lightning flashes in the lifetime of observed storms and those modelled by the new scheme follow mostly similar paths, with an initial peak followed by a rapid decrease in the flash rate and a long tail of low flash rate. The MC09 parameterisation on the other hand is very different. The much larger flash rate is expected and has been commented on. But in terms of the evolution of the flash

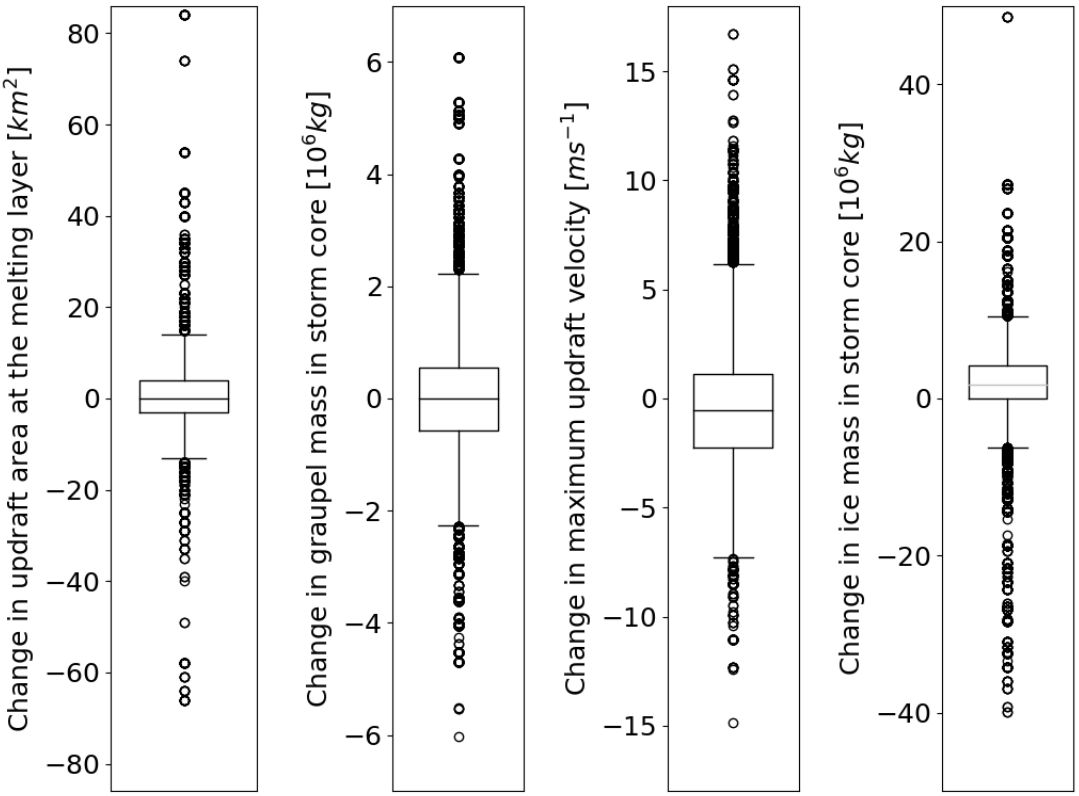

Figure 6.4: As Figure 6.3, but using the MC09 parameterisation for the lightning data.

rate, the peak of the flash rate is on average about 30 minutes after the storm starts to produce lightning. The tail of the flash rate is much more linear than the other two lines, the flash rate reduces less rapidly after the peak than either the observations or the new scheme.

6.3 Discussion

The MC09 parameterisation appears to match the observations of single-cell thunderstorms well in Figure 6.2. In particular there is a similar intensification of the storm core area in the lead up to the onset of lightning within the storms. This suggests that the MC09 parameterisation accurately represents how the size of the storm core changes before the onset of lightning. However the reasons behind it doing this do not appear to be correct. In the 15 minutes prior to the onset of

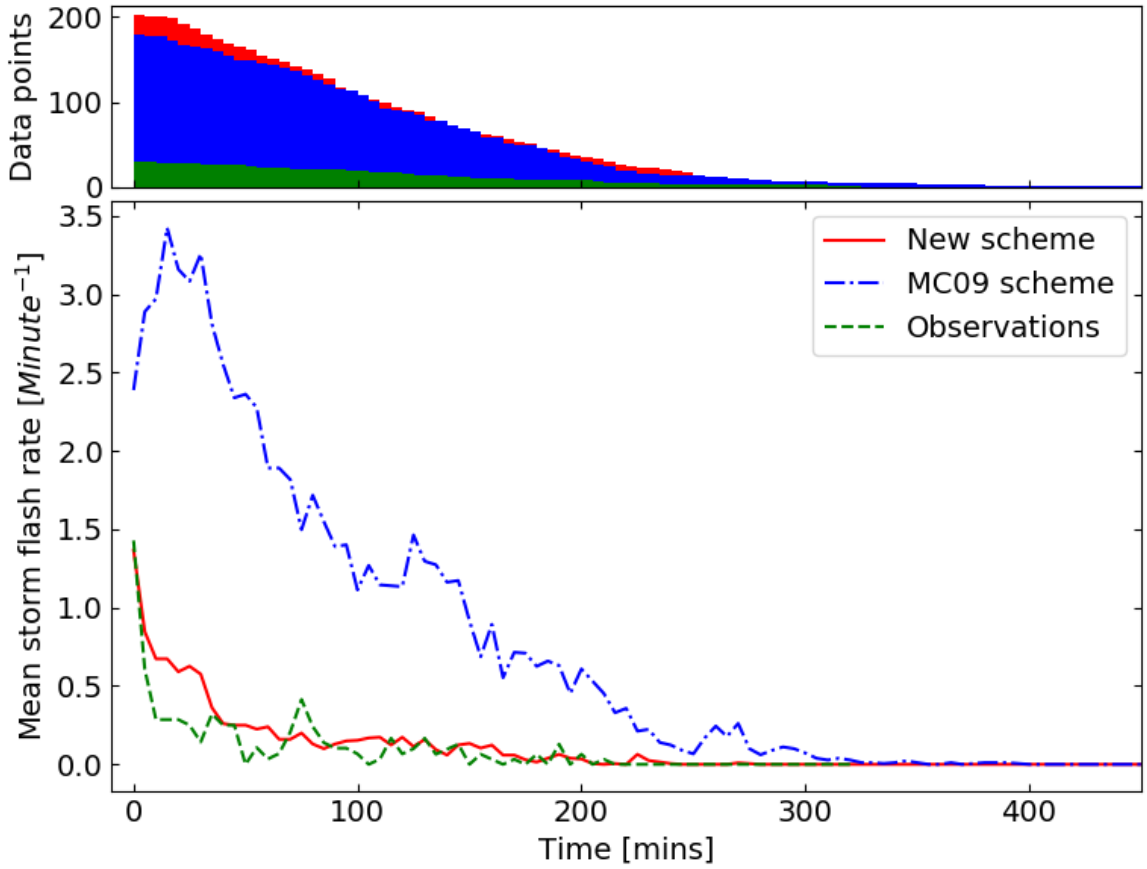

Figure 6.5: Lines showing the mean flash rate in a storm for single cell storms producing lightning in both parameterisation schemes on the day of 31st August 2017. Flashes from the new scheme are shown in red solid lines, flashes from the MC09 scheme are shown in dot dashed blue lines. The x axis is normalised for each line such that lightning begins at time 0 for each method. Storms that dissipate before all storms stop producing lightning are still included in the calculation of the mean.

lightning, shown in Figure 6.4, the change of the updraft area, maximum updraft velocity and graupel mass appear quite different to the change in the same parameters for the intensifications linked to the observations, shown in Figure 5.7. There does not appear to be any signal to the change in these parameters in the MC09 parameterisation. There does appear to be an increase in the cloud ice mass within the storm core prior to the onset of lightning though. This is to be expected, because of the way that the MC09 parameterisation predicts lightning, but again highlights the relative importance of cloud ice compared to graupel for the MC09 parameterisation. Further, the flash rate after the onset of lightning also appears to

be incorrect, compared to the observations for single-cell thunderstorms. The MC09 parameterisation on average increases in lightning flash rate for around 30 minutes after the onset of lightning and then decreases quite linearly, continuing to produce lightning for considerably longer than the observations. This large peak 30 minutes after the onset of lightning suggests that the MC09 parameterisation depends too heavily on parameters that peak too late in the thunderstorm life-cycle.

On the other hand the new scheme appears to be much more physically accurate. The intensification of the storm core prior to the onset of lightning shown in Figure 6.1 is not as strong as that in the observations. However, there is still an increase in the storm core area leading up to the first lightning flash. With this intensification the microphysics occurring within the 15 minutes before the onset of lightning appear to match relatively closely the changes shown in Figure 5.7. Figure 6.3 shows that the updraft area generally increases during the lead up to lightning, while the maximum updraft velocity has no clear signal. The clearest increase is from both the graupel mass and the ice mass in the storm core. This is to be expected as the new electrification scheme depends heavily on both of these factors. In terms of the production of lightning within the lifetime of a single-cell thunderstorm, the new scheme matches the observations well. The peak of the production of lightning in the thunderstorm is right at the onset of lightning (this is due to the fact that the lifetimes have been aligned by the onset of lightning). The new scheme and the observations then both drop quickly towards a flash rate of $0\,\mathrm{min}^{-1}$. Though most storms making up the means do not only have one lightning flash the subsequent flashes are generally rare and sporadic. This suggests that there is not much change in the intensity of the thunderstorm after the intensification leading to the onset of lightning.

6.4 Conclusions

The evolution of the storm core prior to the onset of lightning has been analysed for thunderstorms as modelled by both the new electrification scheme and the MC09

parameterisation. These two methods use the same storms from the model, only changing the production and timing of lightning within those storms. The MC09 parameterisation appears to represent the intensification of the storm core area well prior to the onset of lightning, the new electrification scheme on the other does not reproduce the observations as closely.

In terms of the microphysics the new scheme again represents the observations well, but not perfectly. The strongest increases in the new scheme are seen in the parameters that most directly influence the electrification scheme, that is the graupel and cloud ice mass. This was also seen in the MC09 parameterisation, where the cloud ice was the only parameter which tended to increase before the onset of lightning. The other parameters for the MC09 storms showed no clear increase or decrease before the onset of lightning.

After the first lightning flash, the storms producing lightning in the MC09 parameterisation briefly increase in flash rate to a peak of just less than 3.5 flashes per minute. The storms producing lightning in the new scheme appear much more similar to the observations of thunderstorms. Both, on average, peak immediately at the onset of lightning, before rapidly decreasing to less than 0.5 flashes per minute. The flash rate then remains at this level as flashes are intermittently produced in the storms.

The MC09 parameterisation does not appear to correctly model the evolution of the lightning flash rate after the onset of lightning. Although it does well in capturing the size of the storm core before the onset of lightning, it appears that it may do this for the wrong reasons. The new scheme on the other hand appears to match the physical observations well in most aspects of the timing and evolution of the production of lightning and the microphysics causing lightning.

Chapter 7

Summary

7.1 Overview

The forecasting of lightning is a difficult problem both in terms of the forecasting itself and the verification of the forecast. Any lightning forecast must depend on the convective forecast to produce the parameters that lightning parameterisations are based on. These are often measures of the intensity of convection, such as cloud top height or CAPE. In convection permitting models the parameters used to predict lightning are more related to the production of charge and thunderstorm electrification, however, these still depend on the convection being in the correct location and at the correct intensity.

Two methods of analysing the accuracy of the current lightning parameterisation (the MC09 scheme) in the MetUM are presented. In Chapter 3 a new, physically based, explicit electrification scheme is described and implemented within the infrastructure of the MetUM, examples of the charge structure and other output from the scheme are shown. This new scheme is compared to the MC09 parameterisation in Chapter 4 and both are compared to observations in two case studies. Observations of thunderstorm development in relation to thunderstorm electrification and the production of lightning are shown in Chapter 5, these are compared to the development of thunderstorms as forecast by the lightning schemes in the model in Chapter 6.

Some key findings are:

- The explicit electrification and lightning scheme produces charge structures and electric fields comparable to observed values.

- The explicit electrification scheme performs well in both the UK and US case study. Whereas the MC09 parameterisation only performs well in the US case study.
- Single cell thunderstorm cores are found to intensify prior to the onset of lightning. This is attributed to an increase in updraft velocity, updraft area and graupel mass.
- The explicit electrification scheme represents flash rates in relation to storm evolution more realistically than the MC09 parameterisation.

7.2 The explicit electrification scheme

A new electrification scheme was implemented within the MetUM, the scheme used NIC of graupel and cloud ice to generate charge within clouds. The charge generated was based on the collision-separation rate of graupel and cloud ice and varied depending on the CWC and temperature where the collisions occurred. The charge was transferred to other hydrometeor species and moved throughout the cloud together with the hydrometeors that the charge was carried on. The resulting charge density distribution was used to calculate the electric field across the entire domain. The magnitude of the electric field was then used to initiate lightning flashes. A lightning channel was propagated based on an electric field and a charge magnitude threshold. The lightning channel was used to determine where charge was neutralised, charge was removed along the channel and in the immediately neighbouring points. This updated the charge density distribution which was, in turn, used to recalculate the electric field. The lightning discharge routines repeated until there were no new flashes discharged within the timestep in the domain. The collision-separation efficiency was used to tune the scheme and was set to 0.3.

The charge structure and the magnitude of the charge density produced by the electrification scheme appears to be similar to the structure and magnitudes observed in nature.

7.3 Verification of the lightning forecasts

The output of the electrification scheme was compared against observations and against the MC09 parameterisation for two case studies, one small scale convective day in the UK and one day of supercell convection in the US.

In both case studies the new electrification scheme performed well in terms of total lightning accumulation. The MC09 parameterisation performed well for the US case study but greatly over-forecast the total lightning accumulation for the UK case study. In terms of coverage the new electrification scheme again performed well in both cases. The main issue with the new electrification scheme was in the highest intensity grid boxes. In these locations the new electrification scheme over-forecast the amount of lightning produced. Nevertheless, the scheme did appear able to reproduce the scattered nature of the lightning observations. The MC09 parameterisation did not perform so well in this aspect, the parameterisation consistently produced lightning output that appeared too smoothly contoured, without the individual scattered flashes. This is likely due to the MC09 parameterisation over-producing lightning at mid-intensity rainfall rates. There was little difference between the two forecasting methods in terms of the location forecast and both appeared to be strongly linked to the accuracy of the convection forecast.

Corrections to the MC09 parameterisation showed an improvement to the forecast of total lightning in the UK. However, the change also reduced the total lightning accumulation in the US causing that forecast to become worse.

It is suggested that the high intensity grid boxes within the new electrification scheme may be due to the collision-separation efficiency within regions where graupel may be undergoing wet growth. In these locations (likely to be in the storms cores) graupel and cloud ice particles should be much less likely to separate after colliding, thereby greatly reducing the production of charge and the lightning flash rate.

7.4 Observations of thunderstorm electrification and comparison with the lightning schemes

Observations of single cell thunderstorms in the time before they started to produce lightning showed that the storm core area increases in the 20 minutes before the onset of lightning. The intensifications of the storms were also present in UKV model runs of the same case studies that the intensifications were observed in. The microphysics observed in those intensifications showed that there were increases in the peak updraft velocity, the updraft area and the graupel mass in the storm core during the intensification.

Though almost all single cell thunderstorms intensified before producing lightning for the first time, not all intensifications caused the onset of lightning. This suggests that there are other changes occurring alongside the intensification that also lead to the production of lightning.

Similar analysis using the lightning output produced by the MC09 parameterisation and the new electrification scheme showed that the new scheme better represented the observations in terms of the microphysics, in particular, the new scheme replicated the increases of the graupel mass and the updraft area. The MC09 parameterisation captured the increase in storm core area well, but did not reproduce the microphysics well, the only clear change was an increase in the cloud ice mass. Further, the new scheme matched the evolution of the lightning flash rate in single cell thunderstorms, whereas the MC09 parameterisation produced too much lightning, in particular for the first 30 minutes following the onset of lightning.

Therefore, not only does the new electrification scheme perform better as a lightning forecasting tool than the MC09 parameterisation, but it also represents observations of lightning and electrification in thunderstorm evolution better. This second point is more important for a complex scheme such as this one. The electrification scheme could not be run operationally due to the high computational expense, but given that it has been shown to represent physical thunderstorm pro-

cesses as well as forecasting lightning, this scheme can also be used as a research tool to investigate the role of charge in clouds and thunderstorm processes.

Chapter 8

Future Work

8.1 Thunderstorm electrification scheme

There are numerous elements that can and should be added to this scheme to make it more complete and to aid other areas of study. One of the more pressing issues encountered with this and other explicit electrification schemes is the difficulty of distinguishing between IC and CG flashes. Currently this scheme only deals with total lightning and does not classify flashes. For flash classification to be included, the proportion of IC to CG flashes would need to be analysed and compared to observations, (likely LMA observations as the ATDNet does not classify flashes into IC or CG). Barthe *et al.* (2012) made a decision based on Mansell *et al.* (2005) to classify any channel reaching 2 km above the surface as a CG flash, it is likely a similar assumption will need to be made with this scheme.

Once flashes have been classified into CG and IC another problem is presented. IC flashes are charge conserving across the channel. That is, all charge neutralised within the channel must have originated somewhere else in the storm, therefore there should be no net charge change for an IC flash. This is not the case for a CG flash, where the surface is treated as being an unlimited source of charge of the necessary sign. This means that a charge conservation scheme must also be included for IC flashes.

Other changes, beyond these initial additions, could add detail to the scheme and make the scheme more complete. The inclusion of other methods of charging, such as ion capture and inductive charging, would accomplish this.

Though they would likely not change the charging of convective storms greatly (Helsdon *et al.*, 2002), the inclusion of the Wilson current and differences in con-

ductivity based on the water content of the air would allow for the modelling of charge screening layers. This would allow the representation of charge in layer clouds where there is no graupel present. The inclusion of these charge screening layers, together with the representation of charge effects on microphysical processes, such as collision-coalescence efficiency and evaporation rate (Harrison *et al.*, 2015), would allow for a modelling study on the impact of charge on layer cloud.

In order to increase the accuracy of the physical representation of the model, the collision-separation efficiency should be based on observations, rather than used as a tunable parameter. The collision-separation efficiency should also be a function of several other parameters, most importantly temperature and some measure of the liquid on the surface of the ice particles. This could be a proxy such as LWC or hail mass, or a relevant diagnosed property. It should be possible to diagnose the particle surface temperature from the graupel riming growth rate. This could be used to reduce the collision-separation efficiency to zero, when the particle surface temperature increases above freezing.

8.1.1 High resolution model

In order to allow the model to run at higher resolution than 1.5 km, the code must be changed to allow for gridpoints in the neighbouring processor to be altered by a lightning channel. Once this is changed, the model can be run at higher resolution, such as 500 m or 200 m. The representation of convection at these resolutions has already been examined by Stein *et al.* (2014), who found that these resolutions better represented deep convection in the UK than the 1.5 km resolution. However, the storm core in the higher resolution runs increased and was larger than observed in a composite of radar observed storms.

It would be interesting to examine the response of the electrification scheme, not only to the change of the discharge scheme to including multiple grid points surrounding the channel in each direction, but also the larger storm core in the higher resolution models.

8.2 Lightning parameterisation

Another interesting area of further work would be in developing a new lightning parameterisation, based on the discussion of section 4.5. As mentioned in that section, a new parameterisation should limit the production of lightning on the basis of graupel mass (or graupel number density if convenient). It would be interesting to train the parameterisation on US data and examine whether it still over-predicts lightning within the UK. Conversely, it would also be interesting to train the parameterisation on UK data and examine whether a US forecast is then made less accurate.

Appendix A

Output parameters from the new electrification scheme

Table A.1 shows the parameters introduced in the new electrification scheme that can be output by the scheme. The first four parameters are prognostic variables, others are all diagnostic. The parameters with an item code starting 21/2– were included in the code by Jon Wilkinson.

STASH item code	Diagnostic	Unit
00/615	Charge density on aggregates	Cm^{-3}
00/616	Charge density on ice crystals	Cm^{-3}
00/617	Charge density on rain	Cm^{-3}
00/618	Charge density on graupel	Cm^{-3}
21/107	Electric potential	V
21/108	Electric field in the x direction	Vm^{-1}
21/109	Electric field in the y direction	Vm^{-1}
21/110	Electric field in the z direction	Vm^{-1}
21/111	Electric field magnitude	Vm^{-1}
21/112	Total charge density before advection	Cm^{-3}
21/113	Number of CG flashes	–
21/114	Number of IC flashes	–
21/115	Lightning type	–
21/116	Lightning channel location	–
21/117	Charge density on aggregates before advection	Cm^{-3}
21/118	Charge density on ice crystals before advection	Cm^{-3}
21/119	Charge density on rain before advection	Cm^{-3}
21/120	Charge density on graupel before advection	Cm^{-3}
21/121	Neutralised charge	Cm^{-3}
21/122	Total number of lightning flashes	–
21/201	Aggregate charge density increment	$Cm^{-3}s^{-1}$
21/202	Crystal charge density increment	$Cm^{-3}s^{-1}$
21/203	Rain charge density increment	$Cm^{-3}s^{-1}$
21/204	Graupel charge density increment	$Cm^{-3}s^{-1}$
21/205	Non-inductive charging rate	$Cm^{-3}s^{-1}$
21/206	Aggregate capture charge density transfer rate	$Cm^{-3}s^{-1}$
21/207	Evaporation charge density transfer rate	$Cm^{-3}s^{-1}$
21/208	Sublimation charge density transfer rate	$Cm^{-3}s^{-1}$
21/209	Graupel charge density sedimentation rate	$Cm^{-2}s^{-1}$
21/210	Rain charge density sedimentation rate	$Cm^{-2}s^{-1}$
21/211	Aggregate charge density sedimentation rate	$Cm^{-2}s^{-1}$
21/212	Crystal charge density sedimentation rate	$Cm^{-2}s^{-1}$
21/213	Graupel autoconversion charge density transfer rate	$Cm^{-3}s^{-1}$
21/214	Graupel melting charge density transfer rate	$Cm^{-3}s^{-1}$
21/215	Aggregate melting charge density transfer rate	$Cm^{-3}s^{-1}$
21/216	Crystal melting charge density transfer rate	$Cm^{-3}s^{-1}$
21/217	Crystal capture charge density transfer rate	$Cm^{-3}s^{-1}$
21/218	Crystal sublimation charge density transfer rate	$Cm^{-3}s^{-1}$

Table A.1: Table showing the output from the new electrification scheme

Bibliography

Aufdermaur, A. N. and Johnson, D. A. (1972). Charge separation due to riming in an electric field. *Quarterly Journal of the Royal Meteorological Society*, **98**(416), 369–382.

Baker, B., Baker, M. B., Jayaratne, E. R., Latham, J., and Saunders, C. P. R. (1987). The influence of diffusional growth rates on the charge transfer accompanying rebounding collisions between ice crystals and soft hailstones. *Quarterly Journal of the Royal Meteorological Society*, **113**, 1193–1215.

Barrett, R., Berry, M., Chan, T. F., Demmel, J., Donato, J. M., Dongarra, J., Eijkhout, V., Pozo, R., Romine, C., and Van der Vorst, H. (1994). *Templates for the Solution of Linear Systems Building Blocks for Iterative Methods*.

Barthe, C., Deierling, W., and Barth, M. C. (2010). Estimation of total lightning from various storm parameters: A cloud-resolving model study. *Journal of Geophysical Research Atmospheres*, **115**(24), 1–17.

Barthe, C., Chong, M., Pinty, J.-P., and Escobar, J. (2012). CELLS v1 . 0 : updated and parallelized version of an electrical scheme to simulate multiple electrified clouds and flashes over large domains. *Geoscientific Model Develpment*, (5), 167–184.

Black, R. A. and Hallett, J. (1999). Electrification of the Hurricane. *Journal of the Atmospheric Sciences*, **56**(12), 2004–2028.

Blyth, A. M., Christian, H. J., Driscoll, K., Gadian, A. M., and Latham, J. (2001). Determination of ice precipitation rates and thunderstorm anvil ice contents from satellite observations of lightning. *Atmospheric Research*, **59-60**, 217–229.

Borovsky, J. E. (1995). An electrodynamic description of lightning return strokes and dart leaders: guided wave propagation along conducting cylindrical channels. *Journal of Geophysical Research*, **100**(D2), 2697–2726.

Brooks, I. M., Saunders, C. P. R., Mitzeva, R. P., and Peck, S. L. (1997). The effect on thunderstorm charging of the rate of rime accretion by graupel. *Atmospheric Research*, **43**, 277–295.

Bruning, E. C. and MacGorman, D. R. (2013). Theory and Observations of Controls on Lightning Flash Size Spectra. *Journal of the Atmospheric Sciences*, **70**(12), 4012–4029.

Bruning, E. C., Rust, W. D., Schuur, T. J., MacGorman, D. R., Krehbiel, P. R., and Rison, W. (2007). Electrical and Polarimetric Radar Observations of a Multicell Storm in TELEX. *Monthly Weather Review*, **135**(7), 2525–2544.

Carey, L. D. and Rutledge, S. A. (1996). A multiparameter radar case study of the microphysical and kinematic evolution of a lightning producing storm. *Meteorology and Atmospheric Physics*, **59**(1-2), 33–64.

Carey, L. D. and Rutledge, S. A. (1998). Electrical and multiparameter radar observations of a severe hailstorm. *Journal of Geophysical Research*, **103**, 13979–14000.

Carlson, B. E., Lehtinen, N. G., and Inan, U. S. (2009). Terrestrial gamma ray flash production by lightning current pulses. *Journal of Geophysical Research*, **114**(12), 4–9.

Cecil, D. J., Zipser, E. J., and Nesbitt, S. W. (2002). Reflectivity, Ice Scattering, and Lightning Characteristics of Hurricane Eyewalls and Rainbands. Part I: Quantitative Description. *Monthly Weather Review*, **130**(4), 769–784.

Cecil, D. J., Buechler, D. E., and Blakeslee, R. J. (2014). Gridded lightning climatology from TRMM-LIS and OTD: Dataset description. *Atmospheric Research*, **135-136**, 404–414.

Cifelli, R., Petersen, W. A., Carey, L. D., Rutledge, S. A., and da Silva Dias, M. A. F. (2002). Radar observations of the kinematic , microphysical , and precipitation characteristics of two MCSs in TRMM LBA. *Journal of Geophysical Research*, **107**, 1–16.

Dash, J. G. and Wettlaufer, J. S. (2001). Collisional Charging in Ice and Charge Separation in Thunderstorms. *SAE Technical Paper Series*.

Davies, T., Cullen, M. J., Malcolm, A. J., Mawson, M. H., Staniforth, A., White, A. A., and Wood, N. (2005). A new dynamical core of the Met Office's global and regional modelling of the atmosphere. *Quarterly Journal of the Royal Meteorological Society*, **131**(608), 1759–1782.

Deierling, W. and Petersen, W. A. (2008). Total lightning activity as an indicator of updraft characteristics. *Journal of Geophysical Research Atmospheres*, **113**(16).

Deierling, W., Petersen, W. A., Latham, J., Ellis, S., and Christian, H. J. (2008). The relationship between lightning activity and ice fluxes in thunderstorms. *Journal of Geophysical Research Atmospheres*, **113**(15), 1–20.

DiGangi, E. A., MacGorman, D. R., Ziegler, C. L., Betten, D., Biggerstaff, M., Bowlan, M., and Potvin, C. K. (2016). Journal of Geophysical Research : Atmospheres. *Journal of Geophysical Research: Atmospheres*, **343**, 316–343.

Dwyer, J. R. and Uman, M. A. (2014). The physics of lightning. *Physics Reports*, **534**(4), 147–241.

Dye, J. E. and Bansemer, A. (2019). Electrification in Mesoscale Updrafts of Deep Stratiform and Anvil Clouds in Florida. *Journal of Geophysical Research: Atmospheres*, **124**(2), 1021–1049.

Dye, J. E., Jones, J. J., Winn, W. P., Cerni, T. A., Gardiner, B., Lamb, D., Pitter, R. L., Hallett, J., and Saunders, C. P. R. (1986). Early Electrification and Precipitation Development in a Small , Isolated Montana Cumulonimbus. *Journal of Geophysical Research*, **91**(5), 1231–1247.

Elsom, D. M. and Webb, J. D. C. (2014). Deaths and injuries from lightning in the UK, 1988-2012. *Weather*, **69**(8), 221–226.

Elsom, D. M., Webb, J. D. C., Enno, S.-E., and Horseman, A. (2016). Lightning fatalities and injuries in the UK in 2015 and lightning safety advice for hill and mountain walkers. *The Internation Journal of Meteorology*, **41**(397), 105–126.

Ely, B. L., Orville, R. E., Carey, L. D., and Hodapp, C. L. (2008). Evolution of the total lightning structure in a leading-line , trailing- stratiform mesoscale convective system over Houston , Texas. *Journal of Geophysical Research*, **113**(December 2007), 1–13.

Emersic, C., Heinselman, P. L., MacGorman, D. R., and Bruning, E. C. (2011). Lightning Activity in a Hail-Producing Storm Observed with Phased-Array Radar. *Monthly Weather Review*, **139**, 1809–1825.

Enno, S. E., Anderson, G., and Sugier, J. (2016). ATDnet detection efficiency and cloud lightning detection characteristics from comparison with the HyLMA during HyMeX SOP1. *Journal of Atmospheric and Oceanic Technology*, **33**(9), 1899–1911.

Fierro, A. O., Mansell, E. R., MacGorman, D. R., and Ziegler, C. L. (2013). The Implementation of an Explicit Charging and Discharge Lightning Scheme within the WRF-ARW Model : Benchmark Simulations of a Continental Squall Line , a Tropical Cyclone , and a Winter Storm. *Monthly Weather Review*, **141**, 2390–2415.

Finney, D. L., Doherty, R. M., Wild, O., Huntrieser, H., Pumphrey, H. C., and Blyth, A. M. (2014). Using cloud ice flux to parametrise large-scale lightning. *Atmospheric Chemistry and Physics*, **14**(23), 12665–12682.

Finney, D. L., Doherty, R. M., Wild, O., Stevenson, D. S., Mackenzie, I. A., and Blyth, A. M. (2018). A projected decrease in lightning under climate change. *Nature Climate Change*, **8**(210-213).

Fulton, R. A., Breidenbach, J. P., Seo, D.-J., and Miller, D. A. (1998). The WSR-88D Rainfall Algorithm. *Weather and Forecasting*, **13**, 377–395.

Gilbert, G. K. (1884). Finley's Tornado Predictions. *American Meteorological Journal*, pages 166–172.

Goodman, S. J., Blakeslee, R. J., Koshak, W. J., Mach, D., Bailey, J., Buechler, D., Carey, L., Schultz, C., Bateman, M., McCaul, E., and Stano, G. (2013). The GOES-R Geostationary Lightning Mapper (GLM). *Atmospheric Research*, **125-126**, 34–49.

Hanley, K. E., Plant, R. S., Stein, T. H., Hogan, R. J., Nicol, J. C., Lean, H. W., Halliwell, C., and Clark, P. A. (2015). Mixing-length controls on high-resolution simulations of convective storms. *Quarterly Journal of the Royal Meteorological Society*, **141**, 272–284.

Hare, B. M., Scholten, O., Dwyer, J., Trinh, T. N., Buitink, S., ter Veen, S., Bonardi, A., Corstanje, A., Falcke, H., Hörandel, J. R., Huege, T., Mitra, P., Mulrey, K., Nelles, A., Rachen, J. P., Rossetto, L., Schellart, P., Winchen, T., Anderson, J., Avruch, I. M., Bentum, M. J., Blaauw, R., Broderick, J. W., Brouw, W. N., Brüggen, M., Butcher, H. R., Ciardi, B., Fallows, R. A., de Geus, E., Duscha, S., Eislöffel, J., Garrett, M. A., Grießmeier, J. M., Gunst, A. W., van Haarlem, M. P., Hessels, J. W., Hoeft, M., van der Horst, A. J., Iacobelli, M., Koopmans, L. V., Krankowski, A., Maat, P., Norden, M. J., Paas, H., Pandey-Pommier, M., Pandey, V. N., Pekal, R., Pizzo, R., Reich, W., Rothkaehl, H., Röttgering, H. J., Rowlinson, A., Schwarz, D. J., Shulevski, A., Sluman, J., Smirnov, O., Soida, M., Tagger, M., Toribio, M. C., van Ardenne, A., Wijers, R. A., van Weeren, R. J., Wucknitz, O., Zarka, P., and Zucca, P. (2019). Needle-like structures discovered on positively charged lightning branches. *Nature*, **568**(7752), 360–363.

Harrison, D. L. and Kitchen, M. (2009). High-resolution precipitation estimates for hydrological uses. *Proceedings of the Institution of Civil Engineers: Water Management*, **162**(2), 125–135.

Harrison, R. G., Nicoll, K. A., and Ambaum, M. H. (2015). On the microphysical effects of observed cloud edge charging. *Quarterly Journal of the Royal Meteorological Society*, **141**(692), 2690–2699.

Helsdon, J. H. and Farley, R. D. (1987). A numerical modeling study of a Montana thunderstorm: 2. Model results versus observations involving electrical aspects. *Journal of Geophysical Research*, **92**(D5), 5661–5675.

Helsdon, J. H., Wu, G., and Farley, R. D. (1992). An intracloud lightning parameterization scheme for a storm electrification model. *Journal of Geophysical Research*, **97**(D5), 5865–5884.

Helsdon, J. H. J., Gattaleeradapan, S., Farley, R. D., and Waits, C. C. (2002). An examination of the convective charging hypothesis: Charge structure, electric fields, and Maxwell currents. *JOURNAL OF GEOPHYSICAL RESEARCH*, **107**(D22).

Hill, J. D., Uman, M. A., and Jordan, D. M. (2011). High-speed video observations of a lightning stepped leader. *Journal of Geophysical Research Atmospheres*, **116**(16), 1–8.

Hogan, R. J., O'Connor, E. J., and Illingworth, A. J. (2009). Verification of cloud-fraction forecasts. *Quarterly Journal of the Royal Meteorological Society*, **135**, 1494–1511.

Illingworth, A. J. and Caranti, J. M. (1985). Ice conductivity restraints on the inductive theory of thunderstorm electrification. *Journal of Geophysical Research*, **90**(D4), 6033–6039.

Illingworth, A. J. and Lees, M. I. (1991). Comparison of lightning location data and polaristation radar observations of clouds. In *The 1991 International Aerospace and Ground Conference on Lightning and Static Electricity, Volume 2*, pages 1–10.

Iudin, D. I., Rakov, V. A., Mareev, E. A., Iudin, F. D., Syssoev, A. A., and Davydenko, S. S. (2017). Advanced numerical model of lightning development : Application to studying the role of LPCR in determining lightning type. *Journal of Geophysical Research: Atmospheres*, **122**, 6416–6430.

Jayaratne, E. R. and Saunders, C. P. R. (1985). Thunderstorm electrification: The effect of cloud droplets. *Journal of Geophysical Research*, **90**, 13063–13066.

Jayaratne, E. R., Saunders, C. P. R., and Hallett, J. (1983). Laboratory studies of the charging of soft-hail during ice crystal interactions. *Quarterly Journal of the Royal Meteorological Society*, **109**, 609–630.

Kasemir, H. W. (1960). A contribution to the electrostatic theory of a lightning discharge. *Journal of Geophysical Research*, **65**(7), 1873–1878.

Krehbiel, P. R., Thomas, R. J., Rison, W., Hamlin, T., Harlin, J., and Davis, M. (2000). GPS-based Mapping System Reveals Lightning Inside Storms. *EOS, Transactions, American Geophysical Union*, **81**(3), 21–32.

Lapierre, J., Hoekzema, M., Stock, M., and Merrill, C. (2019). Earth Networks Lightning Network and Dangerous Thunderstorm Alerts. *2019 11th Asia-Pacific International Conference on Lightning (APL)*, pages 1–5.

Latham, J., Blyth, A. M., Christian, H. J., Deierling, W., and Gadian, A. M. (2004). Determination of precipitation rates and yields from lightning measurements. *Journal of Hydrology*, **288**, 13–19.

Liu, C., Cecil, D. J., Zipser, E. J., Kronfeld, K., and Robertson, R. (2012). Relationships between lightning flash rates and radar reflectivity vertical structures in thunderstorms over the tropics and subtropics. *Journal of Geophysical Research Atmospheres*, **117**(6).

Liu, C., Sloop, C., and Heckman, S. (2014). Application of lightning in predicting high impact weaether. In *TECO*.

Lopez, P. (2016). A lightning parameterization for the ECMWF integrated forecasting system. *Monthly Weather Review*, **144**(9), 3057–3075.

Lynn, B. H., Yair, Y., Price, C., Kelman, G., and Clark, A. J. (2012). Predicting Cloud-to-Ground and Intracloud Lightning in Weather Forecast Models. *Weather and Forecasting*, **27**(6), 1470–1488.

Lyons, W. A. and Keen, C. S. (1994). Observations of Lightning in Convective Supercells within Tropical Storms and Hurricanes.

MacGorman, D. R. and Rust, W. D. (1998). *The Electrical Nature of Storms*. Oxford University Press.

Macgorman, D. R., Few, A. A., and Teer, T. L. (1981). Layered lightning activity. *Journal of Geophysical Research*, **86**, 9900–9910.

MacGorman, D. R., Straka, J. M., and Ziegler, C. L. (2001). A Lightning Parameterization for Numerical Cloud Models. *Journal of Applied Meteorology*, **40**, 459–478.

MacGorman, D. R., Rust, W. D., Krehbiel, P., Rison, W., Bruning, E., and Wiens, K. (2005). The electrical structure of two supercell storms during STEPS. *Monthly Weather Review*, **133**(9), 2583–2607.

Mansell, E. R., Macgorman, D. R., Ziegler, C. L., and Straka, J. M. (2002). Simulated three-dimensional branched lightning in a numerical thunderstorm model. *Journal of Geophysical Research*, **107**.

Mansell, E. R., Macgorman, D. R., Ziegler, C. L., and Straka, J. M. (2005). Charge structure and lightning sensitivity in a simulated multicell thunderstorm. **110**.

Mansell, E. R., Ziegler, C. L., and Bruning, E. C. (2010). Simulated Electrification of a Small Thunderstorm with Two-Moment Bulk Microphysics. *Journal of the Atmospheric Sciences*, **67**, 171–194.

Marshall, T. C. and Marsh, S. J. (1993). Negatively charged precipitation in a New Mexico thunderstorm. *Journal of Geophysical Research*, **98**(D8), 14909–14916.

Marshall, T. C. and Rust, W. D. (1991). Electric Field Soundings Through Thunderstorms. *Journal of Geophysical Research*, **96**, 22297–22306.

Marshall, T. C. and Stolzenburg, M. (1998). Estimates of cloud charge densities in thunderstorms. *Journal of Geophysical Research*, **103**, 19769–19775.

Marshall, T. C., Mccarthy, M. P., and Rust, W. D. (1995). Electric field magnitudes and lightning intiation in thunderstorms. *Journal of Geophysical Research*, **100**, 7097–7103.

Maslowski, G. and Rakov, V. A. (2006). A study of the lightning channel corona sheath. *Journal of Geophysical Research*, **111**, 1–16.

Mattos, E. V., Machado, L. A. T., Williams, E. R., and Albrecht, R. I. (2016). Polarimetric radar characteristics of storms with and without lightning activity. *Journal of Geophysical Research: Atmospheres*, **121**, 201–220.

McCaul, E. W., Goodman, S. J., LaCasse, K. M., and Cecil, D. J. (2009). Forecasting lightning threat using cloud-resolving model simulations. *Weather and Forecasting*, **24**(3), 709–729.

Mo, Q., Detwiler, A. G., Helsdon, J., Winn, W. P., Aulich, G., and Murray, W. C. (2007). Hydrometeor charges observed below an electrified cloud using a new instrument. *Journal of Geophysical Research Atmospheres*, **112**(13), 1–13.

Montanya, J., Van Der Velde, O., and Williams, E. R. (2015). The start of lightning: Evidence of bidirectional lightning initiation. *Scientific Reports*, **5**, 1–6.

Mosier, R. M., Schumacher, C., Orville, R. E., and Carey, L. D. (2011). Radar Nowcasting of Cloud-to-Ground Lightning over Houston , Texas. *Weather and Forecasting*, **26**, 199–212.

Petersen, W. A., Christian, H. J., and Rutledge, S. A. (2005). TRMM observations of the global relationship between ice water content and lightning. *Geophysical Research Letters*, **32**(14), 1–4.

Price, C. and Rind, D. (1992). A Simple Lightning Parameterization for Calculating Global Lightning Distributions. *Journal of Geophysical Research*, **97**, 9919–9933.

Rakov, V. A. and Uman, M. A. (2003). *Lightning: Physics and Effects*. Cambridge University Press.

Rawlins, F. (1982). A numerical study of thunderstorm electrification using a three dimensional model incorporating the ice phase. *Quarterly Journal of the Royal Meteorological Society*, **108**(458), 779–800.

Rison, W., Krehbiel, P. R., Stock, M. G., Edens, H. E., Shao, X. M., Thomas, R. J., Stanley, M. A., and Zhang, Y. (2016). Observations of narrow bipolar events reveal how lightning is initiated in thunderstorms. *Nature Communications*, **7**.

Romps, D. M., Seeley, J. T., Vollaro, D., and Molinari, J. (2014). Projected increase in lightning strikes in the united states due to global warming. *Science*, **346**(6211), 851–854.

Rudlosky, S. D., Peterson, M. J., and Kahn, D. T. (2017). GLD360 performance relative to TRMM LIS. *Journal of Atmospheric and Oceanic Technology*, **34**(6), 1307–1322.

Rust, W. D. and Marshall, T. C. (1996). On abandoning the thunderstorm tripole-charge paradigm. *Journal of Geophysical Research Atmospheres*, **101**(18), 23499–23504.

Rutjes, C., Ebert, U., Buitink, S., Scholten, O., and Trinh, T. N. (2019). Generation of Seed Electrons by Extensive Air Showers, and the Lightning Inception Problem Including Narrow Bipolar Events. *Journal of Geophysical Research: Atmospheres*, **124**(13), 7255–7269.

Saunders, C. (2008). Charge separation mechanisms in clouds. *Space Science Reviews*, **137**(1-4), 335–353.

Saunders, C. P. R. (1993). A Review of Thunderstorm Electrificaiton Processes. *Journal of Applied Meteorology*, **32**, 642–655.

Saunders, C. P. R. and Peck, S. L. (1998). Laboratory studies of the influence of the rime accretion rate on charge transfer during crystal / graupel collisions. *Journal of Geophysical Research*, **103**, 949–13.

Saunders, C. P. R., Keith, W. D., and Mitzeva, R. P. (1991). The Effect of Liquid Water on Thunderstorm Charging. *Journal of Geophysical Research*, **96**, 11007–11017.

Schultz, C. J., Carey, L. D., Schultz, E. V., and Blakeslee, R. J. (2017). Kinematic and Microphysical Significance of Lightning Jumps versus Nonjump Increases in Total Flash Rate. *Weather and Forecasting*, **32**, 275–288.

Scovell, R. and Al-Sakka, H. (2016). A Point Cloud Method for Retrieval of High-Resolution 3D Gridded Reflectivity from Weather Radar Networks for Air Traffic Management. *Journal of Atmospheric and Ocean Technology*, **33**, 461–479.

Simpson, G. and Robinson, G. D. (1941). The distribution of electricity in thunderclouds , II. *Proceedings of the Royal Society A: Mathematical, Physical and Engineering Sciences*, **177**, 281–329.

Simpson, G. and Scrase, F. J. (1937). The Distribution of Electricity in Thunderclouds. *Proceedings of the Royal Society A: Mathematical, Physical and Engineering Sciences*, pages 309–352.

Stein, T. H., Hogan, R. J., Hanley, K. E., Nicol, J. C., Lean, H. W., Plant, R. S., Clark, P. A., and Halliwell, C. E. (2014). The three-dimensional morphology of simulated and observed convective storms over Southern England. *Monthly Weather Review*, **142**(9), 3264–3283.

Stein, T. H. M., Hogan, R. J., Clark, P. A., Halliwell, C. E., Hanley, K. E., Lean, H. W., Nicol, J. C., and Plant, R. S. (2015). The DYMECS Project: A Statistical Approach for the Evaluation of Convective Storms in High-Resolution NWP Models. *Bulletin of the American Meteorological Society*, **96**, 939–952.

Stolzenburg, M., Rust, W. D., and Marshall, T. C. (1998). Electrical structure in thunderstorm convective regions 3. Synthesis. *Journal of Geophysical Research*, **103**, 14097–14108.

Stolzenburg, M., Marshall, T. C., Rust, W. D., Bruning, E., MacGorman, D. R., and Hamlin, T. (2007). Electric field values observed near lightning flash initiations. *Geophysical Research Letters*, **34**(4), 1–7.

Stolzenburg, M., Marshall, T. C., and Krehbiel, P. R. (2015). Initial electrification to the first lightning flash in New Mexico Thunderstorms. *Journal of Geophysical Research: Atmospheres*, **120**, 253–276.

Stough, S. M., Carey, L. D., Schultz, C. J., and Bitzer, P. M. (2017). Investigating the Relationship between Lightning and Mesocyclonic Rotation in Supercell Thunderstorms. *Weather and Forecasting*, **32**, 2237–2259.

Takahashi, T. (1978). Riming Electrification as a Charge Generation Mechanism in Thunderstorms. *Journal of the Atmospheric Sciences*, **35**, 1536–1548.

Takahashi, T., Tajiri, T., and Sonoi, Y. (1999). Charges on Graupel and Snow Crystals and the Electrical Structure of Winter Thunderstorms. *Journal of the Atmospheric Sciences*, **56**(11), 1561–1578.

Takahashi, T., Sugimoto, S., Kawano, T., and Suzuki, K. (2017). Riming Electrification in Hokuriku Winter Clouds and Comparison with Laboratory Observations. *Journal of the Atmospheric Sciences*, **74**(2), 431–447.

Tang, Y., Lean, H. W., and Bornemann, J. (2013). The benefits of the Met Office variable resolution NWP model for forecasting convection. *Meteorological Applications*, **20**(4), 417–426.

Wang, K. Y. and Liao, S. A. (2006). Lightning, radar reflectivity, infrared brigthness temperature, and surface rainfall during the 2-4 July 2004 severe convective system over Taiwan area. *Journal of Geophysical Research Atmospheres*, **111**(5).

Wiens, K. C., Rutledge, S. A., and Tessendorf, S. A. (2005). The 29 June 2000 Supercell Observed during STEPS. Part II: Lightning and Charge Structure. *Journal of the Atmospheric Sciences*, **62**(12), 4151–4177.

Wiesmann, H. J. and Zeller, H. R. (1986). A fractal model of dielectric breakdown and prebreakdown in solid dielectrics. *Journal of Applied Physics*, **60**.

Wilkinson, J. M. (2017). A Technique for Verification of Convection-Permitting NWP Model Deterministic Forecasts of Lightning Activity. *Weather and Forecasting*, **32**(2012), 97–115.

Wilkinson, J. M. and Bornemann, F. J. (2014). A lightning forecast for the London 2012 Olympics opening ceremony. *Weather*, **69**(1), 16–19.

Wilson, C. T. R. (1916). On Some Determinations of the Sign and Magnitude of Electric Discharges in Lightning Flashes. *Proceedings of the Royal Society A: Mathematical, Physical and Engineering Sciences*, **92**(644), 555–574.

Wilson, C. T. R. (1924). Electric Field of a Thundercloud and Some of Its Effects. *Proceedings of the Physical Society of London*, **37**, 32D–37D.

Wilson, D. R. and Ballard, S. P. (1999). A microphysically based precipitation scheme for the UK Meteorological Office Unified Model. *Quarterly Journal of the Royal Meteorological Society*, **125**, 1607–1636.

Yair, Y., Lynn, B., Price, C., Kotroni, V., Lagouvardos, K., Morin, E., Mugnai, A., and Llasat, C. (2010). Predicting the potential for lightning activity in Mediterranean storms based on the Weather Research and Forecasting (WRF) model dynamic and microphysical fields. *Journal of Geophysical Research*, **115**, 1–13.

Zhu, Y., Rakov, V. A., Tran, M. D., Stock, M. G., Heckman, S., Liu, C., Sloop, C. D., Jordan, D. M., Uman, M. A., Caicedo, J. A., Kotovsky, D. A., Wilkes, R. A., Carvalho, F. L., Ngin, T., Gamerota, W. R., Pilkey, J. T., and Hare, B. M. (2017). Evaluation of ENTLN Performance Characteristics Based on the Ground Truth Natural and Rocket-Triggered Lightning Data Acquired in Florida. *Journal of Geophysical Research: Atmospheres*, **122**(18), 9858–9866.

Ziegler, C. L. and MacGorman, D. R. (1994). Observed Lightning Morphology Relative to Modeled Space Charge and Electric Field Distributions in a Tornadic Storm. *Journal of the Atmospheric Sciences*, **51**(6), 833–851.

Ziegler, C. L., MacGorman, D. R., Dye, J. E., and Ray, P. S. (1991). A Model Evaluation of Noninductive Graupel-Ice Charging in the Early Electrification of a Mountain Thunderstorm. *Journal of Geophysical Research*, **96**, 833–12.